Department of Physics and Astronomy

University of Heidelberg

Master thesis

in Physics

submitted by

Philipp Saake

born in Stolberg (Rhld.)

2019

General analysis of scale-setting in classically conformal multiscalar models

This Master thesis has been carried out by Philipp Saake

at the

Max Planck Institut für Kernphysik

under the supervision of

Herrn Prof. Manfred Lindner

Allgemeine Analyse der Skalensetzung in klassisch konformen multiskalar Modellen:

In dieser Arbeit untersuchen wir die grundlegenden Eigenschaften von radiativ induzierter, spontaner Symmetriebrechung (RSSB) in multiskalaren Modellen, ohne klassischen Massenterm. Um das Hierarchieproblem mit Hilfe einer Erweiterung des konform-symmetrischen Standard Modells (cSM) anzugehen, präsentieren wir einen allgemeinen Formalismus um die Erzeugung nicht-trivialer Minima des ein-loop effektiven Potentials, anhand einer Reihe von exakten Kritikalitäsgleichungen, zu analysieren. Auf Grund der intuitiven Beschaffenheit dieser Gleichungen sind wir in der Lage systematisch RSSB in klassisch, konformen Modellen zu untersuchen. Im speziellen untersuchen wir das Zusammenspiel von Beiträgen verschiedener Teilchen an der Kondensationsskala und im Renormalisierungsgruppenlaufen der Kopplungen. Wir vergleichen die beobachteten Eigenschaften von RSSB mit Resultaten aus Analysen mit Hilfe der gängigen Gildener-Weinberg Näherung, welche zusätzlich die Existenz einer flachen Richtung auf tree-Level voraussetzt. Ohne der Annahme von klassischer Skaleninvarianz noch weitere hinzu zu fügen finden wir schon Fälle, in denen die ein-loop Eichbeiträge generell von der gleichen Größenordnung sein können wie die skalaren tree-Level Terme. Dies erlaubt das Erzeugen von nicht-trivialen Vacua ohne eine flache Richtung auf tree-Level. Die Analyse mit Hilfe unseres Formalismus offenbart qualitativ neue Szenarien von RSSB, verglichen mit denen der Gildener-Weinberg Näherung und erlaubt daher das intuitive Untersuchen der fundamentalen Eigenschaften der Skalensetzung ohne weitere Annahmen zu der der klassischen Skaleninvarianz hinzu zu fügen.

General analysis of scale-setting in classically conformal multiscalar models:

In this thesis we investigate the fundamental features of radiatively induced spontaneous symmetry breaking (RSSB) in multiscalar models without classical mass terms. Motivated by addressing the hierarchy problem via the extension of the conformal standard model (cSM) we present a general formalism to analyze the generation of non-trivial minima in the one-loop effective potential via a set of exact criticality equations. Given the intuitive nature of these equations we are able to systematically analyze the RSSB in classically conformal multiscalar models. Specifically, we investigate the interplay of contributions by different particles at the scale of condensation and in the renormalization group running of the coupling parameters. We compare the observed features of RSSB to results obtained when using the commonly used Gildener-Weinberg approximation, which additionally assumes the existence of a flat direction at tree-level. Without making further assumptions to classical scale-invariance we already find cases where one-loop gauge contributions can generally be of the same order of magnitude as the scalar tree-level terms. Thus, allowing for the generation of non-trivial vacua without a tree-level flat direction. The analysis using our approach reveals qualitatively new scenarios of RSSB compared to the Gildener-Weinberg approximation and allows for an intuitive investigation of fundamental properties of scale-setting without making further assumptions to classical scale-invariance.

Contents

Conventions and notations

- In this work we use the natural units, such that the speed of light c and the reduced Planck constant $\hbar$ are equal to one

$$c = \hbar = 1 \ .$$

- If not stated otherwise we work in $d = 4$ dimensions such that four-vectors are denoted by $p = p_\mu$, while their spacial part would be written as $\mathbf{p}$.

- Dealing with divergent integrals we use the dimensional regularization method with $d = 4 - \epsilon$ and the $\overline{\text{MS}}$ renormalization scheme. As a result the counter-terms are proportional to

$$C_{\text{UV}} = \left[\frac{1}{\epsilon} - \gamma_{\text{E}} + \ln(4\pi)\right] \ ,$$

  where γ_{E} is the Euler–Mascheroni constant.

- Unless stated otherwise we work in Landau gauge, thus we generally do not require ghost-compensation terms. The free gauge bosons propagator is then given by

$$\frac{-i}{p^2 + i\epsilon}\Delta_{\mu\nu}, \qquad \text{with } \Delta_{\mu\nu} = \left(\eta_{\mu\nu} - \frac{p_\mu p_\nu}{p^2}\right) \ ,$$

  where $\Delta_{\mu\nu}$ denotes a projection operator with its usual properties and $\eta_{\mu\nu}$ the Minkowski metric with the signature $(+,-,-,-)$.

- We use the full Planck mass given in Ref. [1]

$$M_{\text{Pl}} = 1.22089(14) \times 10^{19}\,\text{GeV} \ .$$

Introduction

The standard model (SM) of particle physics is a theoretically self-consistent description of the fundamental interactions of elementary particles. With the recent discovery of the Higgs boson at the LHC in 2012, all of the model's crucial predictions, e.g. new particles are now experimentally validated, and especially the Brout-Englert-Higgs mechanism is confirmed to be responsible for the mass generation of gauge bosons and fermions in the SM. Despite its huge success of explaining almost all observed phenomena in particle physics, there are still several open problems that are not explained by the SM, like dark matter, matter-antimatter asymmetry, inflation, neutrino masses, the hierarchy problem and arguably most important, the unification with gravity. There are lots of attempts to extend the SM to explain either a specific one of these aspects or all together, with the supersymmetric (SUSY) version of the SM being probably the widest studied one. Nevertheless, the lack of experimental confirmation of the predicted supersymmetric partners of the SM particles makes it favorable to consider alternative, more minimalistic extensions of the SM. These have the advantage that if one manages to include problems like dark matter without introducing a new physical scale, one utilizes the fact that the SM already denotes a valid effective field theory for energies up to the Planck mass.

One promising attempt is based on the conformal extension of the SM. The conformal SM (cSM) is set to be classically scale-invariant[1] by omitting the Higgs' mass term in the Lagrangian and was first considered by W. Bardee in Ref. [5] to mitigate the electroweak (gauge) hierarchy problem. In this model the electroweak symmetry is still broken spontaneously by the (physical) Higgs field's non-vanishing vacuum expectation value, yet not due to classical a negative mass-squared term in the Lagrangian, but by including quantum corrections. The corresponding mechanism of radiatively induced spontaneous symmetry breaking (RSSB) in classically conformal systems was introduced in the seminal paper by and named after S. Coleman and E. Weinberg in Ref. [6]. They found that quantum corrections (already at one-loop level) can break conformal symmetry and generate non-trivial vacuum expectation values for the fields. This feature is also called dimensional transmutation, as quantum loops induce dimensionful quantities in a previously scale-invariant theory. Due to the absence of the Higgs boson's mass term in the Lagrangian the necessary fine-tuning of the hierarchy problem between its tree-level mass and its quantum corrections is converted into a (smaller) fine-tuning problem in the values of dimensionless couplings at the scale of renormalization, e.g. the Planck scale M_{Pl}. However, generating the experimentally measured Higgs mass via RSSB in the cSM is prevented by the large top mass, which destabilizes the (one-loop) effective potential, as seen in Refs. [7–10]. Thus, extensions of the cSM are necessary to naturally and dynamically generate the observed VEV of the Higgs field via spontaneous breaking of the initial conformal symmetry by quantum corrections.

Several extensions including different combinations of fields like real or complex scalars, multiple scalars, fermions and gauge bosons have been proposed. In addition

[1] As we always refer to the classical symmetry of a four-dimensional unitary and renormalizable quantum field theory, conformal and scale-invariance are classically equivalent, c.f. Refs [2–4]. Hence we use both terms interchangeably.

to addressing the hierarchy problem these models can incorporate the phenomena not explained by the SM like dark matter, neutrino masses and matter-antimatter asymmetry, c.f. Refs. [11–21]. In Ref. [22] it was shown that additional fermions have a destabilizing effect on the non-trivial vacuum and that the minimal cSM extension model that produces the correct RSSB to match observations is given by two additional scalar singlets. E. Gildener and S. Weinberg introduced a formalism in Ref. [23] that allows to approximately describe RSSB in multiscalar theories. Since the minimization of the general one-loop effective potential in multiscalar models is not trivial, the Gildener-Weinberg approximation is widely used to investigate the above motivated conformal extensions of the cSM (e.g. Refs. [9, 10, 22, 24–27]). In their work they assume the existence of a flat direction at tree-level that allows them to reduce the multidimensional problem of RSSB for multiple scalars to an investigation of the effective potential along the tree-level flat direction. They argue that non-trivial vacua can only be generated along this tree-level flat direction where quantum corrections are large enough to distort the effective potential accordingly. Yet the original S. Coleman and E. Weinberg publication, c.f. Ref. [6], already addressed the fact that a tree-level flat direction is not a necessary condition for RSSB as the gauge sector's quantum corrections can generally be of the same order of magnitude as the tree-level contribution within the applicability of the perturbative expansion. Thus, the commonly used Gildener-Weinberg formalism to describe the dynamical generation of masses in conformal extensions of the SM comes with loss of generality, when considering the natural generation of scales, as the tree-level flat direction only depends indirectly, through the renormalization group running of the scalar couplings, on particle content other than the scalars themselves. As the Gildener-Weinberg method is so widely used to describe RSSB in extensions of the cSM in attempts to solve the hierarchy problem, there has to be quantification of whether this simplification is appropriate. Furthermore, we see that there are forms of RSSB that are not covered by the Gildener-Weinberg formalism such that there might be extension models that were falsely excluded for being phenomenologically ruled out and new ones that were not considered yet.

Therefore, we propose a general formalism for arbitrary multiscalar extensions of the cSM, while directly including contributions of all particle content to analyze their fundamental properties of scale-setting and hence addressing the hierarchy problem by generating the observed Higgs mass via quantum corrections (RSSB). For a n scalar system we do not need to assume the existence of a flat direction at tree-level, but rather give n analytical criticality equations and solve them numerically in generalized n-dimensional spherical coordinates for the vacuum expectation values of the scalar fields. These n criticality equations contain $n-1$ angular and one radial equation in which we nicely see the interplay between contributions of particles with different spin that allow for the generation of non-trivial vacuum expectation values of the fields. In this context we derived general and exact tree- and one-loop level vacuum stability conditions to further ensure that any dynamically generated non-trivial vacuum is stable and in the range of applicability of our theory. These also yield fundamental information on the effects of particles with different spin, thus help to construct successful extensions of cSM. One example is recovering the statement that the large mass of the top quark prevents RSSB in the cSM alone.

To assess unapparent conditions on the initial coupling parameters at the Planck scale, when e.g. assuming the existence of a flat direction at tree-level, we aim to either examine their whole parameter space or the regions that are allowed by the correct RSSB if one assumes random renormalized couplings. Since we do not make further assumptions apart from classical scale-invariance we aim to understand the fundamental properties of mass generation via RSSB in conformal symmetric multiscalar models with gauge contributions.

The intuitive nature of our criticality equations allows for scale-setting to be understood similar to quantum chromodynamics (QCD). While in the non-perturbative case of QCD the scale of spontaneous symmetry breaking is determined by the dimensionless gauge coupling becoming large, in the perurbative breaking of electroweak symmetry, condensation occurs when the couplings reach a certain size, determined by the conditions given by our criticality equations, such that the tree- and loop-level contributions are of the same magnitude. Furthermore, with this exact formalism we are able to determine when the simplification of the Gildener-Weinberg formalism loses general applicability.

This thesis is structured as follows. At first in Section 1 we review the quantum field theoretical formalism that is necessary to calculate the quantum effective potential, the contributions by particles of different spin and the general form of the effective potential itself. Then in Section 2 we briefly discuss spontaneous breaking of conformal symmetry by the example of massless ϕ^4 theory and scalar quantum electrodynamics (QED). Here, we already see differences in mass generation when coupling the scalar to a gauge group, as already pointed out in the original Coleman-Weinberg publication, Ref. [6]. Section 3 is dedicated to introducing our general formalism to describing RSSB in multiscalar field models, explain the numerical methods used to solve for the non-trivial vacua and discuss the importance of the coupling parameters' renormalization group (RG) running. Therefore, we revisit the scalar QED model and gain first insights using the aforementioned approach, while giving a short overview of the Gildener-Weinberg approach to make further comparisons easier. Subsequently, in Section 4, we analyze the simplest conformal symmetric multiscalar models using our general formalism and compare to results obtained by a Gildener-Weinberg analysis. To see the influence on RSSB of the theory's gauge sector we start off with just two massless real scalars and then extend the theory's gauge sector. We first couple one of the massless scalars to a $U(1)$ gauge group, then both to the same gauge group and finally both scalars two independent $U_i(1)$ gauge groups. Respectively we discuss fundamental features of RSSB and compare with the Gildener-Weinberg formalism. At last, in Section 5 we recap and assess the results, discuss their connection to phenomenologically interesting extensions of the cSM and give an outlook of what to expect in the future.

1 Effective action of quantum field theory

To analyze radiatively induced and spontaneous symmetry breaking (RSSB) and therefore the generation of non-trivial vacuum expectation values (VEV) of the quantum scalar fields we need to study the *quantum effective potential* V_{eff}. To derive the said effective potential we must introduce a concept comparable to the classical action which takes into account quantum effects of all loop levels, the *effective action of quantum field theory* or *quantum effective action*. In analogy to the classical action, the quantum field equations are obtained by variation and the correlation functions of the full quantum field theory are given by suitable functional derivatives of the *quantum effective action*. Following Refs. [6, 28–30] we derive the effective action, from there on the effective potential in Section 1.1 and identify at contributions to V_{eff} of particles with different spins in Sections 1.2 to 1.4.

Let us start by considering the theory of one scalar field φ with its general functional Lagrange density $\mathcal{L}[\varphi(x)]$ and its corresponding action

$$S[\varphi] = \int \mathrm{d}^4x \, \mathcal{L}[\varphi(x)] \ . \tag{1.1}$$

Now we introduce the presence of a local, external source,[2] the scalar field $J(x)$, that is coupled linearly to $\varphi(x)$. In the presence of this external source, the generating functional $Z[J]$ of the Green's functions $G_n(x_1, x_2, \ldots, x_n)$ is given by

$$Z[J] = \sum_{n=0}^{\infty} \frac{i^n}{n!} \int \mathrm{d}^4x_1 \, \mathrm{d}^4x_2 \ldots \mathrm{d}^4x_n \, G_n(x_1, x_2, \ldots, x_n) \, J(x_1) J(x_2) \ldots J(x_n) \ . \tag{1.2}$$

Functional differentiation in combination with setting the external sources to zero confirms that $Z[J]$ in Eq. (1.2) is indeed the generating functional for the Green's functions (i.e. time ordered n-point functions)

$$G_n(x_1, x_2, \ldots, x_n) = \langle 0 \,| T\hat{\varphi}(x_1)\hat{\varphi}(x_2) \ldots \hat{\varphi}(x_n) |\, 0 \rangle \tag{1.3}$$

$$= \frac{1}{Z[J]} \frac{\delta^n Z[J]}{\delta i J(x_1) \delta i J(x_2) \ldots \delta i J(x_n)} \bigg|_{J=0} \ . \tag{1.4}$$

Using only the properties of canonical quantization, functional integrating over configuration phase space and regularization,[3] the generating functional of the Green's functions can be written as

$$Z[J] = \int \mathcal{D}\varphi \exp\left(i \left(S[\varphi] + \varphi \cdot J\right)\right) \ , \tag{1.5}$$

where $\mathcal{D}\varphi$ denotes a path integral over φ and $\varphi \cdot J$ is shorthand notation for the

[2] This is applicable since there are many physical situations where external fields are actually present, e.g. the gravitational field or a scalar field with non-vanishing vacuum expectation value.

[3] The need for regularization arises as the integration over configuration space induces a functional measure, which always contains the ill-defined $\delta^4(0)$.

source term

$$\varphi \cdot J = \int \mathrm{d}^4x \, \varphi(x) J(x) \, . \tag{1.6}$$

We want to note here that this form of the generating functional $Z[J]$ of Eq. (1.5) is the consequence of canonical quantization and regularization. It is therefore universal in the sense that it can be derived in analogy for a regularized and arbitrary canonically quantized theory, e.g. different particle content. Furthermore, in a physical sense, the functional $Z[J]$ of Eq. (1.5) represents the transition amplitude between two vacuum states in the presence of an external source $Z[J] = \langle 0_{\text{in}} | 0_{\text{out}} \rangle_{\text{J}}$. It is calculated as the sum over all connected and disconnected Feynman diagrams of the above mentioned amplitude. Here, the Feynman rules for the calculation of the diagrams are given by the Feynman rules of the vanishing external source $J = 0$, i.e. dictated by the classical action $S[\varphi]$, with an additional incorporation of a new vertex induced by the source term $\varphi \cdot J$.

From $Z[J]$, the generating functional of the Green's functions we can derive a generating functional for the connected Green's functions $W[J]$, introducing the relation

$$Z[J] = e^{iW[J]} \, , \tag{1.7}$$

where the connected Green's functions $G_n^c(x_1, x_2, \ldots, x_n | J)$, evaluated at arbitrary source field J, are defined by the functional derivative of $W[J]$

$$G_n^c(x_1, x_2, \ldots, x_n | J) = \frac{\delta^n W[J]}{\delta i J(x_1) \delta i J(x_2) \ldots \delta i J(x_n)} \, . \tag{1.8}$$

Proof that $W[J]$ actually generates connected Green's functions is found through induction and is illustrated by the simplest, non-trivial example, a two-point function ($n = 2$). We can express the full Green's function $G_2(x_1, x_2 | J)$ in terms of one- and two-point connected Green's functions

$$G_2(x_1, x_2) = i G_1^c(x_1 | J) \, i G_1^c(x_2 | J) + i G_2^c(x_1, x_2 | J) \, , \tag{1.9}$$

with $G_1^c(x)$ following from differentiation of Eq. (1.7) with respect to the source for $n = 1$

$$G_1(x) = \frac{1}{Z[J]} \frac{\delta Z[J]}{\delta i J(x)} = i G_1^c(x) \, . \tag{1.10}$$

Furthermore, differentiation of Eq. (1.7) with respect to the source field J and using

Eq. (1.4) leads us to

$$G_2(x_1, x_2|J) = \frac{1}{Z\,[J]} \frac{\delta^2 Z\,[J]}{\delta i J(x_1) \delta i J(x_2)} \,, \tag{1.11a}$$

$$= \frac{1}{Z\,[J]} \frac{\delta Z\,[J]}{\delta i J(x_1)} \frac{1}{Z\,[J]} \frac{\delta Z\,[J]}{\delta i J(x_2)} + i \frac{\delta^2 W[J]}{\delta i J(x_1) \delta i J(x_2)} \,, \tag{1.11b}$$

$$= i G_1^c(x_1) i G_1^c(x_2) + i \frac{\delta^2 W[J]}{\delta i J(x_1) \delta i J(x_2)} \,. \tag{1.11c}$$

Comparing the above Eq. (1.11) to Eq. (1.9) we see that

$$G_2^c(x_1, x_2|J) = \frac{\delta^2 W[J]}{\delta i J(x_1) \delta i J(x_2)} \,, \tag{1.12}$$

and therefore indeed $W[J]$ is the generating functional of the connected Green's functions, as the argument generalizes to arbitrary n. Proof by induction can be found on p. 43-45 in Ref. [28]. In terms of Feynman diagrams the connected Green's functions G_n^c are equivalent to connected Feynman graphs. Since functional derivatives of $Z[J]$ with respect to the source correspond to Fourier transformations, the expectation value (also mean, background or classical field) of $\varphi(x)$ is given by the one-point function

$$\langle \varphi(x) \rangle = G_1(x) = \frac{1}{Z[J]} \frac{\delta Z[J]}{\delta i J(x)} \equiv \phi_J(x) \,. \tag{1.13}$$

Note that, in the context of this work, the external field $J(x)$ is a purely artificial construct with no physical representation. By setting J to zero we go from any theoretical vacuum state to the physical ("true") vacuum state. Thus, one can only discuss the "true" vacuum in the absence of external fields. But for now, combining Eq. (1.7) and Eq. (1.13) we obtain the relation

$$\phi_J = \frac{\delta W[J]}{\delta i J(x)} \,. \tag{1.14}$$

We use this to solve for $J(x)$ since it links $\phi_J(x)$ and $J(x)$ as conjugate objects. Hence, $\phi_J(x)$ becomes an independent functional argument and the external source term $J(x)$ can be express as a functional of the mean field

$$\phi_J(x) \to \phi(x), \qquad J(x) \to J_\phi(x) \,. \tag{1.15}$$

The quantum effective action $\Gamma[\phi]$ is then obtained by a functional Legendre transformation of $W[J_\phi]$

$$\Gamma[\phi] = W[J_\phi] - \int \mathrm{d}^4x \; \phi(x) J_\phi \,. \tag{1.16}$$

Note that the quantum effective action $\Gamma[\phi]$ is now a functional of the mean field $\phi(x)$. Looking at the derivative of the effective action with respect to the mean field

we find the equation of motion for $\phi(x)$ to be

$$\frac{\delta\Gamma[\phi]}{\delta\phi(x)} = -J(x) \,, \tag{1.17}$$

where we differentiated Eq. (1.16), using Eq. (1.14) and the delta distributions definition $\delta^4(x-y) = \delta\phi(x)/\delta\phi(y)$. Here, we see that $\Gamma[\phi]$ plays the role of the classical action in the quantum theory, giving the equations of motion by differentiation. Furthermore, Eq. (1.17) shows that the equation of motion of $\phi(x)$ in absence of the external field reduces to

$$\left.\frac{\delta\Gamma[\phi]}{\delta\phi(x)}\right|_{J=0} = 0 \,. \tag{1.18}$$

Hence, for vanishing external sources the expectation value of the quantum field φ is obtained by a stationary principle of the action functional $\Gamma[\phi]$ analog to the classical theory, but accounting for all quantum corrections.

Furthermore, it was shown that $\Gamma[\phi]$ is the sum of all connected one-particle irreducible graphs in the presence of the external source J and that $W[J]$ may be calculated as the sum of connected tree-level graphs for the vacuum to vacuum amplitudes. The vertices are calculated using the quantum effective action $\Gamma[\phi]$ instead of the classical action $S[\phi]$, as seen e.g. in Ref. [30] on p. 65-67.

In the following we look further into the diagrammatic interpretation of the effective action $\Gamma[\phi]$. Similar to classical action, the effective action is the generating functional for the quantum n-point vertex functions (or correlation functions). These include the classical vertex functions, with the classical action as their generating functional, plus all their quantum corrections.

1.1 Effective potential

Introducing the n-point vertex functions Γ_n as the coefficients in an expansion of the quantum effective action with respect to the mean field $\phi(x)$

$$\Gamma[\phi] = \sum_{n=1}^{\infty} \frac{1}{n!} \int \mathrm{d}^4x_1 \, \mathrm{d}^4x_2 \ldots \mathrm{d}^4x_n \; \Gamma_n(x_1, x_2, \ldots, x_n)\phi(x_1)\phi(x_2)\ldots\phi(x_n) \,, \tag{1.19}$$

the vertex functions are given by functional derivatives

$$\Gamma_n(x_1, x_2, \ldots, x_n) = \frac{\delta^n\Gamma[\phi]}{\delta\phi(x_1)\delta\phi(x_2)\ldots\delta\phi(x_n)} \,. \tag{1.20}$$

In the following we show that the relation Eq. (1.20) is fulfilled and hence $\Gamma[\phi]$ is indeed the generating functional for the quantum vertex functions $\Gamma_n(x_1, \ldots, x_n)$.

For $n = 1$, we simply recognize the one-point vertex function to be given by the source $J(x)$ (up to the arbitrariness of the sign), c.f. Eq. (1.17). For $n = 2$, we use

the relations Eq. (1.14) and Eq. (1.17) to evaluate the following term

$$\int \mathrm{d}^4y \, \frac{\delta^2 W[J]}{\delta J(x)\delta J(y)} \frac{\delta^2 \Gamma[J]}{\delta\phi(y)\delta\phi(z)} = -\int \mathrm{d}^4y \, \frac{\delta\phi(x)}{\delta J(y)} \frac{\delta J(y)}{\delta\phi(z)} = -\delta^4(x-z) \, . \tag{1.21}$$

By considering the result for the connected 2-point function in Eq. (1.12), we arrive at

$$\int \mathrm{d}^4y \, G_2^c(x,y|J) \frac{\delta^2\Gamma[\phi]}{\delta\phi(y)\delta\phi(z)} = \delta^4(x-z) \, . \tag{1.22}$$

Thus, the two-point vertex function $\Gamma_2(y,z)$ is given by the inverted connected two-point function $(G_2^c)^{-1}$

$$\Gamma_2(y,z) = \frac{\delta^2\Gamma[\phi]}{\delta\phi(y)\delta\phi(z)} = \left[G_2^c\right]^{-1}(y,z|J) \, , \tag{1.23}$$

which can be interpreted as the amputated one-particle irreducible (1PI) Green's function. Note that 1PI means that a connected Feynman diagram cannot be made disconnected by cutting one internal line. Furthermore, the example of $n = 2$ corresponds to the inverse propagator. The argument can be extended to arbitrary n by looking at further functional derivative with respect to the mean field $\phi(x_n)$ of the already known $\Gamma_k(x_1,\ldots,x_k)$ with $k = n-1$, leading to the corresponding one-particle irreducible n-point vertex. This is nicely shown in a diagrammatic way in Ref. [28] on p. 47-51.

Now that we know how to calculate the n-point vertices it is advantageous to look at their Fourier transformation, since we are generally interested in translationally invariant quantities (the VEV of the field)

$$\Gamma_n(x_1,\ldots,x_n) = \int \prod_{i=1}^{n} \left[\frac{\mathrm{d}^4p_i}{(2\pi)^4} \exp\left(ip_ix_i\right)\right] (2\pi)^4\delta^4\left(p_1+\ldots+p_n\right) \, \tilde{\Gamma}_n(p_1,\ldots,p_n) \, . \tag{1.24}$$

With Eq. (1.24), the Fourier transformation of the mean field $\tilde{\phi}(p)$ and the integral representation of $\delta^4(p_i,\ldots,p_n)$

$$\delta^4(p_1+\ldots+p_n) = \int \frac{\mathrm{d}^4x}{(2\pi)^4} \exp\left(-ix(p_1+\ldots+p_n)\right) \, , \tag{1.25}$$

we can rewrite the quantum effective action to be

$$\Gamma[\phi] = \sum_{n=1}^{\infty} \frac{1}{n!} \int \prod_{i=1}^{n} \left[\iint \mathrm{d}^4x_i \frac{\mathrm{d}^4p_i}{(2\pi)^4}\phi(x_i)\right] \int \mathrm{d}^4x \, \tilde{\Gamma}_n(p_1,\ldots,p_n) \, \exp\left(i\sum_{i=1}^{n}(x_i-x)p_i\right) \, . \tag{1.26}$$

Expanding the Fourier transformed vertex function $\tilde{\Gamma}_n$ around vanishing momenta,

$$\tilde{\Gamma}(p_1,\ldots,p_n) = \tilde{\Gamma}_n(0,\ldots,0) + \sum_{i=1}^{n} \left.\frac{\partial\tilde{\Gamma}_n(p_1,\ldots,p_n)}{\partial p_i^\mu}\right|_{p_i=0} p_{i,\mu} + \ldots \, , \tag{1.27}$$

we can rewrite the effective action of $\Gamma[\phi]$ Eq. (1.26) as a derivative expansion

$$\Gamma[\phi] = \sum_{n=1}^{\infty} \frac{1}{n!} \int \mathrm{d}^4x \, \tilde{\Gamma}_n(0,\ldots,0) \, \phi(x)^n + \frac{1}{2} \int \mathrm{d}^4x \, Z(\phi) \frac{\partial \phi}{\partial x^\mu} \frac{\partial \phi}{\partial x_\mu} + \ldots \, , \tag{1.28}$$

where $Z(\phi)$ denotes the mean fields normalization factor. Now every term on the right hand side is a function of $\phi(x)$ rather than a functional. We have to note that the expression in Eq. (1.28) implicitly assumes a mean field $\phi(x)$ that is slowly changing in space-time such that the effective action, that is in general a non-local object, is shown in the form of its so-called *local approximation*.

In analogy to the classical action, the non-derivative terms in this local approximation of the effective action (Eq. (1.28)) can be identified as the effective potential $V_{\text{eff}}(\phi)$

$$V_{\text{eff}}(\phi) = -\sum_{n=1}^{\infty} \frac{1}{n!} \tilde{\Gamma}_n(0,\ldots,0) \, \phi(x)^n \, . \tag{1.29}$$

Diagrammatically speaking this means that the effective potential (up to a minus sign) is given by the sum over all 1PI Feynman diagrams with n external legs connected to the constant brackground field $\phi(x) = \phi = \text{const.}$, as implied by evaluation at vanishing external momenta $p_i = 0$. Since we are interested in the non-trivial "true" vacua of the theory, induced by RSSB, we furthermore assume the absence of external fields, i.e. $J = 0$. In the case of constant background field ϕ it is obvious that the calculation of the effective action in Eq. (1.28) yields the effective potential

$$\Gamma[\phi(x) = \phi] = -V_{\text{eff}}(\phi) \int \mathrm{d}^4x \, , \tag{1.30}$$

such that in absence of external sources and for a translation invariant (constant) background field, the stationary principle of the quantum action functional, c.f. Eq. (1.18), reduces to the condition for a stationary point in the effective potential

$$\frac{\partial V_{\text{eff}}(\phi)}{\partial \phi} \stackrel{!}{=} 0 \, . \tag{1.31}$$

Consequently this means that the value of the field for which the effective potential has a total minimum, i.e. fulfills Eq. (1.31), is equivalent to the "true" vacuum expectation value (VEV) of the classical field ϕ. This gives us a geometrical interpretation of the analysis of spontaneous symmetry breaking at quantum loop-level in terms of the investigation of a potential in field space. Even though Eq. (1.31) just requires the effective potential to be stationary, the need for a ground state and hence stability of the potential (being bound from below), makes the analysis of the theories vacua equivalent to the search for minima in the effective potential (local minima correspond to false vacua).

Yet the actual problem of calculating V_{eff} still exists, as it, c.f. Eq. (1.29), is given by an infinite summation of Feynman graphs, i.e. the 1PI n-point quantum vertex functions $\Gamma_n(0,\ldots,0)$ at vanishing external momenta. Thus a sensible approxima-

tion approach is needed. One diagrammatically well understood and convenient approximation approach for calculating the effective potential is the *loop-expansion*. Its main idea is to introduce loop-order specific contributions to the effective potential $V^{(n)}$, that now only contain trivial infinite summations over given n-loop-order diagrams. Therefore, approximating the effective potential only to zero order in loops, V_{eff} is given by the sum over all 1PI tree-level graphs with zero external momenta. Hence, at zero-loop order the effective potential reduces to the tree-level (classical) potential $V_{\text{cl}}(\varphi)$

$$V_{\text{eff}}(\phi) = V^{(0)}(\phi) = V_{\text{cl}}(\phi) \ , \tag{1.32}$$

or equivalently, the n-point quantum vertex functions are equal to the classical vertex functions given by the classical potential $V_{\text{cl}}(\varphi)$ from the Lagrangian $\mathcal{L}$. Moving on to one-loop order in the expansion, the effective potential now contains the tree-level contribution $V^{(0)}$, as discussed above, and a one-loop contribution $V^{(1)}$ (often referred to as the Coleman-Weinberg potential) given by

$$V^{(1)} = \sum_{n=1}^{\infty} \frac{1}{n!} \tilde{\Gamma}_n^{(1)}(0, \dots, 0) \ \phi(x)^n \ . \tag{1.33}$$

In analogy to Eq. (1.29) we can see that the one-loop contribution to the effective potential $V^{(1)}$ is given by the sum over all 1PI Feynman diagrams containing one closed loop and n external legs connected to the mean field ϕ, each contributing a factor ϕ and evaluated at vanishing external momenta. As the one-loop contributions $V^{(1)}$ are renomalizeable, only a finite number of counter-terms need to be added to account for the divergencies (e.g. self-energy diagrams). These counter-terms are denoted by the contribution $\Delta V(\phi)$ and need to be determined self-consistently order by order in the loop-expansion by imposing renormalization conditions for each quantity, i.e. wave-function, mass and coupling constant respectively. Hence, the "full" one-loop effective potential is given by

$$V_{\text{eff}}(\phi) = V^{(0)}(\phi) + V^{(1)}(\phi) + \Delta V(\phi) \ . \tag{1.34}$$

In this manner the effective potential can be calculated for arbitrary order n in the loop-expansion scheme. Yet, we only take into account contributions up to one-loop order to the effective potential as a sensible approximation for the analysis of RSSB. This is not only because of simplicity of calculations but more importantly it is motivated by the fact that contributions of higher loop order n are suppressed by higher powers of the loop factor $(1/16\pi^2)^n$. Hence, we expect the one-loop order contribution to be the leading order of quantum corrections to the initial, classical potential and its vacuum structure and symmetry breaking properties. As we are not interested in the infinite parts of the one-loop effective potential, we from here on discuss V_{eff} in the form of

$$V_{\text{eff}}(\phi) = V^{(0)}(\phi) + V^{(1)}(\phi) \ , \tag{1.35}$$

where $V^{(0)}(\phi)$ and $V^{(1)}(\phi)$ denote the remaining finite contributions after cancella-

tion of the divergences with the counter-terms.

In the following Sections, we show that, using dimensional regularization and the minimal subtraction scheme ($\overline{\text{MS}}$), the remaining one-loop contribution to the effective potential $V^{(1)}$ can be written in the general form

$$V^{(1)}(\phi) = \sum_i V_i^{(1)}(\phi) = \frac{1}{64\pi^2} \sum_i (-1)^{2s_i}\, n_i\, m_i^4(\phi) \left(\ln \left[\frac{m_i^2(\phi)}{\bar{\mu}^2} \right] - c_i \right) , \quad (1.36a)$$

where i runs over all particles contained in the theory, $m_i(\phi)$ denotes the particle's field dependent mass, s_i their spin, n_i the particle's real degrees of freedom and c_i a particle species specific constant. We see that, e.g. the coefficients c_i are determined to be

$$c_i = \begin{cases} \frac{3}{2}, \text{ for scalar fields and fermions} \\ \\ \frac{5}{6}, \text{ for gauge bosons} . \end{cases} \quad (1.37)$$

As the zero-loop order contribution is given by the tree-level (classical) potential, in the follwoing the particle-specific one-loop contributions are calculated in a diagrammatic way, following Refs. [29, 31]. Other examples of calculating the one-loop contributions are, e.g. given in Refs. [32, 33].

1.2 Scalar fields

To illustrate the contribution of a scalar field to the one-loop effective potential $V_{\text{S}}^{(1)}$, we consider the simplest model of one real scalar field ϕ. This can be easily extended to complex scalar fields by rewriting the complex scalar in terms of two real scalar fields and applying the following method to each one respectively.

We consider the Lagrangian of a real scalar field that is given by

$$\mathcal{L} = \frac{1}{2}\partial^\mu\phi\partial_\mu\phi - V^{(0)}(\phi) , \quad \text{with} \quad (1.38)$$

$$V^{(0)}(\phi) = \frac{1}{2}m^2\phi^2 + \frac{1}{4!}\lambda\phi^4 , \quad (1.39)$$

where $V^{(0)}(\phi)$ denotes the classical (tree-level) potential. Recalling Eq. (1.33), the one-loop contribution can be calculated by summing up all Feynman diagrams containing one closed loop, with vanishing external momenta and n external legs connected to the scalar field ϕ. The diagrams contributing to $V_{\text{S}}^{(1)}$ are graphically shown in Fig. 1.1. As seen, every vertex has two external legs,[4] the n-th diagram contains n vertices and therefore $2n$ external legs. Since every external leg is connected to the mean field ϕ, they give the overall factor of ϕ^{2n}. With the Feynman rules from the Lagrangian Eq. (1.38) the n propagators contribute a factor of $i^n \left(p^2 - m^2 + i\epsilon\right)^{-n}$ and the contribution of the n vertices is $\left(-\frac{i}{2}\lambda\right)^n$. While the $\frac{1}{2}$ in the contribution of the vertex is due to a interchange symmetry between the two external legs, the overall symmetry factor of the n-th diagram consists of a factor of $\frac{1}{n}$ due to rotational symmetry and a factor of $\frac{1}{2}$ due to the diagrams symmetry under reflection.

[4] Since the four-point vertex is the only one possible in a ϕ^4 theory, like the one considered here.

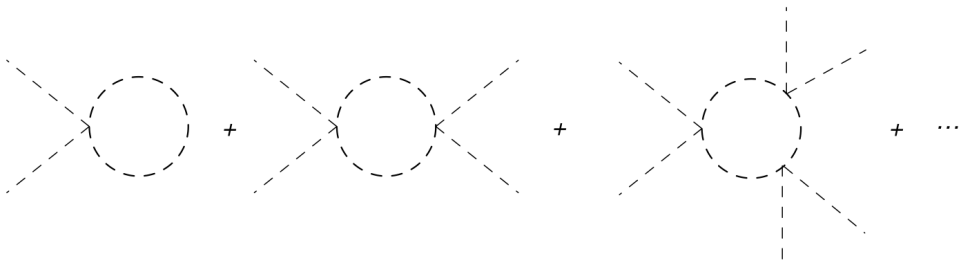

Figure 1.1: The one-loop, 1PI Feynman diagrams that contribute to the effective potential given by the Lagrangian in Eq. (1.38).

Furthermore, under consideration of integration over the loop momentum and an extra factor of i, given by the definition of the generating functional from Eq. (1.7), the one-loop contribution $V_{\mathrm{S}}^{(1)}$, c.f. Eq. (1.33), is calculated to be

$$V_{\mathrm{S}}^{(1)}(\phi) = i \sum_{n=1}^{\infty} \int \frac{\mathrm{d}^4 p}{(2\pi)^4} \frac{1}{2n} \left(\frac{\lambda\phi^2/2}{p^2 - m^2 + i\epsilon} \right)^n , \tag{1.40a}$$

$$= -\frac{i}{2} \int \frac{\mathrm{d}^4 p}{(2\pi)^4} \ln \left[1 - \frac{\lambda\phi^2/2}{p^2 - m^2 + i\epsilon} \right] , \tag{1.40b}$$

where we performed the summation over n after interchanging summation and integration to get from the first to the second line. Introducing the shifted (field dependent) mass $m^2(\phi)$

$$m^2(\phi) = \frac{\partial^2 V^{(0)}(\phi)}{\partial \phi^2} \overset{(1.39)}{=} m^2 + \frac{1}{2}\lambda\phi^2 , \tag{1.41}$$

Wick-rotating into Euclidean space and dropping the field-independent term (as it only denotes an infinite constant) we arrive at

$$V_{\mathrm{S}}^{(1)}(\phi) = \frac{1}{2} \int \frac{\mathrm{d}^4 p}{(2\pi)^4} \ln \left[p^2 + m^2(\phi) \right] . \tag{1.42}$$

Calculating this integral via dimensional regularization and canceling infinite terms using the by the $\overline{\mathrm{MS}}$ scheme determined counter-terms, we are left with the one-loop contribution to the effective potential (the explicit calculation is shown in, e.g. Ref. [29])

$$V_{\mathrm{S}}^{(1)}(\phi) = \frac{1}{64\pi^2} m^4(\phi) \left(\ln \left[\frac{m^2(\phi)}{\bar{\mu}^2} \right] - \frac{3}{2} \right) . \tag{1.43}$$

Since a real scalar field has a spin equal to zero ($s = 0$) and only one real degree of freedom ($n = 1$), comparing this result with Eq. (1.36) and Eq. (1.37) leads to the conclusion, that they are identical.

1.3 Fermion fields

To calculate the contribution of N spin $s = 1/2$ particles ψ_i $(i = 1, \ldots, N)$, linearly coupled to a scalar field ϕ, we start with the general Lagrangian

$$\mathcal{L} = i\bar{\psi}_a \gamma_\mu \, \partial^\mu \psi^a - \bar{\psi}_a \left[M_f(\phi)\right]^a_b \psi^b \, , \tag{1.44}$$

where $\left[M_f(\phi)\right]^a_b = Y^a_b \phi$ already defines the fermionic field dependent mass to be given by the product of the background field ϕ and the Yukawa coupling matrix Y^a_b. We recall that the trace over an odd number of γ-matrices is zero. While every fermion propagator carries the factor of a γ-matrix, this property of the γ-matrices, leads to contributions from diagrams with an odd number of fermion propagators (or vertices) being zero. Hence, the non-zero contributions are given by the sum over all 1PI Feynman diagrams with one fermion loop, $2n$ fermion propagators and $2n$ vertices, connected to $2n$ external legs of the background field ϕ, as seen in Fig. 1.2. The $2n$ propagators contribute a total factor of

$$Tr_s \left[i^{2n} \left(\gamma \cdot p\right)^{2n} \left(p^2 + i\epsilon\right)^{-2n} \right] \, , \tag{1.45}$$

where Tr_s denotes the trace over spinor indices and $(\gamma \cdot p) = (\gamma_\mu \, p^\mu)$. Then the $2n$ vertices give the factor

$$Tr_i \left[-i^{2n} M_f(\phi)^{2n} \right] \, , \tag{1.46}$$

with i indicating a trace over different fermion fields. Combining Eq. (1.45) and Eq. (1.46) with an overall combinatoric factor of $\frac{1}{2n}$ (due to rotation and reflection symmetry of the diagrams), dropping the $i\epsilon$ term for convenience, accounting for the (-1) from the fermion loop and using the relation $(\gamma \cdot p)^2 = p^2$ we arrive at

$$-\frac{1}{2n} \frac{Tr_i \left[M_f(\phi)^{2n}\right]}{p^{2n}} \cdot Tr_s I_s \, . \tag{1.47}$$

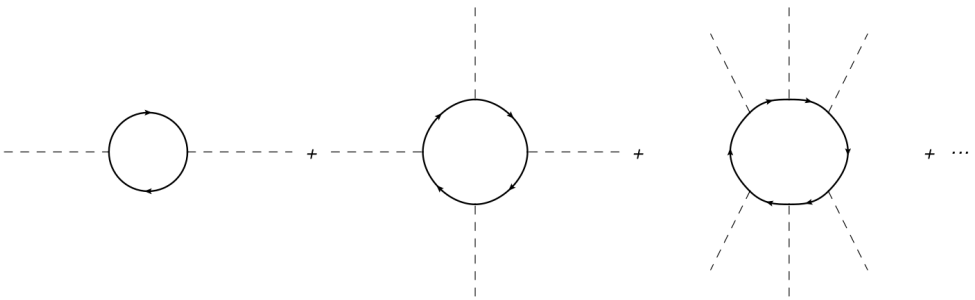

Figure 1.2: The fermionic 1PI Feynman graphs that contribute, as seen in Eq. (1.44), to the one-loop effective potential.

Here I_s denotes the identity matrix of the fermion's spinor space. Hence, the factor $Tr_s I_s$ gives the number of degrees of freedom of the fermion, which is equal to 2 for Weyl and to 4 for Dirac fermions. For simplicity we express this term as

$$Tr_s I_s = \rho = \begin{cases} 2, & \text{Weyl fermion} \\ 4, & \text{Dirac fermion} \end{cases} . \tag{1.48}$$

The one-loop contribution by fermion fields to the effective potential is then given by $V_{\text{F}}^{(1)}(\phi)$

$$V_{\text{F}}^{(1)}(\phi) = -i\rho\, Tr_i \sum_{n=1}^{\infty} \int \frac{\mathrm{d}^4 p}{(2\pi)^4} \frac{1}{2n} \left[\frac{M_f(\phi)^2}{p^2} \right]^n , \tag{1.49}$$

with, analogous to the scalar contribution in Section 1.2, the factor i from the definition of the generating functional Eq. (1.7). Assuming a diagonal mass matrix $M_f(\phi)^2 = m_f^2(\phi) I_{\text{N}}$, the trace over the different fermion fields reduces to the number of fermions with the same mass $m_f^2(\phi)$, i.e the number of flavour states N

$$Tr_i M_f(\phi)^2 = m_f^2(\phi) Tr_i I_{\text{N}} = N m_f^2(\phi) . \tag{1.50}$$

Wick rotating into euclidian space and disregarding field independent terms we arrive at

$$V_{\text{F}}^{(1)}(\phi) = (-\rho N) \frac{1}{2} \int \frac{\mathrm{d}^4 p}{(2\pi)^4} \ln \left[p^2 + m_f^2(\phi) \right] . \tag{1.51}$$

Seeing that the remaining integral is of the same structure as in Eq. (1.42), the final fermion contribution to the one-loop effective potential is given by

$$V_{\text{F}}^{(1)}(\phi) = (-\rho N) \frac{1}{64\pi^2} m_f^4(\phi) \left(\ln \left[\frac{m_f^2(\phi)}{\bar{\mu}^2} \right] - \frac{3}{2} \right) , \tag{1.52}$$

only differing from the scalar contribution in Eq. (1.43) by the factor $(-\rho N)$, that accounts for the fermion's number of degrees of freedom (color, spin, charge) and the sign given by the fermion loop. Identifying $n_i = \rho N$ and given the fermion's spin $s = \frac{1}{2}$ this result is perfectly in agreement with Eq. (1.36) and Eq. (1.37).

1.4 Gauge fields

For the spin $s = 1$ particles contribution we consider one gauge boson coupled to a scalar field. We choose to be in Landau gauge, where the free gauge boson propagator is given by Eq. (1.1) and no ghost-compensation terms are required. The Lagrangian is of the form

$$\mathcal{L} = -\frac{1}{4} Tr \left[F_{\mu\nu} F^{\mu\nu} \right] + \frac{1}{2} \left(D_\mu \phi \right)^\dagger \left(D^\mu \phi \right) , \tag{1.53a}$$

$$\supseteq -\frac{1}{4} Tr \left[F_{\mu\nu} F^{\mu\nu} \right] + \frac{1}{2} q^2 e^2 A_\mu A^\mu \phi^2 , \tag{1.53b}$$

where we highlighted the only vertex that contributes at one-loop level and simultaneously defines the field dependent mass $m_A^2(\phi)$ of the gauge boson to be

$$m_A^2(\phi) = q^2 e^2 \phi^2 \ . \tag{1.54}$$

Furthermore, $D_\mu \phi$ denotes the covariant derivative of ϕ

$$D_\mu \phi = \partial_\mu \phi - iqeA_\mu \phi \ , \tag{1.55}$$

with e denoting the gauge coupling and q the charge of ϕ with respect to the gauge group of A_μ. In this case, we assume $q = 1$. Note here, that this is easily generalized to a theory of multiple scalars and general (more complicated) gauge groups, which can be seen in Ref. [29], while the structure here is still representative of the general calculation. To compute the contribution of the gauge boson $V_{\text{A}}^{(1)}$ to the one-loop effective potential we sum up the one-loop diagrams, depicted in Fig. 1.3. As the diagrams are structurally similar to the scalar ones, c.f. Fig. 1.1, the n-th diagram has n free gauge boson propagators and n scalar-gauge vertices, each connected to two external legs of ϕ. Hence, the n vertices (including the external legs) contribute

$$\left(ie^2\phi^2\eta^{\mu\nu}\right)^n \ , \tag{1.56}$$

while the n propagators contribution can be expressed as

$$\left(p^2 + i\epsilon\right)^{-n} \left(-i\Delta_{\mu\nu}\right)^n \ . \tag{1.57}$$

Here $\Delta_{\mu\nu}$ denotes the projector with the properties

$$\Delta_{\mu\nu} = \left(\eta_{\mu\nu} - \frac{p_\mu p_\nu}{p^2}\right), \qquad (\Delta_{\mu\nu})^n = \Delta_{\mu\nu}, \qquad \Delta^\mu_\mu = Tr\left[\Delta\right] = d - 1 \ , \tag{1.58}$$

where d is the number of space-time dimensions. Collecting the results above and accounting for the overall symmetry factor of $\frac{1}{2n}$, the one-loop gauge boson contri-

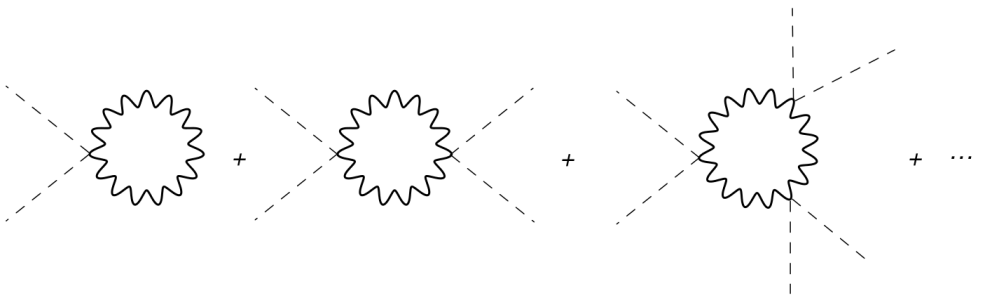

Figure 1.3: The 1PI Feynman graphs that contribute to the one-loop effective potential, given by the Lagrangian in Eq. (1.53).

bution $V_{\text{A}}^{(1)}$ to the effective action is given by

$$V_{\text{A}}^{(1)}(\phi) = \frac{1}{2}\int \frac{\mathrm{d}^4 p}{(2\pi)^4}(d-1)\ln\left[p^2 + m_A^2(\phi)\right] \ , \tag{1.59}$$

having already executed the summation, performed Wick-rotation, used Eq. (1.54) to express it in terms of the field dependent gauge boson mass $m_A^2(\phi)$ and finally dropped field independent terms. Solving the integral via dimensional regularization and $\overline{\text{MS}}$ renormalization, the result is altered by the dimension-dependent factor $(d-1) = (3-\epsilon)$, to finally be

$$V_{\text{A}}^{(1)}(\phi) = \frac{3}{64\pi^2} m_A^4(\phi)\left(\ln\left[\frac{m_A^2(\phi)}{\bar{\mu}^2}\right] - \frac{5}{6}\right) \ . \tag{1.60}$$

While the factor of $n_i = 3$ in front counts the gauge boson's degrees of freedom and is therefore physical, the term $\left(-\frac{5}{6}\right)$ is renormalization scheme dependent and can be arbitrarily altered through redefinition of the technical subtraction (renormalization) scale $\bar{\mu}$, which has mass dimension one. While the form of the one-loop effective potential depends on the regularization method, renormalization scheme and the definition of $\bar{\mu}$, the described physics does not. Hence, one should be careful to use them consistently throughout the calculation of the one-loop effective potential. Furthermore, we see that the result in Eq. (1.60) agrees with Eq. (1.36) and Eq. (1.37). Hence, the general formula in Eq. (1.36) and Eq. (1.37) can be used to derive the one-loop effective potential for an arbitrary particle content with spins 0, $\frac{1}{2}$ and 1.

2 Spontaneous symmetry breaking of conformal symmetry

As we now have established a method to compute the one-loop effective potential for general particle contents of the underlying theory, c.f. Eqs. (1.36) and (1.37), we can now look at the properties of radiatively-induced spontaneous symmetry breaking (RSSB), which corresponds to an analysis of minima of the effective potential. In other words, we analyze the situation, where the quantum one-loop contributions are strong enough (compared to tree-level contributions) such that non-trivial vacua are generated.

In the following we examine examples of the simplest conformal theories to illustrate the underlying Coleman-Weinberg mechanism, compare it to the Gildener-Weinberg approach and comment on stability and applicability. At first we consider the massless ϕ^4 theory in Section 2.1, then massless scalar QED (quantum electro dynamics) in Section 2.2, both originally studied in Ref. [6]. Conformal symmetry requests the theory to only contain scales with vanishing mass dimension, i.e. scale-invariant equations. Since no external scales are present, relevant scales are generated intrinsically by the theory through, e.g. spontaneous symmetry breaking of said conformal symmetry. Thus, conformal extensions of the standard model are particularly interesting in attempting to solve the electroweak hierarchy problem.

Because the tree-level mass term of the Higgs boson is omitted there is no need for fine-tuning it to its quantum corrections. The experimentally observed non-trivial vacuum expectation value of the Higgs field is then dynamically generated by the quantum corrections spontaneously breaking the conformal symmetry.

2.1 Massless ϕ^4 theory

Considering one massless scalar in ϕ^4 theory, its Lagrangian is simply given by Eqs. (1.38) and (1.39) but with tree-level mass equal to zero ($m^2 = 0$), such that the field dependent mass becomes $m^2(\phi) = \frac{1}{2}\lambda\phi^2$. Hence, the one-loop effective potential, calculated via Eqs. (1.36) and (1.37), is given by

$$V_{\text{eff}}(\phi;\bar{\mu}) = V^{(0)}(\phi;\bar{\mu}) \quad + \quad V^{(1)}(\phi;\bar{\mu}) \;, \tag{2.1a}$$

$$= \frac{1}{4!}\lambda\phi^4 + \frac{\lambda^2\phi^4}{256\pi^2}\left(\ln\left[\frac{\lambda\phi^2}{2\bar{\mu}^2}\right] - \frac{3}{2}\right) \;, \tag{2.1b}$$

where we added $\bar{\mu}$ as a separated argument to emphasize the fact that apart from the explicit, there is also an implicit dependency on $\bar{\mu}$, since the coupling depends on the scale of evaluation (also subtraction or running scale) $\lambda \equiv \lambda(\bar{\mu})$. Through renormalization, the coupling λ is fixed at the renormalization scale Λ, which is then called the *bare* coupling $\lambda(\Lambda) = \lambda_0$, while its value at any given scale is determined by renormalization group running (RG running), i.e. its β-function

$$\beta_\lambda(\lambda(\bar{\mu})) = \bar{\mu}\frac{\partial\lambda(\bar{\mu})}{\partial\bar{\mu}} = \frac{\partial\lambda(\bar{\mu})}{\partial\ln\bar{\mu}} \;. \tag{2.2}$$

Enforcing that physical observerables should be independent of the chosen scale, one can use the renormalization group equation (here given in a general form)

$$\left(\bar{\mu}\frac{\partial}{\partial\bar{\mu}} - \gamma_i\phi_i\frac{\partial}{\partial\phi_i} + \beta_i\frac{\partial}{\partial\lambda_i}\right)V_{\text{eff}}(\phi;\bar{\mu}) = 0 \;, \tag{2.3}$$

with γ_i being the fields anomalous dimension, to aquire the RG-improved potential, which only depends on *bare* quantities and the field ϕ. We leave the renormalization group running of couplings to be discussed in more detail later in the analysis of non-trivial vacua.

Furthermore, looking at Eq. (2.1) we see, that the one-loop effective potential becomes singular at the origin of classical field space ($\phi = 0$), which is a consequence of the infrared divergences of the diagrams used to calculate said potential. Using the condition in Eq. (1.31) to derive the ground state of the theory, respectively the vacuum expectation value of ϕ, we arrive at

$$\frac{\partial V_{\text{eff}}(\phi;\bar{\mu})}{\partial\phi} = \phi^3\left\{\frac{\lambda}{6} + \frac{\lambda^2}{64\pi^2}\left(\ln\left[\frac{\lambda\phi^2}{2\bar{\mu}^2}\right] - 1\right)\right\} \stackrel{!}{=} 0 \;, \tag{2.4a}$$

$$\overset{\phi\neq 0}{\Leftrightarrow} \qquad \left\{\frac{\lambda}{6} + \frac{\lambda^2}{64\pi^2}\left(\ln\left[\frac{\lambda\phi^2}{2\bar{\mu}^2}\right] - 1\right)\right\} \stackrel{!}{=} 0 \;. \tag{2.4b}$$

Here we nicely see, that for the generation of non-trivial minima ($\phi \neq 0$), the

one-loop contribution (on the right) has to be of comparable size to the tree-level contribution (on the left). The non-trivial minimum is then determined by

$$\lambda \ln\left[\frac{\lambda\phi^2}{2\bar{\mu}^2}\right] = -\frac{32\pi^2}{3} + \lambda \,. \tag{2.5}$$

From the minimum condition in Eq. (2.5) we see, that for the quantum corrections to shift the minimum away from the origin, either λ or the absolute value of $\lambda \ln\left[m^2(\phi)/\bar{\mu}\right]$ has to be large. This takes us out of the region of the one-loop approximation's applicability, as higher orders in the loop-expansion bring contributions of higher powers in $\lambda \ln\left[m^2(\phi)/\bar{\mu}\right]$ and λ. This leads to the conclusion, that the full effective potential is necessary to analyze the vacuum structure of massless ϕ^4 theory, while the one-loop approximation is not appropriate, as already pointed out in the original work, Ref. [6]. However, this is not the case for conformal symmetric theories in general, but it reminds us to think about the range of applicability in the analysis of further models with more extended particle content. Therefore, in the following section Section 2.2, we investigate the simplest extension of massless ϕ^4 theory, i.e. (massless) scalar quantum electrodynamics (scalar QED).

2.2 Scalar quantum electrodynamics

To analyze massless scalar quantum electrodynamics (scalar QED), we consider a complex scalar $\Phi = \frac{1}{\sqrt{2}}(\phi_1 + i\phi_2)$ with self-coupling λ that is coupled to a $U(1)$ gauge group via the coupling g and with charge $Q(\Phi) = q = 1$. Hence, the part of the Lagrange density necessary for the calculation of the one-loop effective potential contributions is given by

$$\mathcal{L} \supseteq \left(D_\mu \Phi\right)^\dagger \left(D^\mu \Phi\right) - V^{(0)}(\Phi) \,, \tag{2.6}$$

with the tree-level potential

$$V^{(0)}(\Phi) = \lambda \left(\Phi^\dagger \Phi\right)^2 \,. \tag{2.7}$$

As the complex scalar contains one real and one imaginary degree of freedom, we can choose without loss of generality that only the real degree of freedom, in this case ϕ_1, acquires a non-zero VEV

$$\phi_1 \to \phi_1 + \phi, \qquad \phi_2 \to \phi_2 \,. \tag{2.8}$$

Effectively this is a gauge choice and is equivalent to enforcing CP conservation in our model, since we choose a system in which only the CP even, i.e. the real degree of freedom, contributes to the effective potential. Hence, ϕ is the classical (background) field on which the effective potential depends, such that the three field (ϕ) dependent masses are given by

$$m^2_{\phi_1}(\phi) = 3\lambda\phi^2, \qquad m^2_{\phi_2}(\phi) = \lambda\phi^2, \qquad m^2_A(\phi) = g^2\phi^2 \,. \tag{2.9}$$

Note here that $m_A^2(\phi)$ is given in Landau gauge, such that with the methods displayed in Sections 1.2 and 1.4 the one-loop effective potential is calculated to be

$$V_{\text{eff}}(\phi;\bar{\mu}) = V^{(0)}(\phi;\bar{\mu}) \quad + \quad V^{(1)}(\phi;\bar{\mu}) \;, \tag{2.10a}$$

$$= \frac{1}{4}\lambda\phi^4 + \frac{\phi^4}{64\pi^2}\left(9\lambda^2 \ln\left[\frac{3\lambda\phi^2}{\bar{\mu}^2}\right] + \lambda^2 \ln\left[\frac{\lambda\phi^2}{\bar{\mu}^2}\right] - 15\lambda^2 \right.$$
$$\left. +3g^4 \ln\left[\frac{g^2\phi^2}{\bar{\mu}^2}\right] - \frac{5}{2}g^4\right) \;, \tag{2.10b}$$

where the separately displayed dependency on $\bar{\mu}$ reminds us that apart from the explicit $\bar{\mu}$-terms, also the quartic coupling $\lambda \equiv \lambda(\bar{\mu})$ and the gauge coupling $g = g(\bar{\mu})$ depend on the subtraction scale through the renormalization group. Similar to Section 2.1, the one-loop effective potential has a non-trivial minimum at $\langle\phi\rangle = \phi_0 \neq 0$, whereas now there is an additional λ-independent contribution $g^4 \ln m_A^2(\phi)$ for the one-loop contribution to balance out the tree-level contribution. Thus, the non-trivial vacuum can be in the regime of applicability of this theory. Investigating the vacuum structure of scalar QED, we use the stationary condition from Eq. (1.31) and arrive at

$$\frac{\partial V_{\text{eff}}(\phi;\bar{\mu})}{\partial\phi} = \phi^3\left\{\lambda + \frac{1}{16\pi^2}\left(9\lambda^2 \ln\left[\frac{3\lambda\phi^2}{\bar{\mu}^2}\right] + \lambda^2 \ln\left[\frac{\lambda\phi^2}{\bar{\mu}^2}\right] - 10\lambda^2 \right.\right.$$
$$\left.\left. +3g^4 \ln\left[\frac{g^2\phi^2}{\bar{\mu}^2}\right] - g^4\right)\right\} \stackrel{!}{=} 0 \;. \tag{2.11}$$

To simplify the calculation, we use that the value of the subtraction scale $\bar{\mu}$ is arbitrary for physical observables and set it to $\bar{\mu} = \phi_{\text{crit}}$. This is the value the classical field ϕ acquires at the minimum, i.e. when Eq. (2.11) is fulfilled. Following the argument of Section 2.1, we know that both λ and $\lambda \ln m_i^2(\phi)$ have to be small to stay in the region of applicability of our theory. Hence, we can omit the corresponding $\mathcal{O}(\lambda^2)$ one-loop terms, which are subleading with respect to terms of $\mathcal{O}(\lambda)$. Therefore, we rewrite Eq. (2.11) to be

$$\lambda + \frac{3g^4}{16\pi^2}\left(\ln\left[g^2\right] - \frac{1}{3}\right) \stackrel{!}{=} 0 \;. \tag{2.12}$$

We observe, that a non-trivial minimum is generated by one-loop quantum corrections, if the quartic coupling λ and the gauge coupling g^4 are of comparable size (up to the usual loop-suppression factor) $\lambda \simeq \frac{1}{16\pi^2} g^4 \ln[g^2]$. Therefore, one-loop contributions of the same order as the tree-level potential do not violate any assumptions or loop-expansion conditions, and thus lie in the region of applicability of this theory. Here it is important to note that both the quartic as well as the gauge coupling in Eq. (2.12) are evaluated at the scale ϕ_{crit}

$$\lambda = \lambda(\bar{\mu} = \phi_{\text{crit}}) = \lambda_{\text{crit}}, \qquad g = g(\bar{\mu} = \phi_{\text{crit}}) = g_{\text{crit}} \;. \tag{2.13}$$

Consequently the condition of Eq. (2.12) is not a renormalization group invariant statement. This leads to a self-consistent definition of the classical field's VEV ϕ_0, i.e. the scale $\bar{\mu} = \phi_0$ at which the couplings of the theory fulfill the criticality condition Eq. (2.12) and thus marking the transition from the unbroken conformal symmetric phase to the non-trivial vacuum of the broken phase. The actual value of ϕ_{crit} is determined by the renormalization group running of g and λ, which is given by their β-functions. In the case of scalar QED, one can solve analytically for $(\lambda(\bar{\mu}), g(\bar{\mu}))$ and show that there always exists a scale ϕ_{crit} that satisfies Eq. (2.12), if the couplings λ and g are small ($< \mathcal{O}(1)$). This is shown, e.g. in Ref. [34].

Furthermore, with the relation between λ_{crit} and g_{crit} in Eq. (2.12), we can express the one-loop effective potential in terms of $(g_{\text{crit}}, \phi_{\text{crit}})$ instead of $(\lambda(\bar{\mu}), g(\bar{\mu}))$, effectively gaining a parameter with mass dimension one. This feature of SSB in massless theories is called *dimensional transmutation*, see Ref. [6]. It is a result of the fact that the numerical value of the dimensionless couplings depends on the (arbitrary) renormalizion scale. As the criticality condition in Eq. (2.12) is a self-consistent calculation, where a quantity is determined by its individual tree- and one-loop contributions it can be understood as a *gap-equation* similar to the one from the Nambu-Jona-Lasinio (NJL) model. Similarly, Eq. (2.12) gives a condition for the running couplings λ and g, that determines the scale at which their amplitude induces SSB similar to the theory of quantum chromodynamics (QCD), where the *gap-equation* also describes the dynamically induced masses dependent on the coupling α, c.f. Ref. [35]. Using Eq. (2.12) to express λ in Eq. (2.10) in terms of the gauge coupling g, effectively reorganizing the loop-expansion in terms of g^4 instead of λ. The one-loop effective potential then takes the form

$$V_{\text{eff}}(\phi) = \frac{3 g_{\text{crit}}^4 \phi^4}{64\pi^2} \left(\ln\left[\frac{\phi^2}{\phi_{\text{crit}}^2} \right] - \frac{1}{2} \right) + \mathcal{O}(g^8) \,, \tag{2.14}$$

where we only displayed the terms of leading order in the expansion and dropped sub-leading terms of $\mathcal{O}(g^8)$.The one-loop effective potential $V_{\text{eff}}(\phi)$ and the tree-level potential $V^{(0)}(\phi)$ are displayed in Fig. 2.1. There it can be nicely seen, how one-loop contributions induce non-trivial minima. The RSSB induced mass of the classical scalar field ϕ is then given by the second derivative of the effective potential evaluated at the minimum

$$m_\phi^2 = \left. \frac{\partial^2 V_{\text{eff}}}{\partial \phi^2} \right|_{\phi = \phi_{\text{crit}}} = \frac{3}{8\pi^2} g_{\text{crit}}^4 \phi_{\text{crit}}^2 > 0 \,, \tag{2.15}$$

which verifies that the stationary point calculated in Eq. (2.12) is indeed a local minimum of the effective potential. The gauge (vector) boson acquires the mass $m_A^2 = m_A^2(\phi = \phi_{\text{crit}}) = g^2 \phi_{\text{crit}}^2$, such that the mass ratio between the two fields is calculated to be

$$\frac{m_\phi^2}{m_A^2} = \frac{3 g_{\text{crit}}^2}{8\pi^2} \,. \tag{2.16}$$

This result is only valid at leading order in our approximations and has corrections of higher order in g, which are not expected to change the vacuum structure, i.e. that

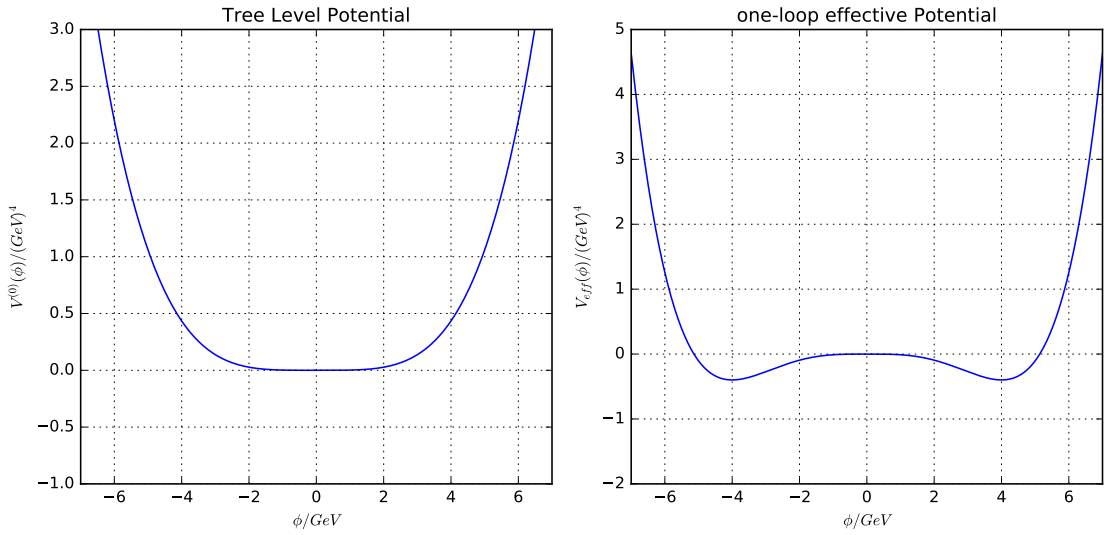

Figure 2.1: The tree-level (left) and one-loop effective potential (right), given respectively by Eq. (2.10) and Eq. (2.14), with exemplary values for $\phi_{\text{crit}} = 4\,\text{GeV}$, $g_{\text{crit}} = 0.9$ and using the criticality condition Eq. (2.12) to calculate $\lambda = \lambda_{\text{crit}} \simeq 0.006781$.

ϕ_{crit} is still the value of the field at which the effective potential has a global minimum. To be more precise, the local minimum at ϕ_{crit} is always lower than any occurring local minimum at $\phi = 0$, whereas our expansion approach is not reliable for large logarithms and hence large ϕ or field values close to the origin. As the effective potential and the above discussed corresponding results are still RG-dependent, in Ref. [6] RG-improvement was used to show that indeed ϕ_{crit} is a global minimum of Eq. (2.10) for all ϕ.

Summing up the case of RSSB in scalar QED, we saw that quantum corrections of magnitude comparable to the tree-level contribution induce a minimum away from the origin, while being still in the range of applicability of the expansion. We arrived at a *gap-equation*, c.f. Eq. (2.12), that introduced us to the feature dimensional transmutation (or transportation). We started with a description with two dimensionless quantities and obtained an equivalent description with one dimensionless and quantity of mass dimension one. Furthermore, and arguably most importantly, the *gap-equation* allows for a self-consistent calculation of the scale at which SSB takes place on the condition that the RG-running of the couplings is known. A more detailed analysis on the scale of SSB depending on renormalized couplings and RG-running is discussed in Section 3.4.

3 Approach for the analysis of RSSB

To further analyze RSSB in theories with a more complex particle content, we introduce a general approach with a minimal amount of quantities that depend on specific models, making it easier to arrive at comparable statements. With this we expect to see the underlying fundamentals of general Coleman-Weinberg symmetry

breaking, by probing and categorizing effects of increasingly complex models. The first step, including a gauge symmetry for a single scalar, was already done in Section 2.2 with the analysis of massless scalar QED and showed us that the quantum one-loop contribution of the gauge boson can generate a non-trivial minimum in the range of applicability of our expansion. In other words, while a massless scalar cannot break conformal symmetry spontaneously on its own, coupling it to a gauge group allows for SSB in the perturbative regime and hence a vacuum at a non-zero field value. Therefore, in Section 3.1 we derive a formalism that describes the contribution of n scalar fields in generalized spherical coordinates, leading to general criticality equations and one-loop vacuum stability conditions. In Section 3.2, we comment on scale-setting in the context of the aforementioned general formalism. Following this, in Section 3.3 we introduce a numerical approach for the calculation of the non-trivial vacuum in dependence on couplings, that are renormalized at high energy (Planck-) scale. In Section 3.4 use this formalism to further investigate the properties of scale-setting, i.e. the critical scale ϕ_{crit}, in massless scalar quantum electrodynamics (scalar QED).

3.1 General formalism of SSB in classically scale-invariant models

With the derivation laid out throughout Section 1, the zero-temperature one-loop effective potential of a theory with n real scalar degrees of freedom $\phi_1, \dots, \phi_n$ is given by

$$V_{\text{eff}}(\phi_1, \dots, \phi_n; \bar{\mu}) = V^{(0)}(\phi_1, \dots, \phi_n; \bar{\mu}) + V^{(1)}(\phi_1, \dots, \phi_n; \bar{\mu}) \,, \tag{3.1}$$

where we again noted the indirect $\bar{\mu}$ dependence of the Lagrangian parameters of the model by including it in the argument. Introducing the generalized spherical coordinates according to Ref. [36](pp. 593-595) with the radial coordinate φ and $n-1$ angular coordinates $\vartheta_1, \dots, \vartheta_{n-1}$, where ϑ_{n-1} ranges over the interval $[0, 2\pi]$ while the other angles $\vartheta_1, \dots, \vartheta_{n-2}$ range over $[0, \pi]$, we can reparameterize the n fields by

$$\begin{aligned}
\phi_1 &= \varphi \ \cos\vartheta_1 \\
\phi_2 &= \varphi \ \sin\vartheta_1 \ \cos\vartheta_2 \\
\phi_3 &= \varphi \ \sin\vartheta_1 \ \sin\vartheta_2 \ \cos\vartheta_3 \\
&\vdots \\
\phi_{n-1} &= \varphi \ \sin\vartheta_1 \cdots \sin\vartheta_{n-2} \ \cos\vartheta_{n-1} \\
\phi_n &= \varphi \ \sin\vartheta_1 \cdots \sin\vartheta_{n-2} \ \sin\vartheta_{n-1} \,,
\end{aligned} \tag{3.2}$$

where the radial coordinate φ has mass dimension one, whereas the angular coordinates ϑ_i with $i = 1, \dots, n-1$ each have mass dimension zero. With this we can rewrite the one-loop effective potential in generalized spherical coordinates to be

$$V_{\text{eff}}(\phi_1, \dots, \phi_n; \bar{\mu}) = \hat{V}_{\text{eff}}(\varphi, \vartheta_1, \dots, \vartheta_{n-1}; \bar{\mu}) = \hat{V}_{\text{eff}}(\varphi, \vec{\vartheta}; \bar{\mu}) \,, \tag{3.3}$$

where the $(n-1)$-component vector $\vec{\vartheta}$ contains all angular coordinates. Considering that we investigate *classically scale-invariant* (conformal symmetric) models, we can make the following statement about the φ dependency of the effective potential

$$\hat{V}^{(0)}(\varphi,\vec{\vartheta};\bar{\mu}) \propto \varphi^4 \ , \ \hat{V}^{(1)}(\varphi,\vec{\vartheta};\bar{\mu}) \propto \varphi^4 \ . \tag{3.4}$$

Indeed, this is just the result of a general dimensional argument that classically conformal models do not contain any Lagrangian parameters (couplings) with non-zero mass dimension. Since φ is the only mass scale, all objects with mass dimension n are proportional to φ^n. Isolating the φ dependecy of $\hat{V}^{(0)}$, the tree-level contribution can generally be rewritten to be

$$\hat{V}^{(0)}(\varphi,\vec{\vartheta};\bar{\mu}) = \frac{1}{N}\kappa(\vec{\vartheta};\bar{\mu})\ \varphi^4 \ , \tag{3.5}$$

where N is the normalization of the tree-level potential and κ is a function only explicitly depending on angular coordinates and implicitly depending on $\bar{\mu}$ through the RG-running of the dimensionless Lagrangian parameters (couplings) of the theory. However, the general φ dependence of the one-loop contributions is not derived as easily, because their explicit form depends on the regularization method and renormalization scheme. Therefore, we choose to investigate one-loop contributions as given in Eq. (1.36), which are calculated using dimensional regularization and the $\overline{\text{MS}}$ renormalization scheme. In the absence of mass terms in the Lagrangian, the field dependent masses m_i^2 have the property that the dependence on the radial component φ and the angular components $\vec{\vartheta}$ can be factorized

$$m_i^2(\varphi,\vec{\vartheta};\bar{\mu}) = \hat{m}_i^2(\vec{\vartheta};\bar{\mu})\ \varphi^2 \ , \tag{3.6}$$

where both the dependence on all angular variables, as well as the implicit $\bar{\mu}$ dependency via the couplings is stored in $\hat{m}_i^2$. With Eq. (3.6), we can rewrite the general one-loop contribution $V^{(1)}(\varphi,\vec{\vartheta};\bar{\mu})$ from Eq. (1.36) as

$$\begin{aligned}\hat{V}^{(1)}(\varphi,\vec{\vartheta};\bar{\mu}) &= \frac{1}{64\pi^2}\sum_i (-1)^{2s_i}\, n_i\, m_i^4(\varphi,\vec{\vartheta};\bar{\mu}) \left(\ln\left[\frac{m_i^2(\varphi,\vec{\vartheta};\bar{\mu})}{\bar{\mu}^2}\right] - c_i\right) \ , \\ &= \frac{1}{64\pi^2}\sum_i (-1)^{2s_i}\, n_i\, \varphi^4\, \hat{m}_i^4(\vec{\vartheta};\bar{\mu}) \left(\ln\left[\frac{\hat{m}_i^2(\vec{\vartheta};\bar{\mu})\,\varphi^2}{\bar{\mu}^2}\right] - c_i\right) \ . \end{aligned} \tag{3.7}$$

Now expanding the logarithm into a sum of logarithms, we can isolate the logarithmic dependency on φ^2 and factor out the tree-level normalization N. This results in

$$\begin{aligned}\hat{V}^{(1)}(\varphi,\vec{\vartheta};\bar{\mu}) &= \left\{\frac{1}{64\pi^2}\sum_i (-1)^{2s_i}\, n_i \hat{m}_i^4(\vec{\vartheta};\bar{\mu}) \left(\ln\left[\hat{m}_i^2(\vec{\vartheta};\bar{\mu})\right] - c_i + \ln\left[\frac{\varphi^2}{\bar{\mu}^2}\right]\right)\right\}\varphi^4 \ , \\ &= \frac{1}{N}\left\{A(\vec{\vartheta};\bar{\mu}) + B(\vec{\vartheta};\bar{\mu})\ln\left[\frac{\varphi^2}{\bar{\mu}^2}\right]\right\}\varphi^4 \ , \end{aligned} \tag{3.8a}$$

where $A(\vec{\vartheta};\bar{\mu})$ and $B(\vec{\vartheta};\bar{\mu})$ are functions of the $\bar{\mu}$-dependent couplings and the angular coordinates $\vec{\vartheta}$, defined as

$$A(\vec{\vartheta};\bar{\mu}) = \frac{N}{64\pi^2}\sum_i (-1)^{2s_i}\, n_i \hat{m}_i^4(\vec{\vartheta};\bar{\mu}) \left(\ln\left[\hat{m}_i^2(\vec{\vartheta};\bar{\mu})\right] - c_i\right) , \tag{3.9a}$$

$$B(\vec{\vartheta};\bar{\mu}) = \frac{N}{64\pi^2}\sum_i (-1)^{2s_i}\, n_i \hat{m}_i^4(\vec{\vartheta};\bar{\mu}) . \tag{3.9b}$$

In analogy to Section 2.2, let us now assume that the minimum of $\hat{V}_{\text{eff}}$ is of non-trivial nature which in spherical coordinates translates to it being located at radial distance φ_0 away from the origin $\varphi > 0$ and of an arbitrary angle $\vec{\vartheta}_0$. Thus, it is convenient to fix the (generally arbitrary) subtraction scale $\bar{\mu}$ at

$$\bar{\mu} = \varphi_{\text{crit}} \equiv \varphi_0 . \tag{3.10}$$

With this choice and using the results from Eq. (3.5) and Eq. (3.8), we separate radial and angular dependencies as best we can, such that the one-loop effective potential of Eq. (3.3) can be written as

$$\hat{V}_{\text{eff}}(\varphi,\vec{\vartheta};\varphi_0) = \frac{1}{N}\left\{\kappa(\vec{\vartheta};\varphi_0) + A(\vec{\vartheta};\varphi_0) + B(\vec{\vartheta};\varphi_0)\ln\left[\frac{\varphi^2}{\varphi_0}\right]\right\}\varphi^4 , \tag{3.11}$$

where the dependency on the angular coordinates is isolated in the quantities κ, A and B, whereas we are left with a logarithmic φ^2 and an overall φ^4 dependency. Now following the condition for a stationary point from Eq. (1.31) the vacuum state $(\varphi_0,\vec{\vartheta}_0)$ must be determined in a self-consistent way by simultaneously solving the set of n stationary (also criticality or gap-) equations

$$\frac{\partial}{\partial\varphi}\hat{V}_{\text{eff}}(\varphi,\vec{\vartheta};\varphi_0)\Big|_{\text{vac}} \overset{(3.11)}{=} \kappa(\vec{\vartheta}_0;\varphi_0) + A(\vec{\vartheta}_0;\varphi_0) + \frac{1}{2}B(\vec{\vartheta}_0;\varphi_0) \overset{!}{=} 0 , \tag{3.12a}$$

$$\vec{\nabla}_\vartheta \hat{V}_{\text{eff}}(\varphi,\vec{\vartheta};\varphi_0)\Big|_{\text{vac}} \overset{(3.11)}{=} \vec{\nabla}_\vartheta \left[\kappa(\vec{\vartheta};\varphi_0) + A(\vec{\vartheta};\varphi_0)\right]_{\vec{\vartheta}=\vec{\vartheta}_0} \overset{!}{=} 0 , \tag{3.12b}$$

where "vac" denotes evaluation at the above mentioned non-trivial vacuum state $(\varphi=\varphi_0,\ \vec{\vartheta}=\vec{\vartheta}_0)$ and $\vec{\nabla}_\vartheta$ is the $(n-1)$ dimensional angular gradient $\vec{\nabla}_\vartheta \equiv \partial/\partial\vec{\vartheta} = (\partial/\partial\vartheta_1,\ldots,\partial/\partial\vartheta_{n-1})^\intercal$ resulting in $(n-1)$ angular stationary equations. Having solved the stationary equations for the vacuum $(\varphi_0,\vec{\vartheta}_0)$ we can simply transform back into regular field space (ϕ_i with $i=1,\ldots,n$), calculating the vacuum expectation values $\phi_{i,\text{crit}}$ of the field (also often called v_i) via Eq. (3.2). Verifying that the calculated stationary point is indeed a local minimum and therefore a viable vacuum state, the Hessian matrix of the effective potential $\text{Hess}(\hat{V}_{\text{eff}})$ with respect to $(\varphi,\vec{\vartheta})$, evaluated at $(\varphi_0,\vec{\vartheta}_0)$ has to be positive definite. Given the general expression for the one-loop effective potential in conformal symmetric models, c.f. Eq. (3.11), its

Hessian at $(\varphi_0, \vec{\vartheta}_0)$ can be written as

$$\mathrm{Hess}(\hat{V}_{\mathrm{eff}})(\varphi_0, \vec{\vartheta}_0; \varphi_0) = \begin{pmatrix} 2\varphi_0^2 B(\vec{\vartheta}_0; \varphi_0) & \frac{\varphi_0^3}{2}\left[\vec{\nabla}_\vartheta B(\vec{\vartheta}; \varphi_0)\right]^\intercal_{\vec{\vartheta}=\vec{\vartheta}_0} \\ \frac{\varphi_0^3}{2}\left[\vec{\nabla}_\vartheta B(\vec{\vartheta}; \varphi_0)\right]_{\vec{\vartheta}=\vec{\vartheta}_0} & \frac{\varphi_0^4}{4}\left[\frac{\partial^2\left(\kappa(\vec{\vartheta};\varphi_0)+A(\vec{\vartheta};\varphi_0)\right)}{\partial\vartheta_i\partial\vartheta_j}\right]_{\vec{\vartheta}=\vec{\vartheta}_0} \end{pmatrix} , \tag{3.13}$$

with the $(n-1)$-dimensional vector $\vec{\vartheta}$, the 2×2 block matrix above represents a $n \times n$ matrix, where the indices i and j range over $i, j = 1, \ldots, n-1$. Since partial derivatives on smooth functions are interchangeable, the Hessian is symmetric by definition. Thus the stability condition of positive definiteness reduces to the statement about the determinant

$$\det h_k > 0 \quad \forall k \in \{1, \ldots, n\} \ , \tag{3.14}$$

where h_k is the upper left $k \times k$ submatrix of $\mathrm{Hess}(\hat{V}_{\mathrm{eff}})(\varphi_0, \vec{\vartheta}_0; \varphi_0)$. From a computational point of view, it is a problem that the elements of the Hessian matrix in Eq. (3.13) contain different powers of φ_0. However, it turns out that all terms in calculating determinants contain the same powers of φ_0 so that it can be factored out in the end. The explanatory calculation is shown in Appendix A.1. Consequentially, the condition to verify that the stationary point found with Eq. (3.12) is actually a minimum is also the condition for one-loop vacuum stability and remains the same as in Eq. (3.14), however h_k is now the $k \times k$ submatrix of $\mathrm{H}(\vec{\vartheta}_0; \varphi_0)$

$$\mathrm{H}(\vec{\vartheta}_0; \varphi_0) = \begin{pmatrix} 2B(\vec{\vartheta}_0; \varphi_0) & \frac{1}{2}\left[\vec{\nabla}_\vartheta B(\vec{\vartheta}; \varphi_0)\right]^\intercal_{\vec{\vartheta}=\vec{\vartheta}_0} \\ \frac{1}{2}\left[\vec{\nabla}_\vartheta B(\vec{\vartheta}; \varphi_0)\right]_{\vec{\vartheta}=\vec{\vartheta}_0} & \frac{1}{4}\left[\frac{\partial^2\left(\kappa(\vec{\vartheta};\varphi_0)+A(\vec{\vartheta};\varphi_0)\right)}{\partial\vartheta_i\partial\vartheta_j}\right]_{\vec{\vartheta}=\vec{\vartheta}_0} \end{pmatrix} . \tag{3.15}$$

From the simplest $k = 1$ case, it follows that $B(\vec{\vartheta}_0; \varphi_0) > 0$ is a necessary condition for one-loop vacuum stability. Considering the structure of $B(\vec{\vartheta}_0; \varphi_0)$, as given in Eq. (3.9b), the tree-level mass contributions of the fermion fields at the minimum $(\varphi_0, \vec{\vartheta}_0)$ have to be smaller than the minimum tree-level contributions of scalar and boson fields combined. At this point we can calculate the vacuum from the criticality equations and verify its stability, i.e. it being not only a stationary point of the effective potential, but a local minimum. To ensure that the minimum is also a global one we need to compare it to the effective potential value at the origin, since all non-trivial vacua in range of applicability come out as solutions to our criticality conditions. We can easily see that the effective potential at the vacuum of $(\varphi_0, \vec{\vartheta}_0)$ is in fact lower than any local minimum that might occur at the origin $(\varphi = 0, \vec{\vartheta} = \vec{0})$. Due to the overall φ^4 dependency, c.f. Eq. (3.11), the effective potential is zero at the origin $\hat{V}_{\mathrm{eff}}(0, \vec{0}) = 0$, while according to Eq. (3.12) the effective potential at $(\varphi_0, \vec{\vartheta}_0)$ is given by

$$\hat{V}_{\mathrm{eff}}(\varphi_0, \vec{\vartheta}_0; \varphi_0) = -\frac{1}{8} B(\vec{\vartheta}_0; \varphi_0)\ \varphi_0^4 < 0 \ . \tag{3.16}$$

Hence, after finding the non-trivial vacuum $(\varphi_0, \vec{\vartheta}_0)$ by solving the criticality conditions and verifying that it is indeed a local minimum of the one-loop effective potential via the Hessian determinant, we can conclude that it is also the global minimum in the range of applicability of our expansion, i.e. the perturbative regime of the theory.

3.2 Scale-setting

So far we have discussed the general form of the criticality equations and the verification that their solution in fact is the non-trivial minimum induced by SSB. In the following we give some comments on solving the stationary (criticality) conditions, their connection to the RG-running of the couplings $(\lambda_i(\bar{\mu}),\ g_i(\bar{\mu}),\ y_i(\bar{\mu}),\ \ldots)$ and therefore the process of scale-setting (i.e. dimensional transmutation) of Coleman-Weinberg symmetry breaking.

Starting off by solving the stationary equations in Eq. (3.12) we notice that they depend explicitly on $\vec{\vartheta}_0$ and implicitly on φ_0 (indicated by the semi-colon). This implicit dependency is due to both Eq. (3.12) not being RG-running invariant, thus φ_0 denotes the scale at which the couplings $(\lambda_i(\bar{\mu} = \varphi_0),\ g_i(\bar{\mu} = \varphi_0),\ y_i(\bar{\mu} = \varphi_0),\ \ldots)$ fulfill the criticality conditions with the angles $\vec{\vartheta}_0$. We deal with this by solving the couplings' set of β-functions, trading the general dependency of the parameter on the energy scale $\bar{\mu}$ against dependencies of initial values and the (energy-) range over which it is integrated. Hence, from here on all calculated numerical values of e.g. $(\varphi_0, \vec{\vartheta}_0)$ are be scheme dependent, while the physics of course are not. Keeping this in mind, there are generally two ways to look at the problem, the *bottom-up* and the *top-down* approach, which arise from the principles of *Effective Field Theory* (EFT). As there is no consistent unified theory (yet), all theoretical descriptions are only valid up to a specific scale (e.g. energy, length, frequency, ...), which in the case of RSSB via Coleman-Weinberg is somewhere between the maximal energy range from the scale of symmetry breaking φ_0 up to the Planck scale M_{Pl}. In terms of RSSB the *bottom-up* approach means renormalizing the theory at the scale of SSB (or condensation), i.e. ensuring the theory is finite by setting the initial values for the couplings at the critical scale $\lambda_{i,0} = \lambda_i(\bar{\mu} = \varphi_0)$, and evolving it to other energies using the RG-running of the couplings given by the corresponding β-functions. Using this approach to determine the upper bound, one must check that evolving the couplings does not violate the applicability conditions of the theory, the stability of the potential, the smallness of couplings (could run into Landau poles) and most importantly that φ_0 is the first instance to fulfill the criticality equations in Eq. (3.12) for any $\vec{\vartheta}_0$. In the *top-down* approach the theory is renormalized at the highest desired scale, i.e. the initial couplings are set at the Planck scale $\lambda_{i,0} = \lambda_i(\bar{\mu} = M_{\text{Pl}} = \bar{\mu}_{\text{Pl}})$. Evolving the theory to lower energies we still have to check for stability of the potential, the smallness of the couplings (now in the infrared (IR) energy regime) and for all n criticality conditions being fulfilled simultaneously. Therefore, the critical scale φ_0 is given by a "most attractive channel" argument, it is the highest scale at which the couplings satisfy the criticality conditions.

For our analysis of RSSB in conformal symmetric models we chose to use the *top-down* approach. Motivated by possible new high energy physics leaving us with

certain (general) values for the couplings at $\bar{\mu}_{\rm Pl}$, which we use to naturally determine at which lower scale the theory transitions from the unbroken, classically scale-invariant phase into the broken phase with masses. Whereas we do not expect new physics around the electroweak scale ($\bar{\mu}_{\rm EW} \approx 100\,\text{GeV}$), which could motivate renormalizing the theory at a lower scale. Furthermore, our main goal is to investigate the hierarchy problem of the exponential scale-separation between $\bar{\mu}_{\rm Pl}$ and the scale of electroweak symmetry breaking $\bar{\mu}_{\rm EW}$. Therefore, we probe whether there implicit conditions on the initial couplings at $\bar{\mu}_{\rm Pl}$ to arrive at critical scales φ_0 close to 100 GeV. Here it is important to note that the scale-separation between the renormalization scale at $\bar{\mu}_{\rm Pl}$ and the scale of electroweak symmetry breaking φ_0 does not result from any logarithms that are explicitly present in the one-loop contributions to the effective potential, c.f. Eq. (3.8), but it is a direct result from the logarithmic running of the coupling parameters. The RG-running of the couplings is determined by their corresponding β-function

$$\beta_{\lambda_i}(\lambda_i(\bar{\mu})) = \frac{\partial\lambda_i(\bar{\mu})}{\partial \ln \bar{\mu}} = \frac{\partial\lambda_i(t)}{\partial t}, \qquad \text{with } t = \ln\left[\frac{\bar{\mu}}{\text{GeV}}\right] . \tag{3.17}$$

As discussed before in Section 2.1, unlike the logarithms arising from RG-running, the logarithms from Eq. (3.8) are part of an expansion parameter and therefore have to be small to ensure applicability of the theory. Depending on the initial conditions, i.e. the renormalized couplings $(\lambda_{i,0},\ g_{i,0}, \ldots)$, a certain "time" of RG-running t_Δ is necessary for the couplings to fulfill the criticality conditions and induce SSB. With the definition for t above, c.f. Eq. (3.17), it follows that the separation (quotient) of critical φ_0 and high energy-scale $\bar{\mu}_{\rm Pl}$ depends exponentially on t_Δ

$$t_\Delta = t_{\rm Pl} - t_{\rm crit} = \ln\left[\frac{\bar{\mu}_{\rm Pl}}{\text{GeV}}\right] - \ln\left[\frac{\varphi_0}{\text{GeV}}\right] = \ln\left[\frac{\bar{\mu}_{\rm Pl}}{\varphi_0}\right] , \tag{3.18a}$$

$$\Leftrightarrow \qquad \frac{\bar{\mu}_{\rm Pl}}{\varphi_0} = e^{t_\Delta} . \tag{3.18b}$$

Furthermore, in Section 3.4 we give the exemplary calculation of scalar QED, that nicely shows how the logarithm provided by the β-function results directly in an exponential scale-separation between high energy $\bar{\mu}_{\rm Pl}$ and breaking scale φ_0.

In conclusion, using the *top-down* approach as described above, to locate the vacuum , which is determined by the scale (and angle) at which the couplings fulfill the criticality equations in Eq. (3.12), we set the renormalized couplings to rather general values (motivated by possible new physics at high energy) at the Planck scale and use β-functions of the couplings to finally determine the highest scale at which SSB can occur in a stable potential. This provides an intuitive formalism to determine scale and angle of radiatively induced symmetry breaking $(\varphi_0, \vec{\vartheta}_0)$ in conformal symmetric models. With respect to the critical scale φ_0 this means that just by renormalizing dimensionless couplings at the Planck scale, the dimensional transmutation feature of Coleman-Weinberg symmetry breaking provides us with the intrinsically preferred non-trivial vacuum scale that is naturally exponentially separated from the Planck scale.

3.3 Numerical determination of the vacuum

As we want to probe conformal symmetric multiscalar models as generally as possible, it is convenient to both solve the criticality and stability conditions as well as to integrate the β-functions numerically. This is sensible since the β-functions, c.f. Eq. (3.17), of the scalar content of the theory become hard to solve analytically if one does not make additional assumptions. Therefore, we choose to restrict our the precision of our analysis and hence its significance by numerical uncertainties that we have to assess throughout the calculation, instead of further assumptions on the scale-dependent, running couplings.

The β-functions have been calculated for most of the common classically conformal theories and can be found in publications, but as we might want to choose a different normalization in the Lagrangian or investigate more exotic models we use the Python script PyR@TE 2, c.f. Ref. [37], to calculate the corresponding β-functions. To calculate the scale dependent coupling functions $(\lambda_i(t), \ldots)$ we fix their initial values at an arbitrary high energy-scale which we choose to be the Planck scale (as motivated above)

$$\lambda_{i,0} = \lambda_i(t_{\text{Pl}}), \qquad \text{with } t_{\text{Pl}} = \ln\left[\frac{\bar{\mu}_{\text{Pl}}}{\text{GeV}}\right] = \ln\left[1.22 \cdot 10^{19}\right] \ . \tag{3.19}$$

Then we integrate their β-functions up to the electro-weak energy-scale $t_{\text{EW}} = \ln\left[\frac{\bar{\mu}_{\text{EW}}}{\text{GeV}}\right] = \ln[100]$ with respect to $t = \ln\left[\frac{\bar{\mu}}{\text{GeV}}\right]$ and as long as the model dependent tree-level stability conditions are fulfilled. We stop at the first scale where any of the tree-level stability conditions is violated, denoting it with t_{stab} and therefore ensure tree-level stability in all our following calculations. As a consequence we get individual interpolation functions for the couplings $\lambda_{\text{i}}(t)$ in the range $t \in [t_{\text{stab}}, t_{\text{Pl}}]$. Due to the $\lambda_i^2 \ln \lambda_i$ terms in the criticality equations, solving them simultaneously causes computational problems. Therefore, we instead calculate the minimum with respect to $\varphi_0 \in [t_{\text{stab}}, t_{\text{Pl}}]$ and $\vec{\vartheta}_0 \in \left[0, \frac{\pi}{2}\right]$ of the sum of squared criticality equations

$$\left(\kappa(\vec{\vartheta}_0;\varphi_0) + A(\vec{\vartheta}_0;\varphi_0) + \frac{1}{2}B(\vec{\vartheta}_0;\varphi_0)\right)^2 + \left(\vec{\nabla}_{\vartheta}\left[\kappa(\vec{\vartheta};\varphi_0) + A(\vec{\vartheta};\varphi_0)\right]_{\vec{\vartheta}=\vec{\vartheta}_0}\right)^2 , \tag{3.20a}$$

$$= \left(f_r(\vec{\vartheta}_0;\varphi_0)\right)^2 + \left(\vec{f}_a(\vec{\vartheta}_0;\varphi_0)\right)^2 , \tag{3.20b}$$

where $f_r(\vec{\vartheta}_0;\varphi_0)$ is the radial criticality equation from Eq. (3.12a) and $\vec{f}_a(\vec{\vartheta}_0;\varphi_0)$ denotes the $n-1$ angular stationary equations of Eq. (3.12b). Since the sum of squares is necessarily greater than 0, a minimum value equal to zero ensures that all terms of the sum are identically zero, hence all stationary conditions would be fulfilled simultaneously. We use the following criteria to check that the found minimum is indeed, up to numerical uncertainties, a zero contour of the criticality equations:

1. Smallness of the minimum: We apply a threshold (e.g. $\alpha^2 = 10^{-9}$) to the value of the squared criticality equations at the found minimum, ensuring that every individual term is numerically close to zero and hence the criticality equations

in Eq. (3.12) are fulfilled up to the numerically accuracy of $\mathcal{O}(\alpha)$.

2. One-loop vacuum stability: Since tree-level stability is already given by only looking for a minimum in the range $t \in [t_{\text{stab}}, t_{\text{Pl}}]$, we additionally check for one-loop stability of the vacuum by requiring the numerical vacuum to fulfill Eq. (3.14), where h denotes the upper left $k \times k$ submatrix of $H(\vec{\vartheta}_0; \varphi_0)$ as given in Eq. (3.15).

3. Leading term quotient: To fulfill the stationary equations there has to be significant cancellation between the individual terms in each stationary equation for it to be equal to zero. To make sure that the minimum of the squared equations is actually the "true" vacuum, and not just the case in which all individual terms of the stationary equations are small, e.g. due to small initial couplings (at the renormalization scale), we apply a threshold to the quotient of leading term of the criticality equations and the sum of squared equations. As $\kappa(\vec{\vartheta}_0; \varphi_0)$ is of $\mathcal{O}(\lambda_i)$, it can be identified as the leading term of both Eq. (3.12). Therefore we require the true vacuum to surpass the threshold

$$q = \frac{\kappa^2(\vec{\vartheta}_0; \varphi_0)}{\left(f_r(\vec{\vartheta}_0; \varphi_0)\right)^2 + \left(\vec{f}_a(\vec{\vartheta}_0; \varphi_0)\right)^2} > \text{ e.g. } 10^3 \,. \tag{3.21}$$

A minimum found to the sum of squared equations in Eq. (3.20a), that passes the three tests mentioned above, is considered the preferred vacuum of the theory for the given initial Lagrangian couplings $(\lambda_{i,0},\ g_{i,0},\ \ldots)$. To investigate the behavior of Coleman-Weinberg symmetry breaking these initial parameters are varied in different ways, e.g. all initial parameters are varied linearly over a certain interval, only two parameters are varied linearly while the others are held constant (gives better visualization options) or generating random independent initial values of different orders of magnitude for the initial couplings. Finally, we calculate the values of the couplings at the critical scale via the interpolation functions $\lambda_i(t)$ from RG-running and investigate the so calculated data with respect to the critical scale φ_0 and angle $\vec{\vartheta}_0$ of RSSB depending on initial coupling values at high energy-scale M_{Pl} and the critical coupling values $\lambda_i(t_{\text{crit}})$.

3.4 Scalar QED analysis

In the following we closely investigate the running of couplings and use the formalism introduced above in Sections 3.1 to 3.3 to further investigate RSSB in the case of massless scalar quantum electrodynamics. Recapping what we already derived in Section 2.2, the one-loop effective potential is calculated to be as in Eq. (2.14) and deriving $V_{\text{eff}}(\phi)$ with respect to the classical field ϕ gave the criticality condition from Eq. (2.12). From the criticality condition we learned that non-trivial minima are induced when $\lambda \simeq \frac{1}{16\pi^2} g^4 \ln[g^2]$ is fulfilled at the critical scale ϕ_0. Now, following the discussion in Section 3.2, we start the analysis of scale-setting by calculating the

scale dependent coupling functions $\lambda(t)$, $g(t)$ from their β-functions

$$(4\pi)^2\,\beta_\lambda(\lambda,g) = 20\lambda^2 - 12\lambda g^2 + 6g^4\,, \tag{3.22a}$$

$$(4\pi)^2\,\beta_g(g) = \frac{1}{3}g^3\,, \tag{3.22b}$$

for given initial couplings at Planck scale $\lambda_0 = \lambda(t_{\rm Pl})$ and $g_0 = g(t_{\rm Pl})$. The $\lambda(t)$ and $g(t)$ are displayed in Fig. 3.1 for different choices of initial couplings λ_0 and g_0. There we see that $g(t)$ is "almost" constant over variation of t while $\lambda(t)$ is increasing with t. This is easily understood by the structure of their β-functions, since the variation of $g(t)$, given by $\beta_g(t)$, is of $\mathcal{O}(g^3)$, such that for $g_0 < 1$ it follows that $\beta_g \ll 1$. On the other hand, $\beta_\lambda(t)$ contains a λ-independent contribution of $\mathcal{O}(g^4)$. With $g(t) \simeq g_0 = \text{const.}$ as discussed above, deriving β_λ with respect to

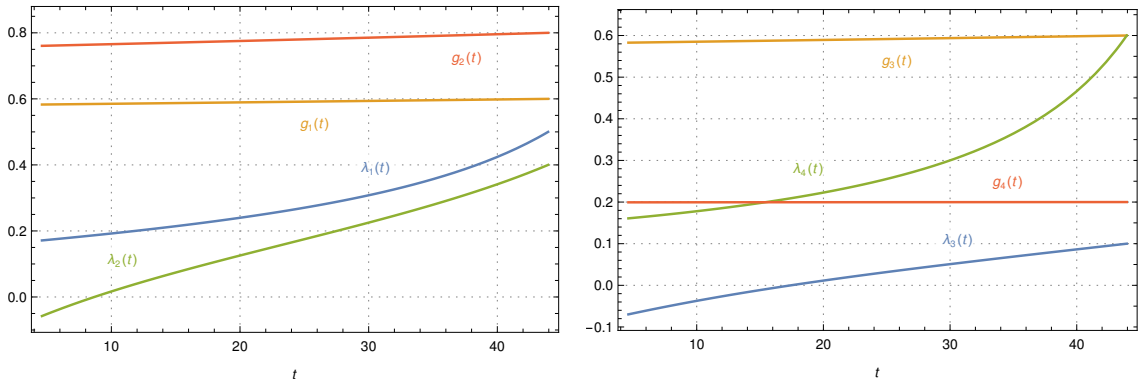

Figure 3.1: The running couplings $\lambda(t)$ and $g(t)$ of scalar QED with different renormalized initial values $(\lambda_{i,0},\ g_{i,0})$, calculated numerically with the β-functions from Eq. (3.22) shown in the range from $t_{\rm Pl}$ to $t_{\rm EW}$. The initial couplings were chosen to be, $i = 1$: $(0.5, 0.6)$, $i = 2$: $(0.4, 0.8)$, $i = 3$: $(0.1, 0.6)$, $i = 4$: $(0.6, 0.2)$.

λ we find that $\beta_\lambda(\lambda) > 0$ (for the calculation see Appendix A.2), for all $\lambda(t)$ This assumes that we start with $\lambda_0 > 0$, which is required by tree-level potential stability. Consequently, if $(\lambda_0, g_0) < \mathcal{O}(1)$ do not already fulfill the criticality condition of Eq. (2.12), $\lambda(\bar{\mu})$ decreases going to lower energy-scales until the criticality condition is fulfilled, inducing SSB or until we reach the end of our investigated stable ($\lambda(\bar{\mu}) > 0$) energy range $\bar{\mu}_{\rm EW}$ without allowing for Coleman-Weinberg symmetry breaking. Applying this finite energy range is a (sensible) truncation of the statement made in Section 2.2, that there always exists a $\phi_{\rm crit}$ such that the couplings satisfy Eq. (2.12) for sufficienlyt small couplings $< \mathcal{O}(1)$. Assuming the initial couplings (λ_0, g_0) are of the same order of magnitude $\mathcal{O}(10^{-1})$, evolving both couplings down to lower energies we quickly arrive in a regime $\bar{\mu}_{\rm crit} < \bar{\mu} < \bar{\mu}_{\rm Pl}$, where $\lambda \ll g(\bar{\mu})^2 \simeq g_0^2$ is fulfilled. Since $\lambda \simeq \frac{1}{16\pi^2} g^4 \ln[g^2]$ is required for SSB we can be assured that we are still in the unbroken phase of the classical conformal symmetry. Since $\lambda \ll g(\bar{\mu})^2 \simeq g_0^2$ implies both $\lambda^2 \ll g_0^4$ and $\lambda g^2 \ll g^4$, we can approximate the β-function of the quartic coupling in this regime by

$$\beta_\lambda(\lambda(\bar{\mu})) \approx \frac{6}{16\pi^2} g^4\,. \tag{3.23}$$

Integrating this from $\bar{\mu}$ to $\bar{\mu}_{\rm Pl}$ we get the energy-scale dependent quartic coupling

$$\lambda(\bar{\mu}) = \frac{6g^4}{16\pi^2} \ln\left[\frac{\bar{\mu}}{\bar{\mu}_{\rm Pl}}\right] + \lambda_0 \ , \tag{3.24}$$

where λ_0 is the initial quartic coupling. Now for the calculation of the critical scale ($\phi_{\rm crit} = \bar{\mu}_{\rm crit}$) where SSB occurs, we solve the criticality condition for $\lambda(\bar{\mu})$ such that $\lambda(\bar{\mu}_{\rm crit})$ is given by

$$\lambda(\bar{\mu}_{\rm crit}) = \frac{3g_{\rm crit}^4}{16\pi^2}\left(\frac{1}{3} - \ln g_{\rm crit}^2\right) = \frac{6g_{\rm crit}^4}{16\pi^2} \ln\left[\frac{\bar{\mu}_{\rm crit}}{\bar{\mu}_{\rm Pl}}\right] + \lambda_0 \ . \tag{3.25}$$

Rearranging for the quotient of critical and Planck scale while omitting terms that are several orders of magnitude smaller than the leading term, we are left with

$$\frac{\bar{\mu}_{\rm crit}}{\bar{\mu}_{\rm Pl}} = \exp\left\{-\frac{16\pi^2}{6}\frac{\lambda_0}{g_0^4}\right\} \ , \tag{3.26}$$

which displays nicely the exponential dependency of scale-separation between critical and high energy-scale with respect to the initial couplings. Now one can already check whether there are any conditions on the initial couplings required to allow for RSSB with a critical scale $\bar{\mu}_{\rm crit}$ around the electroweak scale $\bar{\mu}_{\rm EW}$. For further analysis we use the formalism described in Sections 3.1 to 3.3 to determine the breaking properties for initial couplings $\lambda_0, g_0 \in [0.1, 0.9]$. The result is shown in Fig. 3.2. The red line denotes the upper bound that is set on λ_0, by only allowing RG-running until $t_{\rm EW}$. It shows for a given g_0 the maximal λ_0, such that $\lambda(t)$ can decrease enough through RG-running to satisfy the criticality condition from Eq. (2.12), also shown in the legend of Fig. 3.2. We see that the results from our calculations are in good agreement with the bound given by the red line. Furthermore that there is very little fine-tuning necessary in the renormalized couplings at $\bar{\mu}_{\rm Pl}$ to allow for a spontaneously generated energy-scale around $\bar{\mu}_{\rm EW}$, confirming the relation of exponential scale-seperation, as calculated in Eq. (3.26).

In the case of multiscalar theories it is not as easy to derive (approximate) analytical expressions for the dependency of scale-separations on the initial couplings, compared to scalar QED. Therefore, one either has to make assumptions about e.g. tree-level flat directions (*Gildener-Weinberg* approach) or rely on a numerical analysis. A structurally similar relation to Eq. (3.26) has been derived in Ref. [38] in the context of RSSB in massless two-scalar theory with assumptions similar to the *Gildener-Weinberg* approach. But, since we want to analyze radiatively induced SSB via the Coleman-Weinberg mechanism, we rely on the numerical analysis using the approach described in Sections 3.1 to 3.3 to investigate classically conformal symmetric multiscalar models without any further assumptions. However, first we give a brief summary of the *Gildener-Weinberg* approach, originally derived in Ref. [23], since it is widely used in various applications in the literature (e.g. Refs. [9, 10, 22, 24–27]. This allows us to easily compare our findings with the corresponding *Gildener-Weinberg* results.

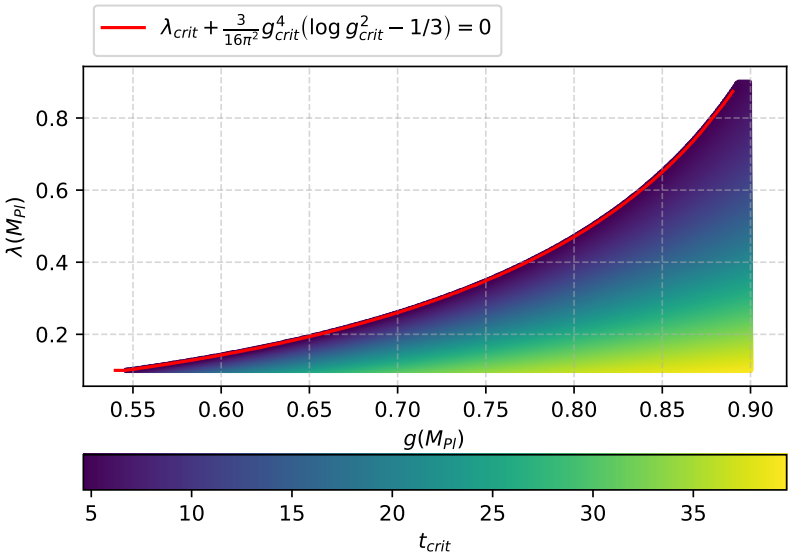

Figure 3.2: The condensation scale t_{crit} depending on the values of the couplings at renormalization, i.e. the initial values at Planck scale $(\lambda(M_{\text{Pl}}), g(M_{\text{Pl}}))$. The calculation allows for $t_{\text{crit}} \in [t_{\text{EW}}, t_{\text{Pl}}]$.

3.5 Gildener-Weinberg approach

In the following we review the formalism introduced by E. Gildener and S. Weinberg in Ref. [23], which describes a systematic approach for minimizing the effective potential in a (classical conformal symmetric) theory with multiple scalar fields. They assume couplings of order g^2, with g denoting the gauge coupling. As a result, the tree-level contribution to the effective potential is of $\mathcal{O}(g^2)$, whereas the one-loop contribution is of $\mathcal{O}(g^4)$. Consequently, for the one-loop contribution to perturb the potential, the tree-level term has to vanish at a specific scale, the Gildener-Weinberg (GW) scale Λ_{GW}. With the tree-level potential given by

$$V(\vec{\Phi}) = \frac{1}{24} f_{ijkl} \phi_i \phi_j \phi_k \phi_l \ , \tag{3.27}$$

where $\vec{\Phi}$ is the collection of the theory's real scalar degrees of freedom, the condition of vanishing tree-level contribution at the Gildener-Weinberg scale Λ_{GW} translates to a condition on the scalar couplings f, the so called Gildener-Weinberg conditions. In general they can be written in the following way

$$R(f)|_{\Lambda=\Lambda_{\text{GW}}} = 0 \ . \tag{3.28}$$

Note that the scalar couplings in Eq. (3.27) are subject to RG-running $f = f(\Lambda)$, with Λ denoting the renormalization scale. That the scalar couplings f fulfill the condition in Eq. (3.28) corresponds to a valley along a ray in field space with a minimal value of zero. This ray in field space denotes the *flat direction* and can be parameterized by a unit vector of field space $\vec{n}$ and the value φ that determines the

position away from the origin on the ray

$$\vec{\Phi}_{\text{flat}} = \vec{n}\varphi \ . \tag{3.29}$$

Along the flat-direction, the one-loop quantum corrections can induce non-trivial minima, while the other directions in field space are dominated by the tree-level contributions and therefore only contain trivial minima. These minima along the flat direction lies slightly shifted from the GW scale Λ_{GW} at $\langle\varphi\rangle$

$$\langle\varphi\rangle = \Lambda_{\text{GW}} \cdot \exp\left(-\frac{1}{4} - \frac{A}{2B}\right) \ , \tag{3.30}$$

with the one-loop terms A, B given as in Eq. (3.9), up to factors that drop out while calculating A/B. A derivation of the expression in Eq. (3.30) is found in Appendix A of Ref. [22]. Then, radiatively induced spontaneous symmetry breaking along $\vec{\Phi}_{\text{flat}}$ corresponds to the mass generation of the pseudo-Goldstone boson of broken scale invariance. Its mass is then proportional to the curvature of the effective potential at its minimum. Thus, the Gildener-Weinberg formalism reduces the scale dependent n field dimensional problem of SSB to an analysis of the potential along the flat direction and at Λ_{GW}.

The above reviewed Gildener-Weinberg approach seems, at first glance, similar to the approach used by us to investigate Coleman-Weinberg symmetry breaking, as it is also built around an equation that determines the scale at which the effective potential is minimal by requiring the couplings to fulfill certain conditions. But here lies already the first difference. The Gildener-Weinberg conditions only apply to the scalar couplings, while our n criticality equations depend on couplings (e.g. quartic, gauge, yukawa) from all sectors (e.g. scalars, fermions, gauge bosons). In addition, the Gildener-Weinberg formalism assumes domination of the tree-level contribution generically in the field space, which we do not assume. If this is not the case, the GW formalism still gives a correct local minimum along the flat direction. However this local minimum is not necessarily also the global minimum of the effective potential. The possibility that the one-loop contribution can compete with the tree-level potential in general field space is commonly not considered. Thus, in the following Section 4 we investigate classically scale invariant multiscalar models, not restricting ourselves to an analysis along possible flat directions but rather investigating the effective potential in full field space. We also focus on effects caused by the interplay of the scalar sector with e.g. gauge sector instead of mostly focusing on the scalar sector itself, as it is done in the GW-method.

4 Classically conformal symmetric two-scalar theories

In the following we introduce different classical scale-invariant models to investigate RSSB in the Coleman-Weinberg formalism in the most general way. We want to develop a systematic or physical intuition of the symmetry breaking properties of the different particle sectors and especially their interplay. Therefore, we use the

methods and general formalism introduced in Section 3 to investigate characteristics of RSSB at the critical scale and its connection to initial couplings through RG-running. Starting off with the simplest massless two-scalar model we continue by adding different forms of couplings (e.g. just one scalar coupled to it, both or individual gauge groups) to a $U(1)$ gauge group, trying to give an intuitive approach that may be generalized to more complex (toy) models. We compare our results with findings from a Gildener-Weinberg type analysis and highlight differences that result from the general approach including non-scalar contributions in the criticality equations instead of having them contribute only implicitly through RG-running of scalar couplings as it is done in the Gildener-Weinberg approach. We see that we are able to fundamentally distinguish different cases of RSSB, while also qualitative new features of symmetry breaking appear. These are understood given the intuitive nature of our general criticality equations.

4.1 Two massless scalars

Let us consider a toy model which only features two massless real scalar fields ϕ and S that both can acquire a non-vanishing vacuum expectation value. The corresponding Lagrangian reads

$$\mathcal{L} = \tfrac{1}{2}\partial_\mu\phi\partial^\mu\phi + \tfrac{1}{2}\partial_\mu S\partial^\mu S - V_{\text{tree}}(\phi, S) \tag{4.1}$$

with the tree-level potential

$$V_{\text{tree}}(\phi, S) = \frac{\lambda}{4}\phi^4 + \frac{\lambda_p}{4}\phi^2 S^2 + \frac{\lambda_s}{4}S^4 \,. \tag{4.2}$$

Note here, that excluding dimension-4 operators such as e.g., ϕS^3 is equivalent to implicitly assuming a $\mathbb{Z}_2$ symmetry between the two fields ϕ and S. Now following Section 3.1 for $n = 2$ scalar degrees of freedom $\vec{\vartheta}$ reduces to ϑ. We rewrite the effective potential with respect to the spherical coordinates

$$\phi = \varphi\sin\vartheta, \qquad S = \varphi\cos\vartheta \,, \tag{4.3}$$

such that the angular part of the tree-level contribution $\kappa(\vartheta;\varphi_0)$ (evaluated at the critical scale $\bar{\mu} = \varphi_0$) is simply given by

$$\kappa(\vartheta;\varphi_0) = \lambda\sin^4\vartheta + \lambda_p\sin^2\vartheta\cos^2\vartheta + \lambda_s\cos^4\vartheta \,. \tag{4.4}$$

Whereas, the one-loop contributions result from two field dependent mass terms $\hat{m}^2_\pm(\vartheta;\varphi_0)$ originating from the two-scalar degrees of freedom and hence contributing to the one-loop terms $A(\vartheta;\varphi_0)$ and $B(\vartheta;\varphi_0)$ with constants $c_\pm = \frac{3}{2}$, multiplicities $n_\pm = 1$ and spin $s_\pm = 0$, c.f. Eq. (3.9). These field dependent masses are calculated to be

$$\begin{aligned}\hat{m}^2_\pm(\vartheta;\varphi_0) = \frac{1}{4}\Big(&6\left(\lambda\sin^2\vartheta + \lambda_s\cos^2\vartheta\right) + \lambda_p \\ &\pm\left[16\lambda_p^2\sin^2\vartheta\cos^2\vartheta + \left(6\left(\lambda\sin^2\vartheta - \lambda_s\cos^2\vartheta\right) - \lambda_p\left(\sin^2\vartheta - \cos^2\vartheta\right)\right)^2\right]^{\frac{1}{2}}\Big) \,,\end{aligned} \tag{4.5}$$

where the implicit φ_0 dependence again denotes that the Lagrangian couplings $(\lambda(t), \lambda_s(t), \lambda_p(t))$ are subject to renormalization group running. How exactly the couplings change over varying running scale is quantified by their corresponding β-functions, that are calculated to be

$$16\pi^2\beta_\lambda = 18\lambda^2 + \tfrac{1}{2}\lambda_p^2 \,, \tag{4.6a}$$

$$16\pi^2\beta_{\lambda_s} = 18\lambda_s^2 + \tfrac{1}{2}\lambda_p^2 \,, \tag{4.6b}$$

$$16\pi^2\beta_{\lambda_p} = 2\lambda_p(3\lambda + 3\lambda_s + 2\lambda_p) \,. \tag{4.6c}$$

The resulting functions for the scale dependent Lagrangian couplings $(\lambda(t), \lambda_s(t), \lambda_p(t))$ are exemplary shown in Fig. 4.1. Here we may already note that the portal coupling cannot become negative due to RG-running if not initially already $\lambda_{p,0} < 0$, since the portal coupling's β-function depends on λ_p itself in a multiplicative way, c.f. Eq. (4.6). In addition we observe, that the absolute value of all couplings mono-

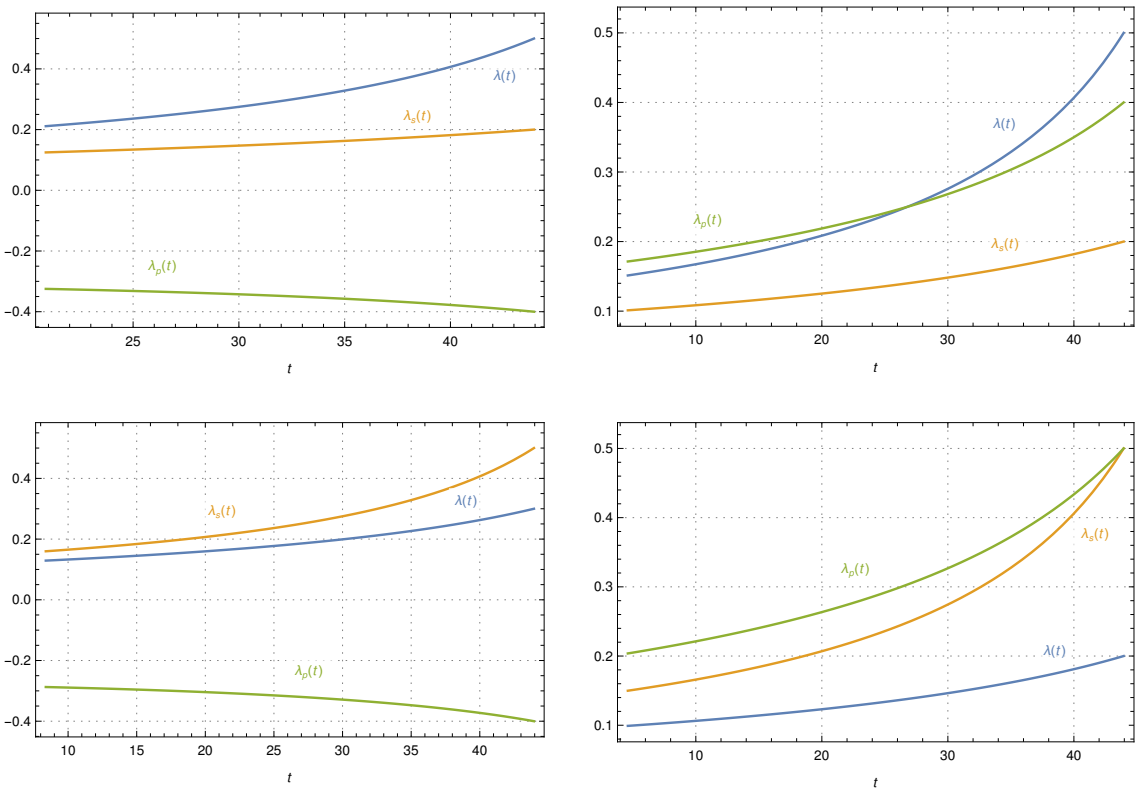

Figure 4.1: The renormalization group running of the Lagrangian couplings $(\lambda, \lambda_s, \lambda_p)$ with respect to $t = \ln[\bar{\mu}/\mathrm{GeV}]$ in the "interesting" energy range of $[t_{\mathrm{EW}}, t_{\mathrm{Pl}}]$ corresponding to the β-functions from Eq. (4.6). Here displayed with different initial couplings $(\lambda_0, \lambda_{s,0}, \lambda_{p,0})$, i.e. upper left: $(0.5, 0.2, -0.4)$, upper right: $(0.5, 0.2, 0.4)$, lower left: $(0.3, 0.5, -0.4)$, lower right: $(0.2, 0.5, 0.5)$.

tonically decreases towards lower energies and initially zero couplings only stay equal to zero in the case of no portal coupling $\lambda_p = 0$. Furthermore, we need to ensure vacuum stability for the tree-level and the one-loop effective potential in the region of interest and especially at the minimum of the effective potential φ_0. From stability of the tree-level potential, we get the following conditions for the Lagrangian

couplings

$$\lambda(t) > 0, \qquad \lambda_s(t) > 0, \qquad \lambda_p(t) > -2\sqrt{\lambda(t)\lambda_s(t)}, \qquad \forall\, t \in [t_{\mathrm{EW}}, t_{\mathrm{Pl}}]\,, \tag{4.7}$$

where t is the natural logarithm of the running scale $\bar{\mu}$, while t_{EW} denotes the lower end of the energy range, as we arenot interested in SSB at scales below 100 GeV, and accordingly t_{Pl} makes M_{Pl} the upper bound for investigated energies as we would expect our effective field theory to transition into unknown physics at energy-scales that high. Hence, t_{Pl} is the scale at which we set the theory to be finite by fixing the Langrangian parameters at that scale. This corresponds to "matching conditions" between two phases of effective field theories and with that we focus on understanding the effects the choice of initial conditions has on the properties of RSSB. For the stationary point, calculated using Eq. (3.12), to denote the global one-loop stable minimum of the effective potential the following conditions have to be fulfilled

$$\mathrm{H}(\varphi_0, \vartheta_0) > 0 \qquad \text{and} \qquad B(\vartheta_0; \varphi_0) > 0\,, \tag{4.8}$$

with the one-loop contribution term $B(\vartheta_0; \varphi_0)$ as given in Eq. (3.9b) and the Hessian determinant H evaluated at the vacuum (φ_0, ϑ_0)

$$\mathrm{H}(\varphi_0, \vartheta_0) = \frac{\varphi_0^6}{4}\left(2B(\vartheta_0;\varphi_0)\left[\frac{\partial^2\left(\kappa(\vartheta;\varphi_0) + A(\vartheta;\varphi_0)\right)}{\partial\vartheta^2}\right]_{\vartheta=\vartheta_0} - \left[\frac{\partial B(\vartheta;\varphi_0)}{\partial\vartheta}\right]^2_{\vartheta=\vartheta_0}\right). \tag{4.9}$$

The condition arising from combining Eq. (4.8) with Eq. (4.9) is checked numerically for all points to ensure that only the "true" non-trivial vacuum is found. Detailed calculations for the determinant of the Hessian and partial derivatives for the classical scale-invariant two-scalar model are displayed in Appendix A.3. With the stability of the potential and the conditions for the stationary point being the global minimum, we want to turn to the criticality equations before looking at results from simulations to assess what kind of symmetry breaking we expect to take place. Given the tree-level contribution in Eq. (4.4) and that only the two field dependent masses from Eq. (4.6a) contribute to the one-loop term in the effective potential, it is easily seen that the tree-level contribution is generally of $\mathcal{O}(\lambda_i)$ while the one-loop terms are of $\mathcal{O}(\lambda_i^2)$. Thus, we expect only Gildener-Weinberg like symmetry breaking, since there are no other particle sectors that could compete with the contributions of the scalars. In other words, we expect an almost flat direction and therefore κ is close to zero, such that the one-loop effects can shift the vacuum of the theory from the origin to a non-trivial solution. An exact flat direction develops if the couplings at a certain scale t fulfill one of the following Gildener-Weinberg conditions

$$\text{For } \lambda_p > 0 \;:\quad \lambda(t) = 0, \qquad \lambda_s(t) = 0\,, \tag{4.10a}$$

$$\text{For } \lambda_p < 0 \;:\quad \lambda(t) = 0, \qquad \lambda_s(t) = 0, \qquad \lambda_p(t) = -2\sqrt{\lambda(t)\lambda_s(t)}\,. \tag{4.10b}$$

Following here the same principle of a tree-level flat direction as Gildener and Weinberg did in their analysis, our formalism offers a different perspective to understand

how symmetry breaking can take place. As the tree-level term κ depends only on an odd power in λ_i and there is more than one coupling (mixing of scalar fields), there can be cancellations such that the absolute value of the tree-level term is much smaller than λ_i, while at the same time the one-loop terms depend on an even power in the couplings, resulting in no cancellations among themselves. Therefore, unlike in the massless ϕ^4 theory, c.f. Section 2.1, RSSB in this theory's region of applicability is possible if the tree-level potential becomes flat enough for the quantum corrections to induce a non-trivial vacuum.

With these we have a complete description in the context of the general formalism introduced in Section 3.1 and start with a linear variation of one of the quartic couplings and the portal coupling, while holding the other quartic coupling constant. This gives us a simple access to the symmetry breaking properties, as the Lagrangian and therefore the effective potential is invariant under exchange of ϕ and S. Additionally, only varying two parameters allows for an easier visualization of the dependence on the initial conditions of the vacuum (φ_0, ϑ_0). The results for critical scale $\varphi_0 \equiv \langle\varphi\rangle$ and critical angle $\vartheta_0 \equiv \theta$ of symmetry breaking for varying $\lambda_0 \in [0.1, 0.9]$ and $\lambda_{p,0} \in [-0.9, 0.9]$, while the other fields quartic initial coupling is given by $\lambda_{s,0} \in \{0.1, 0.3, 0.5\}$ are displayed in Figs. 4.2 and 4.3.

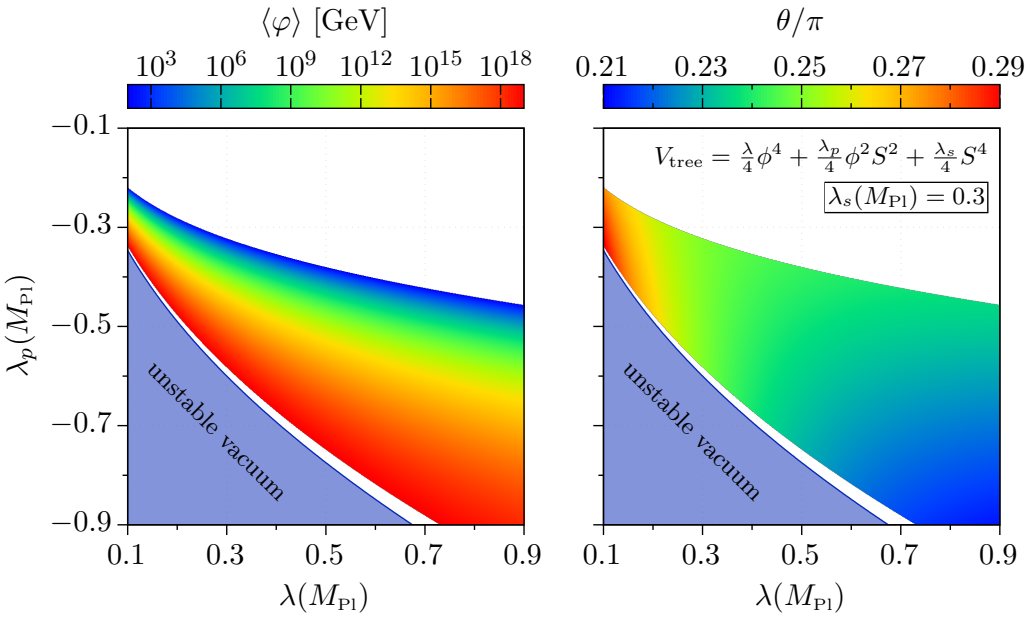

Figure 4.2: The condensation scale $\varphi_0 \equiv \langle\varphi\rangle$ and angle $\vartheta_0 \equiv \theta$ depending on the initial couplings at the Planck scale $(\lambda(M_{\rm Pl}), \lambda_p(M_{\rm Pl})) \in ([0.1, 0.9], [-0.9, 0.9])$ with $\lambda_{s,0} = 0.3$. The displayed range of the initial couplings is limited to the areas of viable solutions and was scanned using a step-size of $\Delta\lambda_0 = 0.001$.

Looking at Fig. 4.2, the first important observation is that for initial couplings of the same order of magnitude ($\lambda_{i,0} = \mathcal{O}(1)$), RSSB cannot occur for positive initial portal couplings. This can be understood quite intuitively if one looks closely at the criticality equations, especially the radial one from Eq. (3.12a) and its individual terms. Considering that λ_p cannot become negative due to RG-running, if $\lambda_{p,0} \geq 0$ and tree-level stability dictates $\lambda, \lambda_s \geq 0$ then all terms in $\kappa\,(\vartheta_0; \varphi_0)$ are greater or

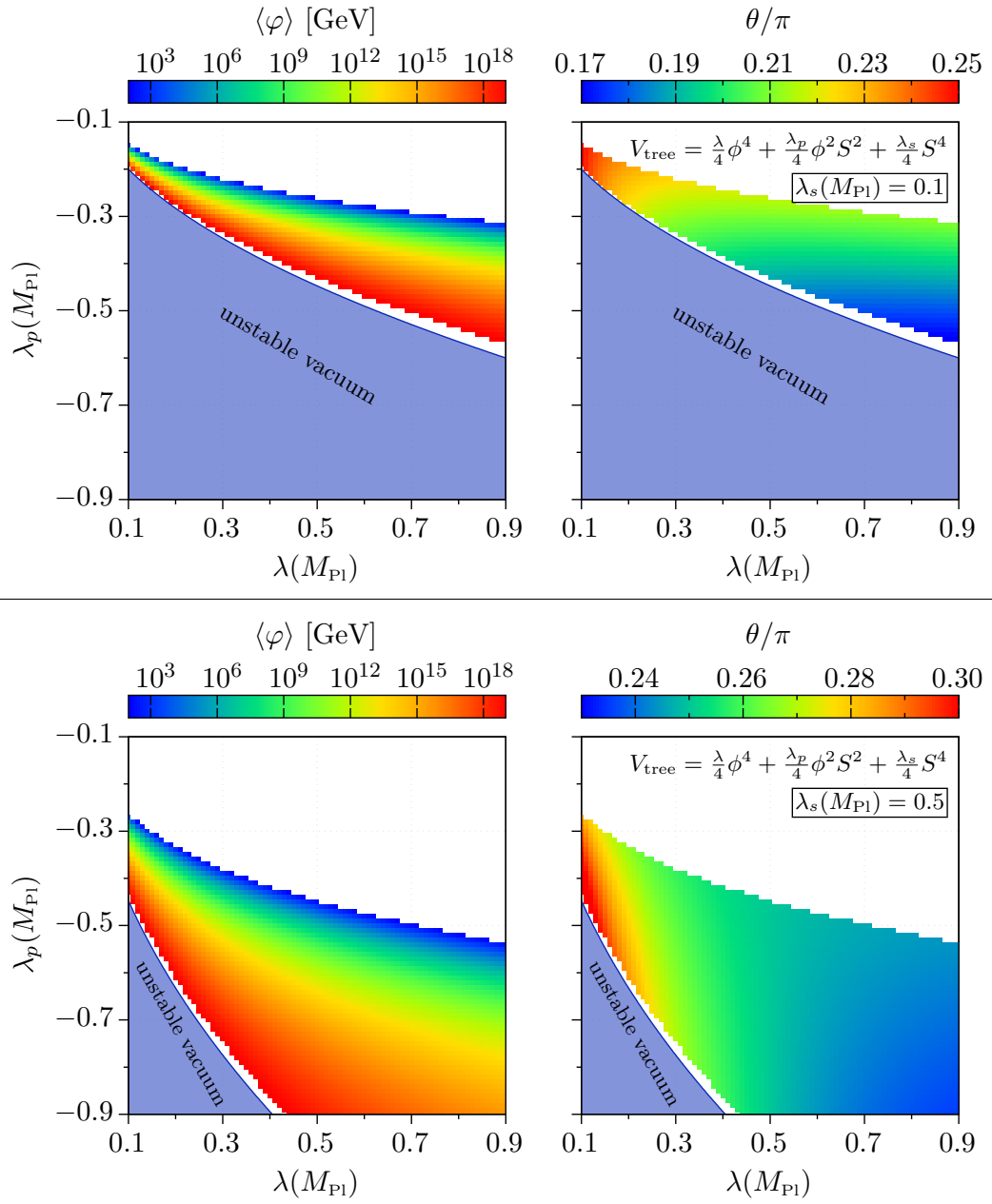

Figure 4.3: The condensation scale $\varphi_0 \equiv \langle\varphi\rangle$ and angle $\vartheta_0 \equiv \theta$ depending on the initial couplings at the Planck scale $(\lambda(M_{\rm Pl}), \lambda_p(M_{\rm Pl})) \in ([0.1, 0.9], [-0.9, 0.9])$ with $\lambda_{s,0} = 0.1$ (top) and $\lambda_{s,0} = 0.5$ (bottom). The displayed range of the initial couplings is limited to the areas of viable solutions and was scanned using a step-size of $\Delta\lambda_0 = 0.01$.

equal to zero, c.f. Eq. (4.4), or in other words no cancellation can occur in $\kappa(\vartheta_0; \varphi_0)$. Therefore $\kappa(\vartheta_0; \varphi_0) = \mathcal{O}(\lambda_i)$, with λ_i being one of the couplings, since all are of the same order of magnitude, while the one-loop terms are of $A(\vartheta_0; \varphi_0), B(\vartheta_0; \varphi_0) = \mathcal{O}(\lambda_i^2)$, such that Eq. (3.12a) cannot be fulfilled. This is important again when we look at couplings of different orders of magnitude with negative and positive portal couplings. Secondly, one sees that the region of allowed RSSB is bound from

above and below. The boundary from below, as displayed e.g. in Fig. 4.2, originates from ensuring initial tree-level potential stability via $\lambda_p > -2\sqrt{\lambda\lambda_s}$ from Eq. (4.7). Whereas, the boundary from above is due to our restriction in the range of RG-running (only down to t_{EW}), as already seen in Section 3.4, Fig. 3.2. Understanding the observed structure of symmetry breaking scales is directly linked to the expected similarity to the Gildener-Weinberg case. The "rainbow"-like structure, where points with the same critical scale have similar distances to the boundary that is set by tree-level potential stability, originates from the fact, that said stability condition, if it is exactly fulfilled ($\lambda_p = -2\sqrt{\lambda\lambda_s}$),, denotes the Gildener-Weinberg condition for SSB with non-vanishing VEVs for both scalar fields. Fulfilling the stationary equations in the massless two-scalar models requires a "kind of flat" direction such that one-loop and tree-level contributions can be of the same order of magnitude. Thus, the more an initial point in coupling parameter space deviates from the "flatness" condition of Gildener-Weinberg, the longer RG-running needs to flatten out the tree-level potential, resulting in a lower scale of symmetry breaking. In Fig. 4.4 the quartic coupling λ and the portal coupling λ_p are shown with their values at the critical scale t_{crit}. There we see all the points from before moved way closer to the boundary that is set by GW "flatness" condition, distorting the shape of symmetry breaking points along the conditions curve. Furthermore, we see that there are no holes

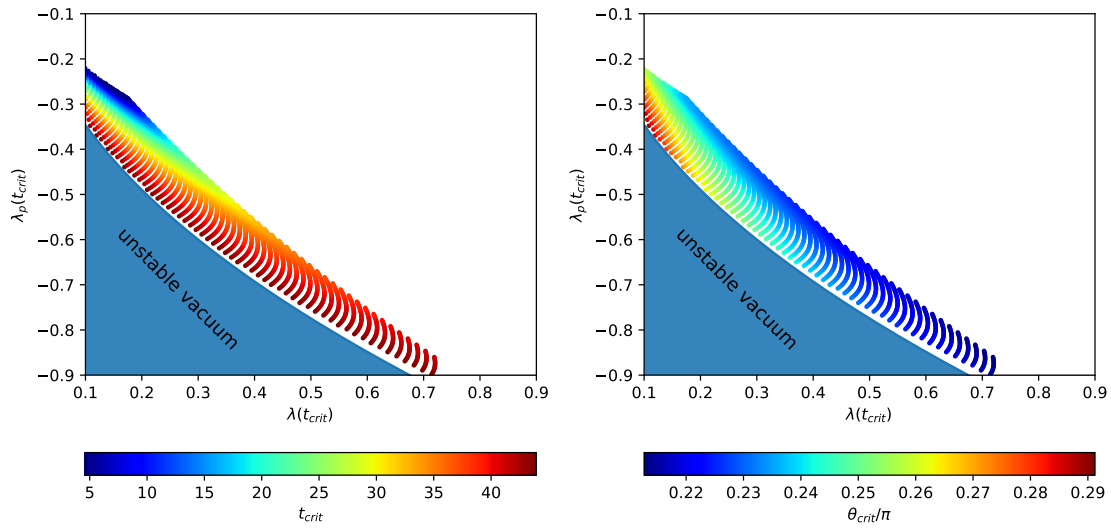

Figure 4.4: Condensation scale t_{crit} and angle θ_{crit} plotted against the portal and quartic coupling at the scale of symmetry breaking $(\lambda(t_{\mathrm{crit}}), \lambda_p t_{\mathrm{crit}})$. The calculations are based on the classical scale-invariant two-scalar model given in Section 4.1 and varied initial conditions at the Planck scale $(\lambda(M_{\mathrm{Pl}}), \lambda_p(M_{\mathrm{Pl}})) \in ([0.1, 0.9], [-0.9, 0.9])$ with $\lambda_{s,0} = 0.3$. For comparison the displayed parameter space is identical with the one in Figs. 4.2 and 4.3 while again a step-size of $\Delta\lambda = 0.01$ was used.

or unexpected unstable regions, but rather a smooth distribution of condensation points. This was expected since all the quantities in the criticality conditions are smooth functions of the scale and angle of condensation $(\vartheta_0; \varphi_0)$. While we find the

full range of possible symmetry breaking scales, the critical angles θ only varies a little around a symmetric value, e.g. $\approx \frac{\pi}{4}$ for $\lambda_{s,0} = 0.3$ in Fig. 4.2. As a result the total (maximal) variation throughout the scanned range of initial couplings is only about $\Delta\theta \approx 0.08\pi$. Seeing as ϑ (and therefore also $\vartheta_0 \equiv \theta$) describes the mixing of the two-scalar fields ϕ and S

$$\vartheta = \arctan\left(\frac{\phi}{S}\right) \ , \tag{4.11}$$

the maximal cancellation in the tree-level contribution $\kappa(\vartheta_0; \varphi_0)$, c.f. Eq. (4.4), for given couplings is reached for maximal mixing of the fields, i.e. $\vartheta = \pi/4$. And since cancellation in $\kappa(\vartheta_0; \varphi_0)$ is essential for RSSB in a theory with only scalar degrees of freedom, it is only natural that the case of symmetry breaking at maximal mixing angle is the intrinsically preferred one. In other words, since there is no preferred direction in field space, the theory aligns around the (symmetrical) angle of maximal mixing. In the calculation of data for Fig. 4.3 and Fig. 4.4 we used a different step-size.

Now varying the second quartic coupling $\lambda_s(M_{\text{Pl}})$ to be either 0.1 or 0.5 instead of 0.3 (see Fig. 4.3), we observe that the structure of condensation points of both plots seems to be almost unaffected, while the by tree-level stability excluded region and the angle of condensation seem to vary. This is exactly what we would expect as the condition for determining the unstable vacuum region, c.f. Eq. (4.7), depends directly on λ_s and as the cancellations in $\kappa(\vartheta_0; \varphi_0)$ not only depend on the angle of mixing ϑ but also on the scalar couplings, an asymmetry among the quartic couplings results in a shift of the angle for which the cancellations are maximized, which is equivalent to a rotation in field space and matches the observations from comparing Fig. 4.2 and Fig. 4.3. This effect is transported from the scale of setting initial couplings to the critical scale by the RG-running of the couplings.

So far, we only considering initial couplings of the same order of magnitude. Now we turn to the analysis of RSSB for three random individual initial couplings with absolute values of $|\lambda_{i,0}| \in [10^{-5}, 1]$. While $\lambda_0, \lambda_{s,0} > 0$, as required by tree-level vacuum stability, this includes both positive and negative portal couplings. In Fig. 4.5 the critical angle is plotted against the scale of condensation, while distinguishing points originating from initial positive or negative portal couplings. Recollecting that the portal coupling cannot change its sign throughout RG-running we observe the expected Gildener-Weinberg like symmetry breaking. Namely, that for positive portal coupling at the GW scale the tree-level potential can only develop a flat direction and therefore allows for GW symmetry breaking along one of the fields ($\vartheta = 0, \pi/2$) with the quartic coupling of that field equal to zero, c.f. Eq. (4.4). Yet for negative portal coupling at the GW scale, there can be a flat direction for an arbitrary ϑ, depending on the ratios between the quartic and portal couplings. Even though the results of the calculations agree with the findings from the Gildener-Weinberg formalism, there are two interesting insights to be gained here:

1. While there is SSB for positive portal couplings for couplings of different orders of magnitude, there is none if the scalar couplings are of the same order of magnitude. Hence a hierarchy in the (initial) couplings is necessary.

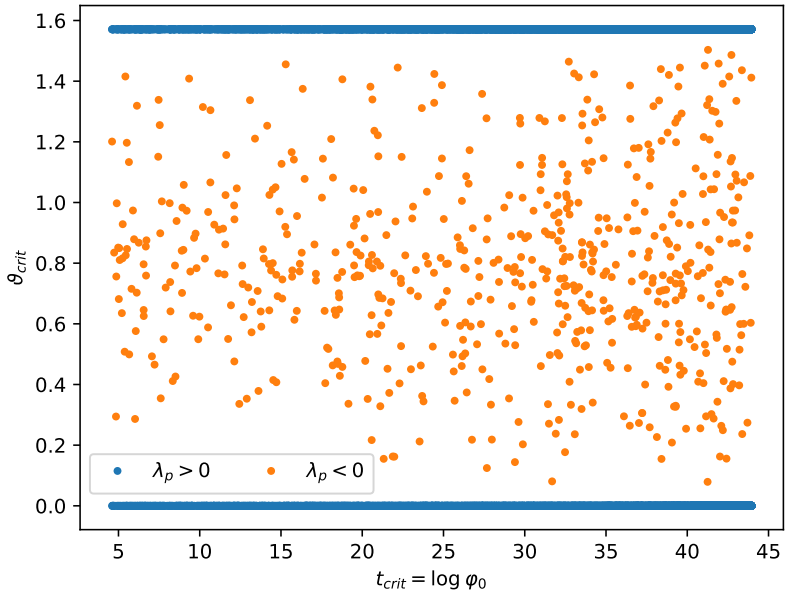

Figure 4.5: The critical angle $\vartheta_{\text{crit}} = \vartheta_0$ against the condensation (critical) scale $t_{\text{crit}} = \ln \varphi_0$, while the color of the points distinguishes between negative and positive portal couplings (both at Planck and condensation scale).

2. In both cases (with or without coupling hierarchy) SSB in all directions in field space (all angles ϑ) is generally expected for negative portal couplings, yet we do not find points with SSB (up to numeric uncertainties) along one of the fields. Thus, a mixed condensation state seems to be preferred.

Both of these observations can be understood in the context of the general approach that is presented in this work, c.f. Section 3.1. Starting with explaining insight number one, we want to recall that there is no cancellation possible in $\kappa(\vartheta_0; \varphi_0)$ as all individual terms are positive and at least the portal term is not equal to zero, given $\lambda_p > 0$, yet the tree-level contribution has to be small, i.e. the same order of magnitude as the suppressed one-loop contributions. Not assuming there is a hierarchy in the initial couplings then for critical angles of $\vartheta_0 \neq 0, \frac{\pi}{2}$ the tree-level term is of $\kappa(\vartheta_0; \varphi_0) = \mathcal{O}(\lambda_{\text{largest}})$, while the one-loop contributions are still of $A(\vartheta_0; \varphi_0), B(\vartheta_0; \varphi_0) = \mathcal{O}(\lambda^2_{\text{largest}})$. Consequently, there cannot be any SSB under this conditions, since the one-loop terms cannot cancel the tree-level contribution, such that the criticality equation of Eq. (3.12a) cannot be fulfilled. For critical mixing angles $\vartheta_0 = 0, \frac{\pi}{2}$ there is still no cancellation in $\kappa(\vartheta_0; \varphi_0)$, but now it only depends on one of the quartic couplings λ or λ_s,

$$\kappa(\vartheta_0; \varphi_0) = \begin{cases} \mathcal{O}(\lambda), & \vartheta_0 = \frac{\pi}{2} \\ \mathcal{O}(\lambda_s), & \vartheta_0 = 0 \end{cases}, \tag{4.12}$$

such that it can become "almost" flat if the corresponding quartic coupling is initially hierarchically smaller, with this effect being amplified by RG-running while going to

lower energy-scales. An example of the amplifying nature of RG-running for hier-

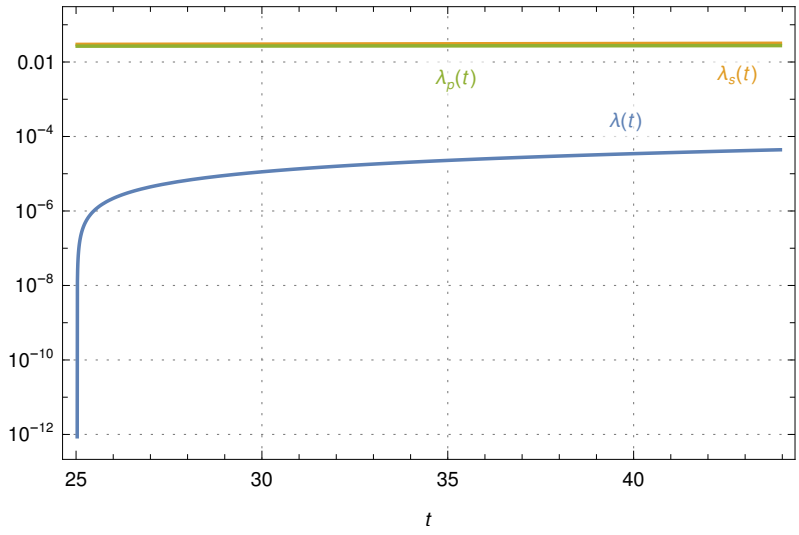

Figure 4.6: The RG-running of the scalar couplings with hierarchically initial values of $(\lambda_0, \lambda_{s,0}, \lambda_{p,0}) = (0.0000440, 0.0318, 0.0276)$ that result in the non-trivial vacuum $(\varphi_0, \vartheta_0) = (1.57, 27.7)$. For reasons of clarity and comprehensibility the numerical values are rounded to their third non-zero digits. The shown energy range is truncated by ensuring tree-level vacuum stability, particularly $\lambda(t) > 0$. Note here the logarithmic scale for the strength of the couplings.

archic initial couplings is shown in Fig. 4.6. Whereas, for a tree-level flat direction, the one-loop contributions still depend on the largest contributing scalar coupling in this scenario, the portal coupling λ_p, $A(\vartheta_0;\varphi_0)$ and $B(\vartheta_0;\varphi_0) = \mathcal{O}(\lambda^2_{\text{largest}}) = \mathcal{O}(\lambda^2_p)$. As a result the one-loop contributions, even though depending on λ^2_p, can be the same order of magnitude as the the tree-level term $\kappa(\vartheta_0;\varphi_0)$ due to a large enough hierarchy between one of the quartic couplings and the portal coupling. Therefore, allowing for the criticality condition in Eq. (3.12a) being fulfilled for positive portal couplings resulting in possible spontaneously symmetry breaking. The explanation for the second insight is then rather simple. This theory of purely scalar particle content needs either cancellations in the tree-level contribution or a large enough hierarchy between the portal and a quartic coupling, whereas the effect of tree-level cancellations is much bigger, needs less fine tuning and does not depend on amplification through RG-running and hence is the preferred one in the *top-down* approach of analysis. With tree-level cancellation being the preferred mechanism in this scenario, it is clear that with the tree-level contribution $\kappa(\vartheta_0;\varphi_0)$ as given in Eq. (4.4), that a critical angle of $\vartheta_0 = 0, \frac{\pi}{2}$ would result in no cancellation in the tree-level contribution. RSSB rather occurs at the mixing angle of maximal tree-level cancellations, which is not necessarily identical to the angle of maximal mixing but depends on the ratios between the scalar couplings. This result is further motivation to consider general Coleman-Weinberg symmetry breaking via the *top-down* approach, since there is initially no reason for the theory to prefer any "form" of RSSB when looking at the couplings at the critical scale. However, renormalizing the theory at high energy and evolving it towards low energies shows that through

the properties of RG-running the preferred (or more natural) solutions for RSSB are separated from the ones that would need fine-tuning. We also want to note that the result of a preferred type of Gildener-Weinberg like symmetry breaking in the $\lambda_p > 0$ parameter space, is a result entirely based on RSSB in theories containing only scalar degrees of freedom. An analysis in the Gildener-Weinberg framework only focuses on the theories scalar sector and hence one might think that this statement generalizes to theories with arbitrary particle content, while our approach, including explicit contributions from non-scalar degrees of freedom, shows that this statement does not generalize for arbitrary particle content in the most general approach to RSSB. We see that this is indeed the case when introducing complex scalars that are coupled to a gauge group in Section 4.2. Somewhat quantifying how well our general

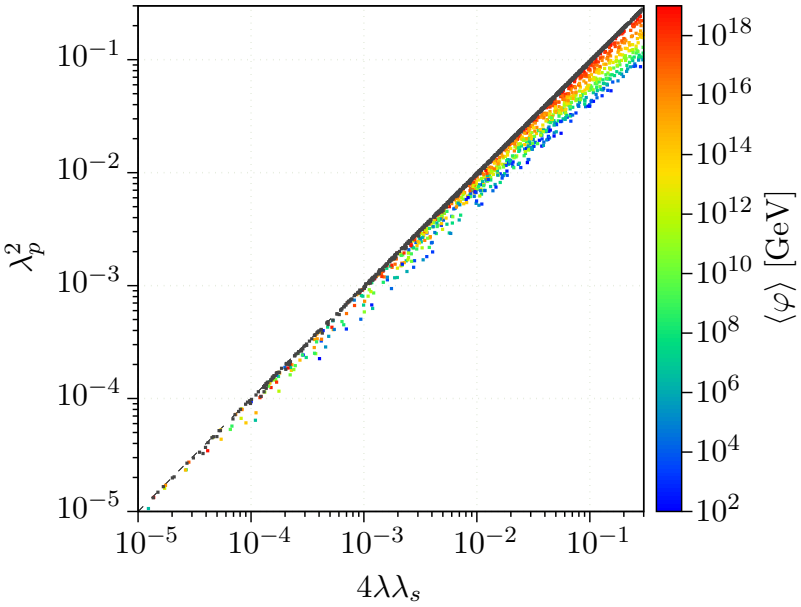

Figure 4.7: Deviation from the Gildener-Weinberg condition for spontaneous symmetry breaking, that is preferred for $\lambda_p < 0$, i.e. $\lambda_p^2 = 4\lambda\lambda_s$ (equivalent to the one in Eq. (4.10)). The colored data points show the initial couplings at Planck scale with the resulting criticality scale, while the black data points denote the couplings evaluated at the condensation scale $\varphi_0 \equiv \langle\varphi\rangle$.

approach reproduces the findings of Gildener-Weinberg we used the *top-down* approach to determine when the scalar couplings would fulfill the GW conditions and found that deviations of the scale and angle of the non-trivial vacuum (φ_0, ϑ_0) were of the $\mathcal{O}(10^{-2})$. Furthermore, to analyze the RG-runnings effect on deviations from Gildener-Weinberg conditions, in Fig. 4.7 we both look at initial deviations from the condition for GW symmetry breaking with non vanishing VEVs for both scalar fields ($\lambda_p < 0$), as well as at the coupling parameters deviations at the critical scale. Here it is seen, that the initial deviations are smoothed out by the renormalization group running of the couplings, such that a smaller initial deviation from the GW condition results in less RG-running until condensation and therefore higher critical scale φ_0.

In conclusion the model of two real and massless scalar fields ϕ and S behaves like

one would expect using the Gildener-Weinberg approximation. This is reproduced by the analysis following our general approach to RSSB, yet it also allowed us to find systematics that are not obvious from a solemn Gildener-Weinberg analysis, e.g. that one needs a hierarchy in initial couplings that is amplified by RG-running to allow for RSSB with $\lambda_p > 0$. Using this more general approach of analysis our results are in agreement with current literature and publications, e.g. Refs. [31, 38]. Yet we do not need to assume a Gildener-Weinberg case like in Ref. [38], where they use this to calculate the explicit exponential scale-separation between high energy renormalization and critical scale and also do not make any statements about the tree-level and one-loop contribution on generically scales as in Ref. [31] but rather acknowledge that RG-running can drastically change the hierarchy between the two terms. While a theory consisting merely of scalar degrees of freedom was expected to behave like described by Gildener and Weinberg we expect that including particles of different spin $s_i \neq 0$ changes this. Particularly including the coupling of gauge groups to the scalars is expected to establish the option of scalar QED like symmetry breaking.

4.2 Two massless scalars one coupled to a $U(1)$ gauge group

After analyzing the symmetry breaking properties of the scalar sector with two real degrees of freedom, we now extend the particle content by charging the scalar ϕ under a $U(1)$ gauge group with charge $Q(\phi) = 1$, gauge field A_μ and gauge coupling g. Still enforcing classical scale-invariance in the Lagrangian leaves us with the massless and real scalar field S and the massless and complex scalar field $\phi = \frac{1}{\sqrt{2}}(\phi_r + i\phi_i)$, which can be expressed by two real scalar fields ϕ_r and ϕ_i, but only has one real degree of freedom, i.e. ϕ_r. Via gauge fixing we choose that only the real degree of freedom acquires a non-vanishing VEV, while the imaginary degree of freedom ϕ_i is (later) "eaten" by the Goldstone boson. This is equivalent to enforcing that the theory is invariant under CP transformation, as the effective potential only depends on the CP-even degree of freedom ϕ_r. As a consequence we consider the theory's Lagrangian to be

$$\mathcal{L} = (D_\mu\phi)^\dagger (D^\mu\phi) + \frac{1}{2}\partial_\mu S \partial^\mu S - V_{\text{tree}}(\phi^\dagger, \phi, S) \,, \tag{4.13}$$

with the covariant derivative $D_\mu\phi$ and the tree-level potential $V_{\text{tree}}(\phi^\dagger, \phi, S)$ given by

$$D_\mu\phi = \partial_\mu\phi - igA_\mu\phi \,, \tag{4.14a}$$

$$V_{\text{tree}}(\phi^\dagger, \phi, S) = \lambda\left(\phi^\dagger\phi\right)^2 + \frac{\lambda_p}{2}\left(\phi^\dagger\phi\right)S^2 + \frac{\lambda_s}{4}S^4 \,. \tag{4.14b}$$

Again we exclude dimension-4 operators that are odd in one of the fields, e.g. ϕS^3, by assuming a $\mathbb{Z}_2$ symmetry and follow the general formalism introduced in Section 3.1 to derive the one-loop effective potential. With only the two real degrees of freedom contributing, the tree-level contribution $\kappa(\vartheta_0; \varphi_0)$ is equal to the one from Eq. (4.4),

with the two contributing fields in spherical coordinates

$$\phi_r = \varphi \sin\vartheta, \qquad S = \varphi \cos\vartheta \ . \tag{4.15}$$

The one-loop terms $A(\vartheta_0;\varphi_0)$ and $B(\vartheta_0;\varphi_0)$, c.f. Eq. (3.9), on the other hand still get the same contributions from field dependent masses given as in Eq. (4.6a), but also gain two additional contributions. A scalar contribution $\hat{m}_3^2(\vartheta;\varphi_0)$

$$\hat{m}_3^2(\vartheta;\varphi_0) = \lambda \sin^2\vartheta + \frac{1}{2}\lambda_p \cos^2\vartheta \ , \tag{4.16}$$

that contributes with the constant $c_3 = \frac{3}{2}$ and multiplicity $n_3 = 1$ and the field dependent mass term $\hat{m}_A^2$ of the gauge boson

$$\hat{m}_A^2(\vartheta;\varphi_0) = g^2 \sin^2\vartheta \ , \tag{4.17}$$

that originates from the kinetic term of ϕ, $(D_\mu\phi)^\dagger (D^\mu\phi)$. It contributes to Eq. (3.9) with the constant $c_A = \frac{5}{6}$ and multiplicity $n_A = 3$. Note again, that the as implicit marked dependency in the field dependent masses denotes that the displayed couplings are subject to RG-running and thus their contributions to the criticality equations depend on the scale φ_0 at which the effective potential develops a non-trivial vacuum. The functions for the running couplings $(\lambda_i(t), g(t))$ are then determined by integrating their β-functions

$$16\pi^2\beta_g = \tfrac{1}{3}g^3 \ , \tag{4.18a}$$
$$16\pi^2\beta_\lambda = 20\lambda^2 + \tfrac{1}{2}\lambda_p^2 - 12\lambda g^2 + 6g^4 \ , \tag{4.18b}$$
$$16\pi^2\beta_{\lambda_s} = 18\lambda_s^2 + \lambda_p^2 \ , \tag{4.18c}$$
$$16\pi^2\beta_{\lambda_p} = 2\lambda_p(4\lambda + 3\lambda_s + 2\lambda_p - 3g^2) \ . \tag{4.18d}$$

Since the resulting functions depend on the choice of initial conditions for the renormalized couplings, some examples are shown in Fig. 4.8. There we see the impact of the gauge coupling g on the running of the scalar couplings, as the g's running itself is only very small as for the case of scalar QED, c.f. Fig. 3.1. It is seen that the RG-running of λ_s is almost not affected, which is what we expected, since β_{λ_s} only depends indirectly through λ_p on the gauge coupling g. Furthermore, the RG-running of the portal coupling is slowed down by the g dependent term of opposite sign in Eq. (4.18) and for a sufficient hierarchy between the gauge coupling g and the scalar couplings the sign of the whole β-function can be changed. This results in $\lambda_p(t)$ increasing in absolute value going to lower t (see upper left and right in Fig. 4.8) instead of decreasing as before. Note that $\lambda_p(t)$ still cannot become negative due to RG-running. If positive at the renomalization scale $\lambda_{p,0} > 0$, then it stays positive at all scales $\lambda_p(t) > 0$, since its β-function has still only terms that contain a factor of λ_p itself (see arguments in Section 4.1). For the quartic coupling λ of the field that is coupled to the gauge group the β-function gains additional terms both with opposite and identical sign with respect to the terms originating from the self- and portal coupling. Since the term with opposite sign is of $\mathcal{O}(\lambda g^2)$, whereas the other term is rather constant and $\mathcal{O}(g^4)$ (as $g(t)$ is quite constant),

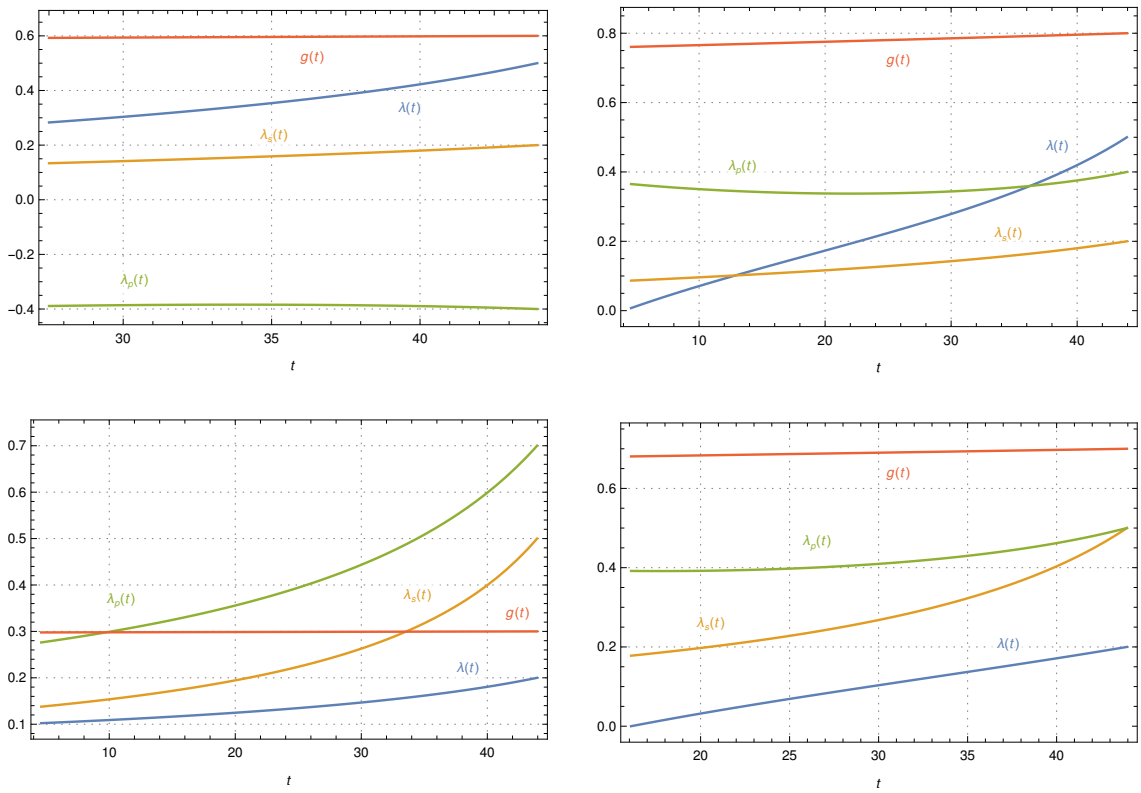

Figure 4.8: The renormalization group running of the Lagrangian couplings $(\lambda(t), \lambda_s(t), \lambda_p(t), g(t))$ in energy range of $[t_{\text{stable}}, t_{\text{Pl}}]$, where the tree-level potential is stable, corresponding to the β-functions from Eq. (4.18). Here displayed with different initial couplings $(\lambda_0, \lambda_{s,0}, \lambda_{p,0}, g_0)$, i.e. upper left: $(0.5, 0.2, -0.4, 0.6)$, upper right: $(0.5, 0.2, 0.4, 0.8)$, lower left: $(0.2, 0.5, 0.7, 0.3)$, lower right: $(0.2, 0.5, 0.5, 0.7)$.

the opposing term dominates for couplings of the same order of magnitude and hence slows down the RG-running of λ. For sufficiently large g_0 it can cause the curvature of $\lambda(t)$ to change its sign, as it is seen in the two right hand plots in Fig. 4.8. But if there exists a hierarchy between the quartic, and portal coupling and the gauge coupling, then the $\mathcal{O}(g^4)$ term dominates and accelerate the decrease of $\lambda(t)$ towards small t. The hierarchy can already be sufficient for both couplings $\mathcal{O}(10^{-1})$. Additionally, the conditions for tree-level and one-loop vacuum stability, as given in Eqs. (4.7) to (4.9) , as well as the Gildener-Weinberg conditions from Eq. (4.10) do not change when one includes coupling to gauge groups of the scalar. Yet the one-loop terms $A(\vartheta_0; \varphi_0)$ and $B(\vartheta_0; \varphi_0)$ change according to the previously introduced additional field dependent masses (see Eqs. (4.16) and (4.17)). Thus, we now can turn to the analysis of non-trivial vacua for different choices of initial conditions at renormalization scale.

As we did in Section 4.1, we start with investigating the systematics of RSSB for initial couplings of the same order of magnitude. For comparability we again choose to vary the initial quartic coupling λ_0 and the portal coupling $\lambda_{p,0}$, while keeping the other quartic coupling $\lambda_{s,0}$ and the gauge coupling g_0 constant. To see the effect of varying g_0 we calculate the condensation scales and angles in Figs. 4.9 to 4.11 for different constant values of initial portal coupling. There we see that the

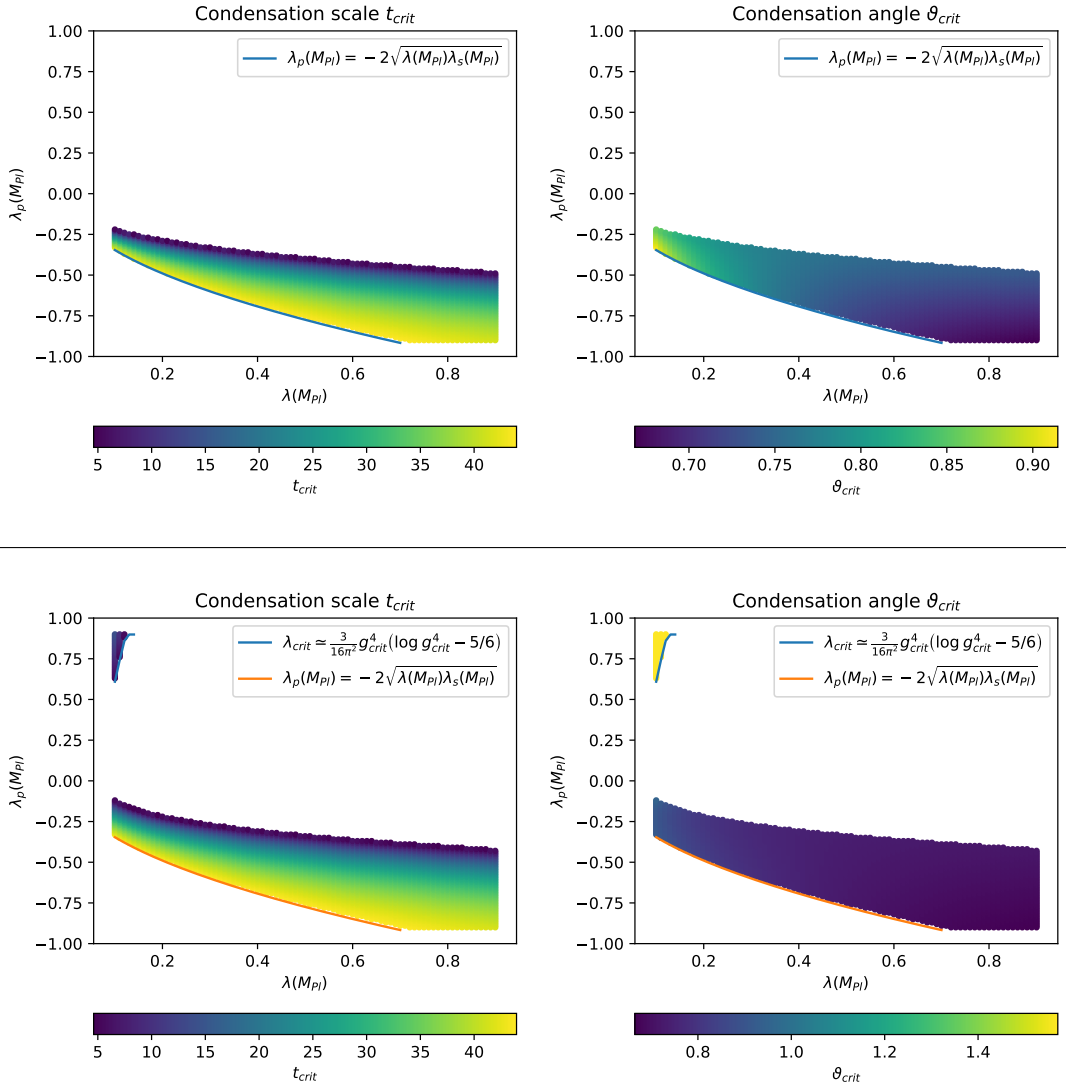

Figure 4.9: Condensation scale and angle depending on the initial portal $\lambda_{p,0}$ and quartic coupling λ_0, with constant $\lambda_{s,0} = 0.3$, $g_0 = 0.2$.(top) and $g = 0.5$ (bottom). Additionally the tree-level stability condition and gauge-breaking bounds are plotted.

calculations with "small" $g_0 = 0.2$ (see Fig. 4.9) give the same results as before in Fig. 4.2, namely only condensation for $\lambda_{p,0} < 0$ at non-trivial angles $\vartheta_{\text{crit}} \neq 0, \frac{\pi}{2}$ and arbitrary scales bound from below and above respectively by stability conditions and truncation of the running scale t at t_{EW}. Now with increasing initial gauge coupling we see that there is condensation possible at positive portal couplings already at values of $g_0 = 0.5$ as seen in Fig. 4.9. This effect is due to the contribution of the gauge coupling to only the one-loop terms such that, in a scalar QED like fashion, the one-loop contributions $A(\vartheta_0; \varphi_0)$ and $B(\vartheta_0; \varphi_0)$ can cancel out the tree-level term $\kappa(\vartheta_0; \varphi_0)$ at the vacuum to fulfill the criticality equations from Eq. (3.12). Thus, when the one-loop contribution of the gauge boson is of equal order of magnitude to

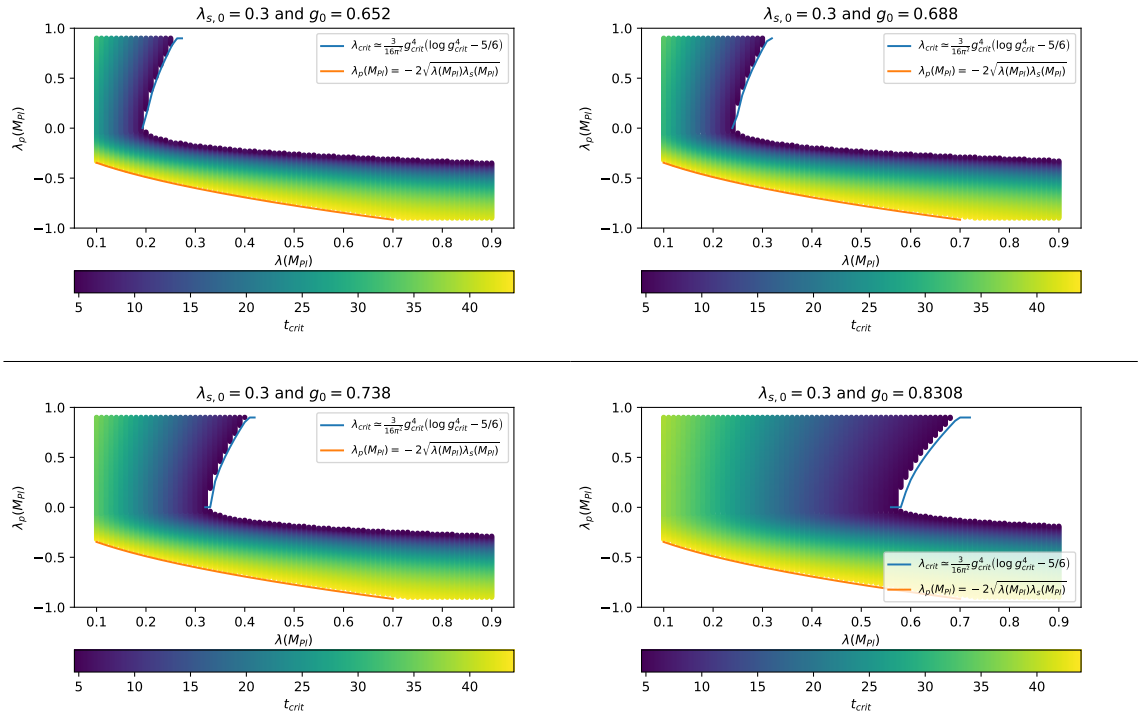

Figure 4.10: Condensation scale t_{crit} depending on the initial portal $\lambda_{p,0}$ and quartic coupling λ_0, with different but constant $\lambda_{s,0}$ and g_0. Additionally, the tree-level stability condition and the gauge-breaking bounds (like in scalar QED) are plotted.

the tree-level contribution of the scalar and hence allow for spontaneous symmetry breaking, we call this *gauge-breaking*. Whereas condensation as seen in Section 4.1 is called *scalar-breaking*. In analogy to RSSB in scalar QED, we expect the due to gauge breaking allowed parameter space to be bound by the condition that at the critical scale

$$\lambda_{crit} \simeq \frac{3}{16\pi^2} g^4_{crit} \left(\ln\, g^2_{crit} - 5/6\right) \ , \tag{4.19}$$

where the right hand side is generally negative, such that the condition contains an implied absolute value for the right hand side, comparing the sizes of the contributions rather than their sign. Therefore, in Figs. 4.9 to 4.11 we plotted the lowest possible $\lambda_{p,0} > 0$ for which the condition in Eq. (4.19) can still be fulfilled through RG-running up to t_{EW}. The scale dependence of this condition is nicely displayed in Fig. 4.10 where we see that the lowest possible breaking scale from our calculations fits very nicely the above explained condition that is plotted as a the red line. Note, that there would actually be a $\sin^2 \vartheta_0$ dependency in the natural logarithm of Eq. (4.19), but via the most attractive channel argument, the first scale that allows for SSB is always the one with maximal gauge contribution, hence $\vartheta_0 = \frac{\pi}{2}$. For further investigation Figs. 4.10 and 4.11 display the effect of increasing initial gauge coupling's fourth power g_0^4 in a linear way. Given the condition in Eq. (4.19), we expect the allowed condensation parameter space to depend on g_0^4 such that critical scale and angle are displayed for $g_0 = 0.652, 0.688, 0.738, 0.8308$, which is confirmed

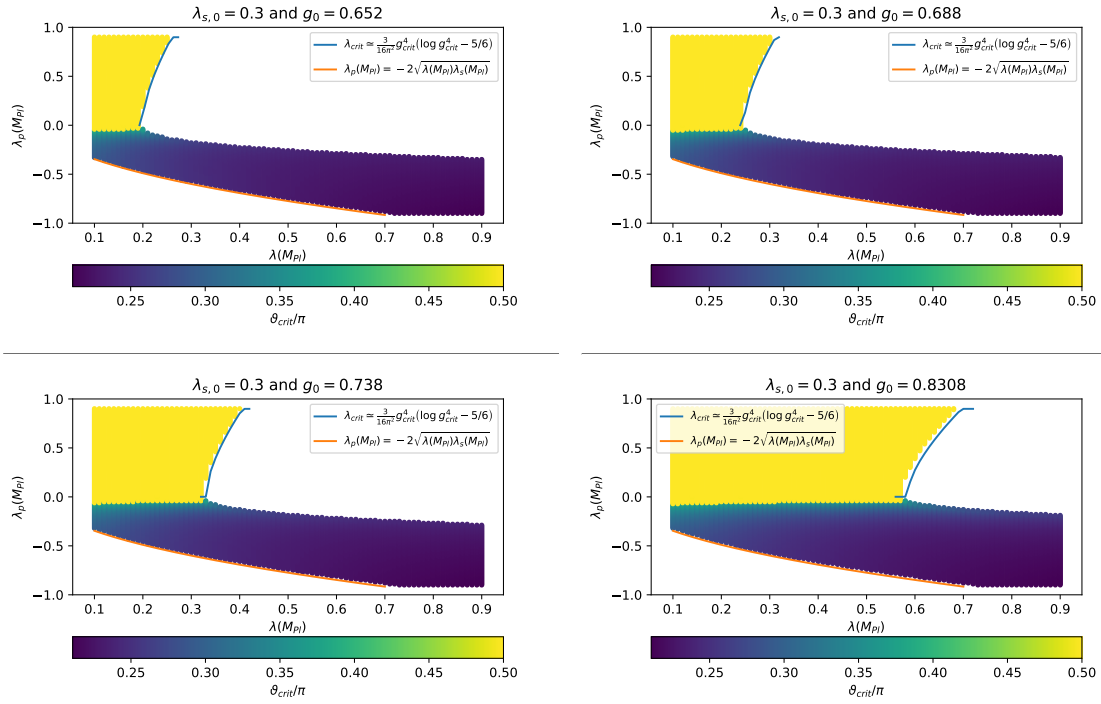

Figure 4.11: Condensation angle ϑ_{crit} depending on the initial portal $\lambda_{p,0}$ and quartic coupling λ_0, with different but constant $\lambda_{s,0}$ and g_0. Additionally, the tree-level stability condition and the gauge-breaking bounds are plotted.

by Figs. 4.10 and 4.11. Looking specifically at the angles of condensation for initial couplings of the same $\mathcal{O}(10^{-1})$ as displayed in Fig. 4.11 we see that there is a clear separation between *scalar-* and *gauge-breaking*. The *gauge-breaking* is only possible in the direction of the field that is coupled to the gauge group, here $\phi_r = \varphi \sin\vartheta$, resulting in a condensation angle of $\vartheta_0 = \frac{\pi}{2}$. This can be understood in different ways, in the case of our criticality equations the angle $\vartheta_0 = \frac{\pi}{2}$ means that both ϕ_r and A_μ contribute maximally to the equations, while S does not contribute. Therefore, the tree-level is dominated by λ and the one-loop terms by $g^4 \ln g^2$ with "small" $\lambda_p^2 \ln \lambda_p$ contributions. Deviating from this angle, the tree-level would gain contributions that are proportional to λ_p and λ_s, whereas the one-loop level only gains additional terms proportional to λ_p^2 and λ_s^2, resulting in an even larger discrepancy that would need "more" RG-running such that tree-level and one-loop terms are of the same magnitude and hence induce symmetry breaking, by fulfilling the criticality conditions Eq. (3.12). This means solutions for $\lambda_p > 0$ and non-trivial angles $\vartheta_0 \neq 0, \frac{\pi}{2}$ are in general possible but spontaneous symmetry breaking was already induced by quantum corrections at a higher scale, leaving it unclear how the theory evolves in the phase of spontaneously broken conformal symmetry. This opens up a whole different discussion about possible sequential symmetry breaking (or *Coleman-Weinberg tumbling*), which would need some more time to investigate and is beyond the scope of this work. Another way to understand that, *gauge-breaking* only occurs at trivial angles $\vartheta_0 = 0, \frac{\pi}{2}$ for positive critical portal couplings is to look at the geometry of the one-loop effective potential. Here, we have the usual quartic

rising tree-level with only a minimum at the origin that gains a negative contribution from the quantum corrections induced by the gauge field A_μ. But since the gauge field is only coupled to one of the scalars (here ϕ) its contribution is orientated along the axis of the scalar ϕ and therefore, if large enough, can only induce non-trivial minima in the direction of the field.

Because of the homogeneous breaking along $\vartheta_0 = \frac{\pi}{2}$ for $\lambda_p > 0$, the structure in the $\lambda_p < 0$ region of the plots in Fig. 4.11 is not accessible with respect to the analysis of critical angles. Therefore, in Fig. 4.12 the parameter region for $\lambda_p < 0$ and breaking along angles $\vartheta_0 \neq \frac{\pi}{2}$ is shown at the example of $\lambda_{s,0} = 0.3$ and $g_0 = 0.8308$. There we see, that the structure is similar to *scalar-breaking* of the

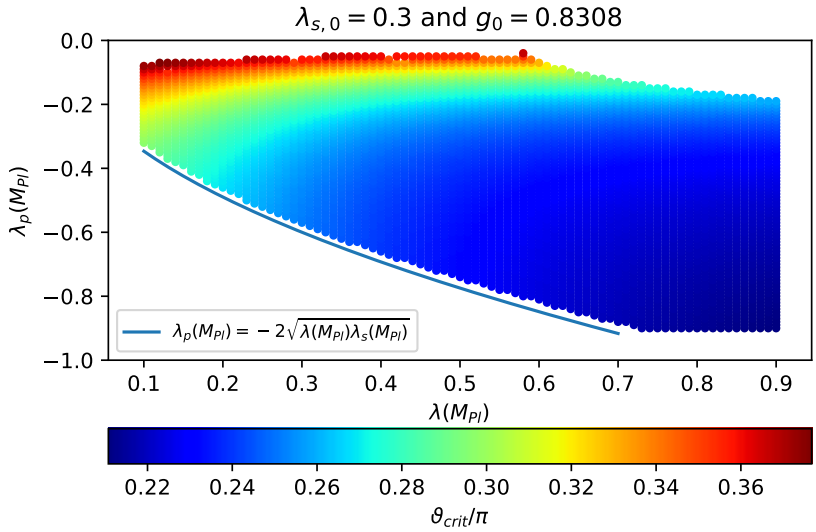

Figure 4.12: The critical angles ϑ_{crit} depending on initial portal $\lambda_{p,0} > 0$ and quartic coupling λ_0, for constant $\lambda_{s,0} = 0.3$ and $g_0 = 0.8308$. Additionally the lower bound, given by tree-level stability of the potential, is plotted.

conformal two massless scalar model, c.f. Fig. 4.5, yet the range of critical angles has dramatically increased from $\Delta\theta \approx 0.08\pi$ to $\Delta\vartheta_{\text{crit}} \approx 0.15\pi$, and is not centered around $\frac{\pi}{4}$ but rather shifted towards $\frac{\pi}{2}$. This result matches nicely with what we would have expected with the explanation above. On the one hand we still have the tree-level mechanism of flat direction dominating the properties of symmetry breaking, which prefers maximal tree-level cancellations, hence for $\lambda_{s,0} = 0.3$ critical angles around $\vartheta_0 \approx \frac{\pi}{4}$ and on the other hand we have the quantum one-loop effects that are still suppressed enough to not dominate SSB but pull towards the axis of the ϕ_r field. Since this effect is not linear in λ_p, λ but rather scales like g^4, which has a big impact on the RG-runnings of the scalar couplings. It results in a shift towards higher critical angles and an extension of the range of possible breaking angles. Furthermore, looking at the distribution of critical scale φ_0 in the region of possible RSSB for given g_0 (see Fig. 4.10), we see that the parameter space of condensation is bound from the upper right and from the lower left. The boundary in the lower left given by the tree-level stability condition (or the GW-condition),

as already discussed above in Section 4.1, is not altered by the introduction or variation of g_0, since the tree-level stability conditions do not change. Unlike this, the boundary to the upper right does depend strongly on g^4, as it denotes how much deviation from the Gildener-Weinberg condition (in the *scalar-breaking* case) can be compensated by the RG-running and what value of $\lambda_{p,0}$ is necessary for RG-running to still allow the couplings to fulfill the breaking condition of *gauge-breaking* from Eq. (4.19). For sufficiently large g_0 the RG-running of λ is accelerated towards lower scales which results in the fact that points with larger initial deviations from the GW condition still allow for SSB at scales $\approx t_{\text{EW}}$, yet since only the RG-running of λ is accelerated while the running of λ_s stays the same, at the same time the angle for maximal cancellation is shifted towards $\frac{\pi}{2}$. Comparing our results with a Gildener-Weinberg type analysis, we find (up to uncertainties) the same features of e.g. allowed SSB for positive portal coupling and renormalization values of the same order for the couplings. The plots for comparison are found in Appendix A.4. Initially it seemed surprising that Gildener and Weinberg, demanding a flat direction in the scalar tree-level potential, also fully includes the coupling to a another particle sector just because the RG-running of the scalar couplings depend on it. This however just enhances the significance RG-running has in the context of RSSB in conformal symmetric models and shows that so far even though our approach seems more general the non-scalar sector is not prominent enough to disturb the scalar sector that so far is dictating the properties of radiatively generated non-trivial minima. On the other hand we now have two different formalisms in which we can understand the calculated features of symmetry breaking to understand the fundamental characteristics of exponential scale generation in classically scale-invariant theories. Varying the second initial quartic coupling to $\lambda_{s,0} = 0.5$ has the same effect as already in Section 4.1, which is expected as it does not couple to the gauge field A_μ. We display the corresponding plots in the same manner as above but for $\lambda_{s,0} = 0.5$ and $g_0 = 0.5$ in Appendix A.4.

Turning towards the analysis of renormalized couplings with possible initial hierarchy (orders of magnitudes), we again generate individual random values for the initial scalar couplings $\lambda_{i,0} \in [10^{-5}, 1]$ and gauge coupling $g_0 \in [10^{-2}, 1]$. With our results so far pointing towards a g_0^4 dependency for symmetry breaking properties, the gauge coupling is only varied to lowest value of 10^{-2}, even though initial couplings $g_0^4 = \mathcal{O}(10^{-8})$, result in condensation like in the two massless scalar model, c.f. Section 4.1. The corresponding possible non-trivial vacua are shown in Fig. 4.13, where we distinguish between cases with negative and with positive portal coupling λ_p. There we see similar structures to the case only containing two massless scalars, c.f. Fig. 4.5, but we also see deviations, e.g. for positive portal couplings at the condensation scale. There are only a few points with non-trivial critical angles $\vartheta_{\text{crit}} \neq 0, \frac{\pi}{2}$ while the rest only allow for SSB along one of the fields and hence can be denoted as Gildener-Weinberg like symmetry breaking. Furthermore, we see the already discussed effect of the gauge contribution pulling the angle of condensation towards breaking along ϕ_r and hence angles of $\vartheta_{\text{crit}} \approx \frac{\pi}{2}$. With just the two massless scalars in Fig. 4.5 there was a symmetrical gap between points of non-trivial vacua and the critical angles $\vartheta_{\text{crit}} = 0, \frac{\pi}{2}$, whereas coupling only one scalar to a gauge group introduces an asymmetry in contributions such that this symmetrical gap is

now highly asymmetric, i.e. towards $\frac{\pi}{2}$ there is no gap anymore, while the gap towards 0 seems unchanged. Furthermore, it can be seen that condensation in general becomes more "natural" when adding a gauge group, since the number of points that allow for non-trivial vacua has roughly doubled compared to the case of the two massless scalars, from around 5% to roughly 10%. Now investigating the con-

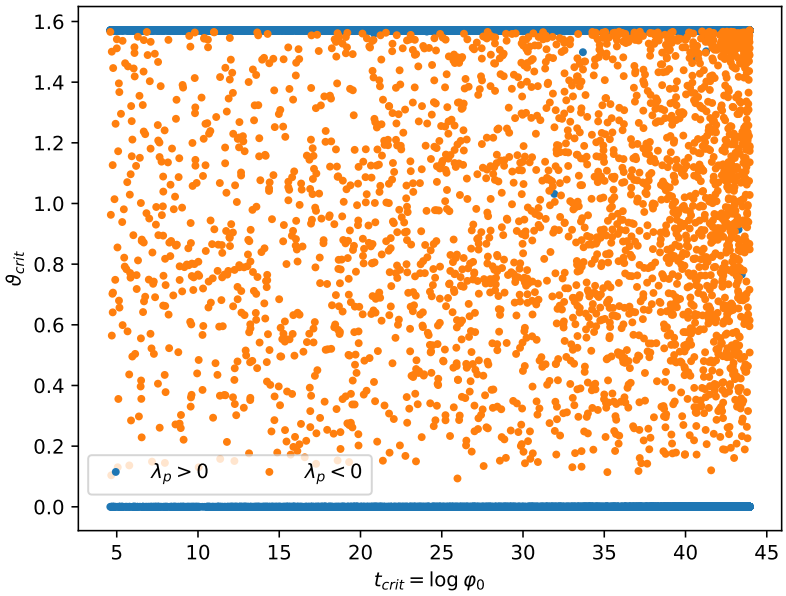

Figure 4.13: The critical angles ϑ_{crit} and scales t_{crit} that are allowed by randomly chosen individual initial couplings. The points are separated by the sign of the portal coupling at condensation scale.

densation for non-trivial angles and positive portal couplings, we find that almost all observed points have initial couplings of "large" gauge coupling $g_0 = \mathcal{O}(10^{-1})$, smaller initial quartic coupling $\lambda_0 = \mathcal{O}(10^{-2})$ and suppressed portal as well as other quartic coupling $\lambda_{p,0}, \lambda_{s,0} = \mathcal{O}(10^{-5})$. Therefore, we again look at points of possible condensation with $\lambda_p > 0$ for initial couplings in the ranges $\lambda_0 \in [10^{-3}, 1]$, $\lambda_{s,0}, \lambda_{p,0} \in [10^{-4}, 10^{-6}]$ and $g_0 \in [10^{-1}, 1]$ and display the results in Fig. 4.14. Here we see that there is still the GW condensation in the direction of ϕ_r and hence $\vartheta_{\text{crit}} = \frac{\pi}{2}$ but also a lot more allowed vacua for non-trivial angles. Their distribution is (highly) focused to the upper right corner, meaning that even though there are deviations from the non-trivial GW condensation-angle, they are mostly very small and in cases where the theory almost instantly spontaneously breaks the classical scale-invariance of the model. Further analysis of the properties of these points yield, that they are somewhat numerically unstable, in the sense that up to numerical uncertainties both criticality equations (c.f Eq. (3.12)) are zero for a range of angles, that include $\frac{\pi}{2}$, and scales. Sadly, a more analytic approach of treating $\lambda_s(t_{\text{crit}}), \lambda_p(t_{\text{crit}})$ as small perturbations and expanding the criticality equations around zero was not successful in explaining the observed data points for condensation at non-trivial angles in the case of $\lambda_p(t_{\text{crit}}) > 0$, whether they are a physical

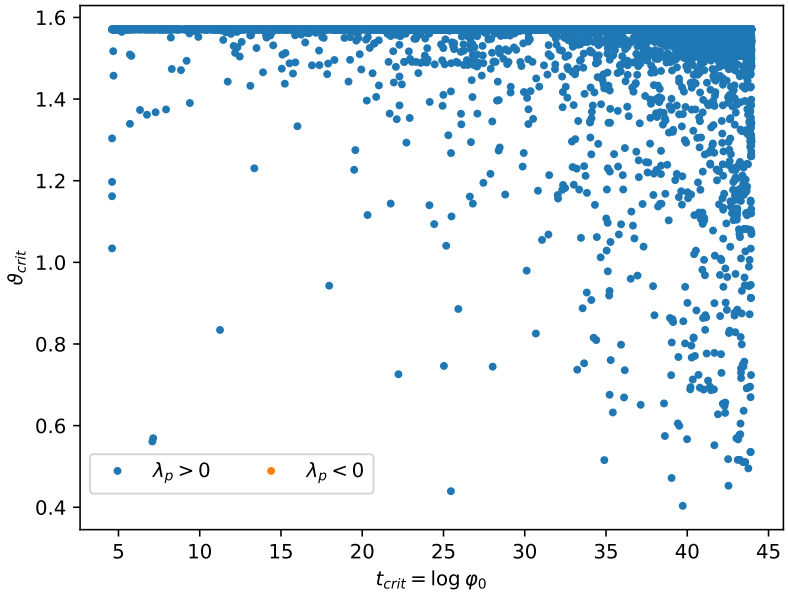

Figure 4.14: The critical angles ϑ_{crit} and scales t_{crit} that are allowed by randomly chosen individual initial couplings $\lambda_0 \in [10^{-3}, 1]$, $\lambda_{s,0}, \lambda_{p,0} \in [10^{-4}, 10^{-6}]$ and $g_0 \in [10^{-1}, 1]$. The initial portal coupling and therefore the portal coupling at all t is chosen to be positive.

feature or purely numerical. At this point, using the previous arguments and results, we figure that the observed points are rather due to numerical uncertainties than of physical effects. The most prominent argument for this interpretation is the fact, that the maximal contribution of the gauge boson is aligned along the coupled scalar contribution of ϕ_r, such that it can only induce non-trivial minima along a ray parallel to ϕ_r, i.e. $\frac{\pi}{2}$, as the one-loop contributions are generally suppressed, such that the maximal contribution is necessary. With this argument we would expect the situation to change if one couples the other scalar S also to a gauge group ($U(1)$), either to the same one or to an individual one. In Sections 4.3 and 4.4 we analyze these two cases with respect to the already obtained results for RSSB with gauge and scalar particle content.

With the results from the "linear scans", that we can distinguish between *gauge-* and *scalar-breaking*, we want to analyze how those statements transfer to initial couplings of different order of magnitude. Hence, in Fig. 4.15 we investigate how the critical scales and angles $(t_{\text{crit}}, \vartheta_{\text{crit}})$ dependence on the initial quartic λ_0 and gauge coupling g_0^4, motivated by the condition for *gauge-breaking* from Eq. (4.19). For reasons of clarity we split the analysis by whether the portal coupling λ_p is positive or negative. In the plots displaying the angles of condensation (right hand side) we nicely see the separation between *scalar-* and *gauge-breaking*, as the feature (dark red) that roughly corresponds to $\lambda_0 \approx g_0^4$ and can be identified with fulfilling the condition for *gauge-breaking* from Eq. (4.19) at the vacuum. Furthermore, outside the parameter region of *gauge-breaking* we find the usual properties of *scalar-breaking*

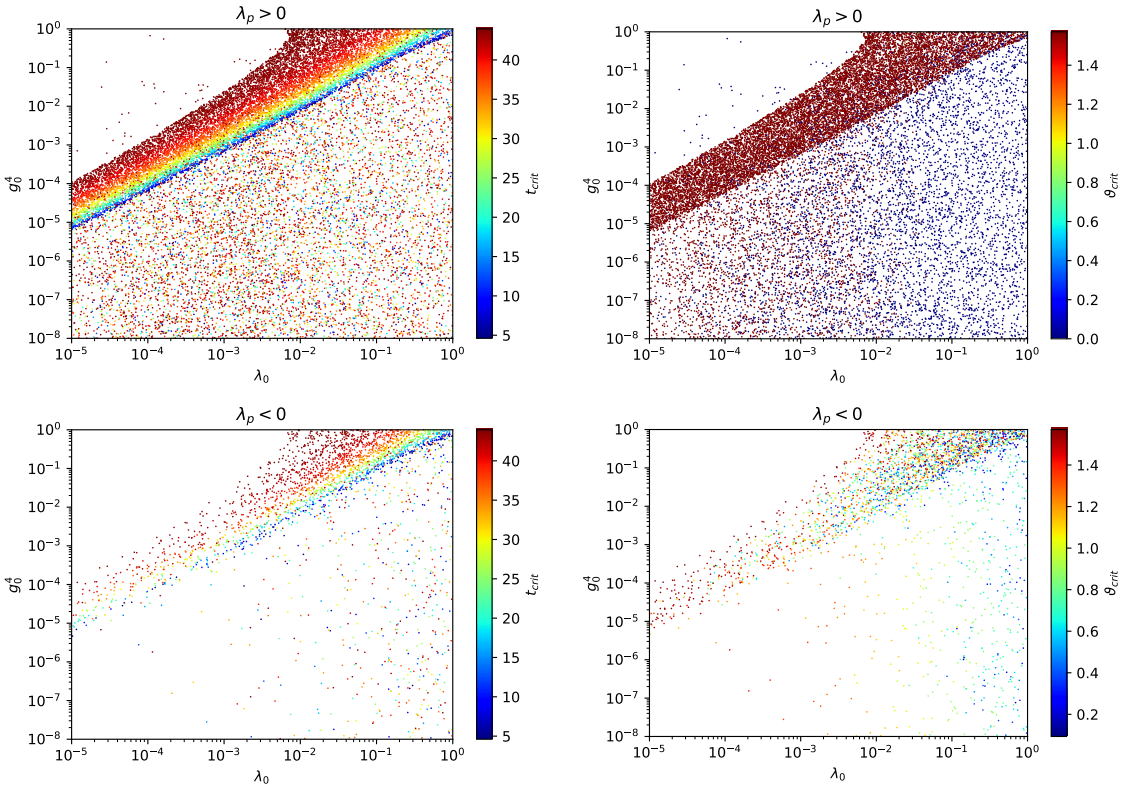

Figure 4.15: The critical angles ϑ_{crit} and scales t_{crit} that are allowed by randomly chosen individual initial couplings $\lambda_{i,0} \in [10^{-5}, 1]$, and $g_0 \in [10^{-2}, 1]$. The initial portal coupling and therefore the portal coupling at all t is chosen to be positive in the upper two plots, while it is negative in the lower two .

like discussed above and also in Section 4.1, i.e. only breaking along one of the fields for $\lambda_p > 0$ and along non-trivial angles for $\lambda_p < 0$. On the other hand, the plots displaying the critical scales, or radial location of the vacua, t_{crit} (left hand side), show the same features that with the analysis of the critical angle can be assigned either the type of *gauge-* or *scalar-breaking*. The upper left feature of *gauge-breaking* displays again the region allowed due to RG-running. Starting off from the upper left with the highest scale, where the *gauge-breaking* condition and therefore also the criticality equations from Eq. (3.12) are almost immediately fulfilled we see the boundary set by truncating RG-running at t_{EW}. The boundary is set to show the lowest g_0^4 that allows for condensation for a given λ_0, which would extend with "longer" RG-running, since $\lambda(t)$ decreases faster towards lower t than g^4 as seen in the β-functions in Eq. (4.6). In the region of *scalar-breaking* the fulfillment of the criticality equations and therefore the scale at which the non-trivial minimum is induced t_{crit}, depends much more on the initial second quartic $\lambda_{s,0}$ and portal coupling $\lambda_{p,0}$. Since these are random for every data point in the plot it is expected to not see any (smooth) structure in the distribution of critical scales in the *scalar-breaking* region of these plots. These results are well reproduced by an analysis in the Gildener-Weinberg formalism, where one has to additionally account for the case that the full one-loop effective potential might be dominated entirely by the quantum corrections of the gauge sector (this could be the case for the region above

the *gauge-breaking* feature), such that the Gildener-Weinberg method might find a non-trivial minimum, which would violate potential stability at one-loop level, i.e. render the effective potential imaginary at the vacuum.

In conclusion, we saw that including the simplest gauge group coupled to only one of the scalars creates an asymmetry that allows for *gauge-breaking* along the coupled scalar field. Therefore, it allows condensation for initial couplings of the same order of magnitude for positive portal couplings. Thus, we can determine the regions of *scalar-* and *gauge-breaking* by analysis of the critical angle and comparison with the results from the model of two massless scalars in Section 4.1. Here we want to note, that in some cases it can be easily distinguished that the SSB properties of the theory are dominated by *gauge-breaking*, while for other cases one has to account for a mixed state of the two, e.g. seen in Fig. 4.12 where we are in a *scalar-breaking* case but the range of angles is broadened by the influence of the gauge sector. Another effect of including a gauge group is the amplification of the RG-running of the scalar coupling such that even the allowed region for *scalar-breaking* increases. This leads us to believe that our approach is well suited to describe RSSB in a more general way including the contributions of the gauge sector explicitly in the criticality equations while at the same time accounting for the renormalization group running. At last, we find that a classically scale-invariant multiscalar theory gains new ways of scale generation (*gauge-breaking*) and needs less fine-tuning in the initial conditions for the generation of exponential scale hierarchies by introducing (even) a simple gauge group.

4.3 Two scalars coupled to the same $U(1)$ gauge group

Now coupling both scalars ϕ and S to the same $U(1)$ gauge group with general charges $Q(\phi) = q_\phi$ and $Q(S) = q_s$ renders them both complex

$$\phi = \frac{1}{\sqrt{2}}\left(\phi_r + i\phi_i\right), \qquad S = \frac{1}{\sqrt{2}}\left(S_r + iS_i\right) \ , \tag{4.20}$$

where ϕ_r, ϕ_i, S_r, S_i are real scalar fields that respectively denote the complex field's real and imaginary degree of freedom. Like before, we disregard any dimension-4 operators that are of an odd power in one of the fields by assuming a $\mathbb{Z}_2$ symmetry between the fields, such that the Lagrangian with the corresponding tree-level potential and covariant derivatives are given by

$$\mathcal{L} = \left(D_\mu\phi\right)^\dagger \left(D^\mu\phi\right) + \left(D_\mu S\right)^\dagger \left(D^\mu S\right) - V_{\text{tree}}(\phi^\dagger, \phi, S^\dagger, S) \ , \tag{4.21a}$$

$$V_{\text{tree}}(\phi^\dagger, \phi, S^\dagger, S) = \lambda\left(\phi^\dagger\phi\right)^2 + \lambda_p\left(\phi^\dagger\phi\right)\left(S^\dagger S\right) + \lambda_s\left(S^\dagger S\right)^2 \ , \tag{4.21b}$$

$$D_\mu\phi = \partial_\mu\phi - iq_\phi g A_\mu\phi \ , \tag{4.21c}$$

$$D_\mu S = \partial_\mu S - iq_s g A_\mu S \ . \tag{4.21d}$$

By fixing the gauge accordingly we choose only the real degrees of freedom of the scalar fields to acquire a non-vanishing VEV and consequently only get tree- and one-loop level contributions that depend on ϕ_r and S_r. They given in the 2d

spherical coordinates

$$\phi_r = \varphi \sin\vartheta, \qquad S_r = \varphi\cos\vartheta \ . \tag{4.22}$$

As a result the general angular tree-level contribution $\kappa(\vartheta;\varphi_0)$ does not change compared to the one in Eq. (4.4). On the other hand, the gauge fields contribution $\hat{m}_A^2(\vartheta;\varphi_0)$ to the one-loop terms $A(\vartheta;\varphi_0)$ and $B(\vartheta;\varphi_0)$ changes to be charge dependent

$$\hat{m}_A^2(\vartheta;\varphi_0) = g^2\left(q_\phi^2\sin^2\vartheta + q_s^2\cos^2\vartheta\right) \ , \tag{4.23}$$

while scalar contributions still consist of $\hat{m}_\pm^2(\vartheta;\varphi_0), \hat{m}_3^2(\vartheta;\varphi_0)$ as given in Eqs. (4.6a) and (4.16) plus an additional contribution by $\hat{m}_4^2(\vartheta;\varphi_0)$

$$\hat{m}_4^2(\vartheta;\varphi_0) = \lambda_s\cos^2\vartheta + \frac{1}{2}\lambda_p\sin^2\vartheta \ . \tag{4.24}$$

Determined by the spin of their corresponding fields the masses $\hat{m}_\pm^2(\vartheta;\varphi_0)$, $\hat{m}_3^2(\vartheta;\varphi_0)$, $\hat{m}_4^2(\vartheta;\varphi_0)$ contribute with multiplicity $n_i = 1$ and constants $c_i = \frac{3}{2}$ $(i = \pm, 3, 4)$ and $\hat{m}_A^2(\vartheta;\varphi_0)$ with $n_A = 3$, $c_A = \frac{5}{6}$. As usual the implicit scale dependency marked with the semi-colon in all the quantities denotes that the couplings are subject to RG-running, such that the above contributions depend on the scale of evaluation, which is following the approach in Section 3.1 already chosen to be the scale of condensation φ_0. The mentioned RG-running of the couplings is determined by their β-functions, which in this theory are calculated to be

$$16\pi^2\beta_g = \frac{q_\phi^2 + q_s^2}{3}g^3 \ , \tag{4.25a}$$

$$16\pi^2\beta_\lambda = 20\lambda^2 + \lambda_p^2 - 12q_\phi^2\lambda g^2 + 6q_\phi^4 g^4 \ , \tag{4.25b}$$

$$16\pi^2\beta_{\lambda_s} = 20\lambda_s^2 + \lambda_p^2 - 12q_s^2\lambda_s g^2 + 6q_s^4 g^4 \ , \tag{4.25c}$$

$$16\pi^2\beta_{\lambda_p} = 2\lambda_p\left(2\lambda_p + 4\lambda + 4\lambda_s - 3(q_\phi^2 + q_s^2)g^2\right) + 12q_\phi^2 q_s^2 g^4 \ . \tag{4.25d}$$

Here we already see, that the only difference in the RG-running of λ and λ_s is determined by the ratio of their charges q_ϕ and q_s with respect to their common $U(1)$ gauge group. Having already discussed the effect a gauge group has on the coupled scalars RG-running, c.f. Fig. 4.8, we discuss examples of fields that are charged asymmetrically $q_\phi \neq q_s$ under their gauge group in Fig. 4.16. With the β-functions given in Eq. (4.25), the RG-runnings displayed in Fig. 4.16 confirm what we expect, i.e. that the quartic couplings $\lambda(t)$ and $\lambda_s(t)$ now both behave individually like the quartic coupling λ in Section 4.2, whereas the portal coupling's behavior becomes more complex than before. Due to the additional term, λ_p does not renormalize in a multiplicative way anymore, such that it can change its sign throughout RG-running. This is a fundamental difference to the models before and consequently we now need to check whether the portal coupling is indeed still positive at the scale of condensation when setting it initially to $\lambda_{p,0}$. This is displayed in the context of the analysis of non-trivial condensation angles for positive portal coupling at the critical scale in Figs. 4.17 and 4.18. With the full description of the theory we turn to

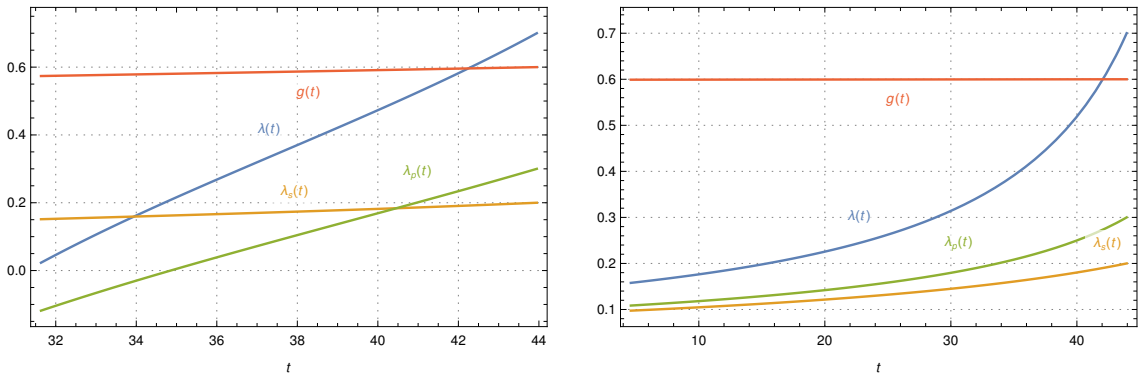

Figure 4.16: The Lagrangian couplings $(\lambda(t), \lambda_s(t), \lambda_p(t), g(t))$ in $[t_{\text{stable}}, t_{\text{Pl}}]$ corresponding to the β-functions from Eq. (4.25). Here displayed with different charges under the field's $U(1)$ gauge group $Q(\phi, S) = (2, 1)$ (left) and $Q(\phi, S) = (0.2, 0.1)$ (right). The renormalized couplings are chosen to be $(\lambda_0, \lambda_{s,0}, \lambda_{p,0}, g_0) = (0.7, 0.2, 0.3, 0.6)$.

inspect the results for randomly set initial couplings of (potentially) different orders of magnitude like in Fig. 4.13, which are displayed for equal charges $q_\phi = q_s = 1$ in Fig. 4.17 and for asymmetric field charges $q_\phi = 1,\ q_s = 2$ in Fig. 4.18. Comparing the plots in Fig. 4.17 where the points are separated by the corresponding initial portal coupling's sign (left) with the ones where they are separated by the portal coupling's sign at the critical scale (right) we see that, up to very few points (like before), condensation for non-trivial angles only takes place for negative critical portal coupling. Since, equal charges of the fields under the gauge group lead to angle invariance of the gauge contribution to the one-loop effective potential

$$\text{if } q_\phi = q_s = q \qquad \Rightarrow \qquad \hat{m}_A^2(\vartheta; \varphi_0) = g^2 q^2 \equiv \hat{m}_A^2(\varphi_0)\ , \tag{4.26}$$

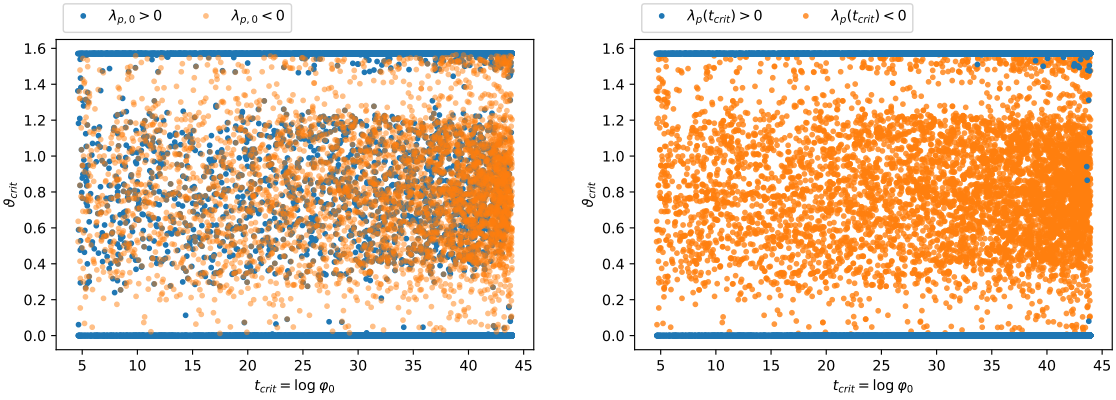

Figure 4.17: The critical angles ϑ_{crit} and scales t_{crit} that are allowed by randomly chosen individual initial couplings $\lambda_{i,0} \in [10^{-5}, 1]$ and $g_0 \in [10^{-2}, 1]$. The points are separated by the sign of the portal coupling at condensation scale and the fields' charges under the $U(1)$ gauge group are $Q(\phi) = Q(S) = 1$.

we expect that this leads to problems fulfilling the criticality equations. Because of $\hat{m}_A^2$ being angle independent the gauge boson's contribution drops out of the second criticality equation, c.f. Eq. (3.12b), such that we are only left with contributions from the theory's scalar sector that cannot allow for non-trivial angles of condensation as already discussed and seen in Section 4.1. Therefore, we chose unequal or asymmetric charges which results (Fig. 4.18) in a picture similar to the one from Section 4.2 with two massless scalars where only one is coupled to the gauge group, c.f. Fig. 4.13. In addition to numerical uncertainties for these points of non-trivial critical angles for $\lambda_p(t_{\text{crit}})$, (almost) all of them are now at scales $t_{\text{crit}} \approx t_{\text{Pl}}$, such that one always has to account for the possibility that these points of condensation are rather numerical solutions at the boundaries of parameter space than actually physical. At this point we can already infer that by not seeing the desired points

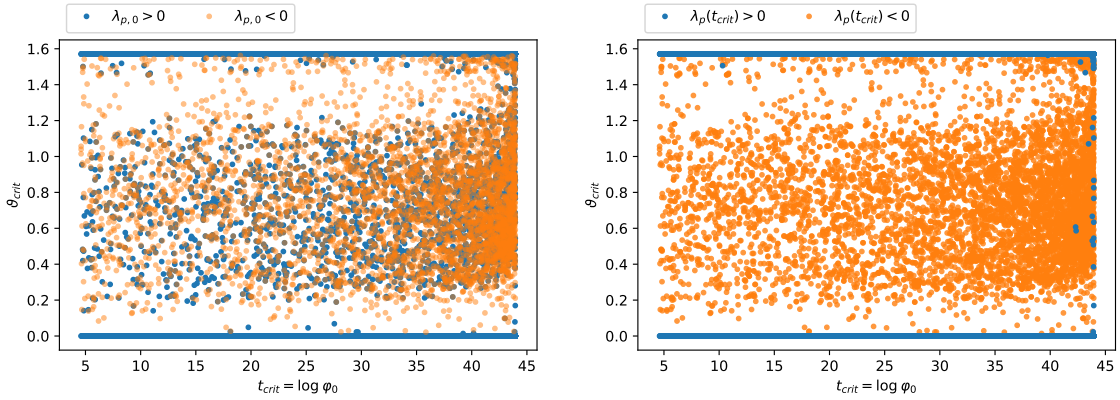

Figure 4.18: The critical angles ϑ_{crit} and scales t_{crit} that are allowed by randomly chosen individual initial couplings $\lambda_{i,0} \in [10^{-5}, 1]$ and $g_0 \in [10^{-2}, 1]$. The points are separated by the sign of the portal coupling at condensation scale and the fields' charges under the $U(1)$ gauge group are $Q(\phi) = 1$ and $Q(S) = 2$.

of non-trivial angles for positive critical portal couplings so far, they are either not allowed in this toy-model or they are associated with necessary fine-tuning. Therefore, they are only conceptional interesting for our analysis to distinguish when the non-scalar sector of the theory becomes "important" enough to induce effects that are qualitatively new and not considered by an analysis via the Gildener-Weinberg approximation. To see when this is the case we turn to two massless complex scalars that are each coupled to an individual $U(1)$ gauge group in Section 4.4.

Furthermore, we also see the effect of unequal or asymmetrical coupling in Fig. 4.18 as the condensation points with a non-trivial angle $\vartheta_{\text{crit}} \neq 0, \frac{\pi}{2}$ are "drawn" towards the direction of the more strongly coupling field S. Further investigation of this asymmety is done for couplings of with random orders of magnitudes $\lambda_{i,0} \in [10^{-5}, 1]$ and $g_0 \in [10^{-2}, 1]$ and equal charges $q_\phi = q_s = 1$ in Figs. A.6 and A.7. We see that there is the same structure of *gauge-breaking* as seen in Fig. 4.15, but now for both of the initial quartic couplings λ_0 and $\lambda_{s,0}$. For reasons of visibility we again separated the points of positive and negative critical portal coupling. For the points of positive portal coupling we expect either *gauge-breaking* identically along ϕ ($\vartheta_{\text{crit}} = \frac{\pi}{2}$) or S ($\vartheta_{\text{crit}} = 0$). For fields with equal charges we would expect a smooth transition of angles in the case of negative portal couplings, as they now

lack a preferred direction, since both *scalar-* as well as *gauge-breaking* are now symmetrical in the couplings λ and λ_s. This is confirmed in Fig. 4.19, where we exactly see a sharp distinction at the line of equal initial couplings $\lambda_0 = \lambda_{s,0}$ for the angle of condensation in the $\lambda_{p,0} > 0$ case (left) and the expected smooth transition with the symmetrical angle $\vartheta = \frac{\pi}{4}$ for equal initial couplings $\lambda_0 = \lambda_{s,0}$ and $\lambda_{p,0} < 0$ (right). Now choosing asymmetric charges for the fields, i.e. $q_\phi = 1$ and $q_s = 2$ as seen in Fig. 4.20, we find that the structures only slightly shift towards the corner of large λ and small λ_s. This can be understood by looking at the individual terms in the

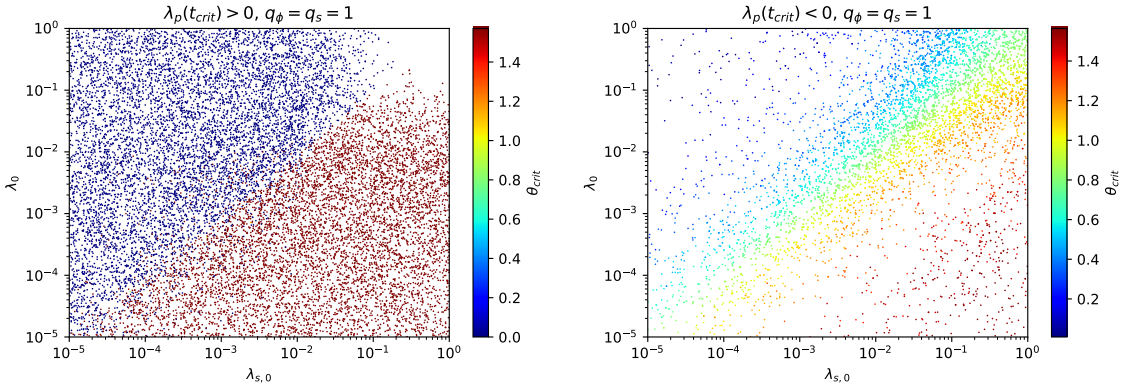

Figure 4.19: The critical angles ϑ_{crit} that are allowed by randomly chosen individual initial couplings $\lambda_{i,0} \in [10^{-5}, 1]$ and $g_0 \in [10^{-2}, 1]$. The points are separated by the sign of the portal coupling at condensation scale, $\lambda_{p,0} > 0$ (left) and $\lambda_{p,0} < 0$ (right).

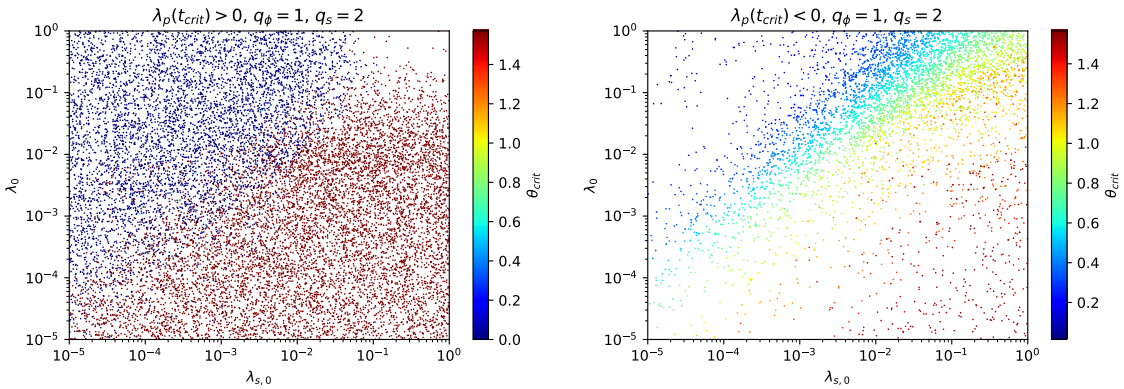

Figure 4.20: The critical angles ϑ_{crit} that are allowed by randomly chosen individual initial couplings $\lambda_{i,0} \in [10^{-5}, 1]$ and $g_0 \in [10^{-2}, 1]$. The points are separated by the sign of the portal coupling at condensation scale, $\lambda_{p,0} > 0$ (left) and $\lambda_{p,0} < 0$ (right).

criticality equations, especially the radial equation from Eq. (3.12a) and the fact, that the *gauge-breaking* condition's, c.f. Eq. (4.19) left hand side now also depends on λ_s and also λ_p if the portal coupling is negative at the scale of condensation.

Therefore the angle of condensation via *gauge-breaking* is determined by

$$\text{for } \lambda_{p,\text{crit}} > 0 \ : \ \lambda \sin^4\vartheta + \lambda_s \cos^4\vartheta \simeq \frac{3}{16\pi^2} g^4 (q_\phi^2 \sin^2\vartheta + q_s^2 \cos^2\vartheta)^2 \ , \tag{4.27a}$$

$$\text{for } \lambda_{p,\text{crit}} < 0 \ : \kappa(\vartheta;\varphi) \simeq \frac{3}{16\pi^2} g^4 (q_\phi^2 \sin^2\vartheta + q_s^2 \cos^2\vartheta)^2 \ , \tag{4.27b}$$

where we again compare the sizes of contributions rather than the sign, such that we also left out the natural logarithm that would add a factor of $\mathcal{O}(1)$ and imply that this equation has to be fulfilled as a simplification of the radial criticality equation such that all couplings are evaluated at $\lambda = \lambda_i(t = t_{\text{crit}})$, $g = g(t_{\text{crit}})$ and the critical angle $\varphi_0 \equiv \varphi_{\text{crit}}$. With these equations we can understand the shift in Fig. 4.20, as a higher charge only effects the one-loop contribution, resulting in a compensation via the angle towards the weaker coupled field and hence moving the points of condensation towards the upper left corner. While this simple consideration gives some explanation one should never forget to account for the effects of RG-running when discussing condensation conditions in dependence of initial couplings. Thus, also the statement above, e.g. depends on whether g_0^4 is large compared to the scalar couplings and all the other factors that are important in the renormalization group running. This is also a nice reason to explain (small) irregularities in the plots, as these are probably points where the RG-running and therefore the SSB is affected by the not displayed quantities, like $\lambda_{p,0}$ and g_0.

In conclusion, a system of two massless scalars that are both coupled (symmetrically or asymmetrically) to the same $U(1)$ gauge group does not provide systematically new features of RSSB but extends the already observed feature of *gauge-breaking* to both scalar fields. We find that this model is still within the margin of applicable particle content for a Gildener-Weinberg type analysis as we do not find additional features. On the other hand our approach reproduces the statements made by Gildener and Weinberg and therefore provides a consistency check as well as a different point of view to understand the observed features. There is one feature here that has to be particularly noted, i.e. that the portal coupling λ_p can change its sign throughout RG-running allowing for condensation at non-trivial angles $\vartheta_0 \neq 0, \frac{\pi}{2}$ at initial portal couplings $\lambda_{p,0} > 0$, yet still at critical portal couplings $\lambda_p(t_{\text{crit}}) < 0$.

4.4 Two scalars coupled to two individual $U(1)$ groups

In this section we only briefly discuss the contributions of this model in the context of our general formalism from Section 3.1 and give a simple example for new features that are not covered by a Gildener-Weinberg type analysis, i.e. RSSB at not trivial angles for positive critical portal coupling. Since with now two individual gauge groups and thus couplings g_ϕ and g_s there are now five parameters that can be adjusted to gain certain insights or investigate areas of parameter space, we restrict ourselves to a simple symmetric case and setting them randomly to investigate the most general ("natural") case of quantum one-loop induced non-trivial minima. Further analysis for more combinations of varied parameters is left for upcoming works and therefore beyond the scope of this thesis.

Now with two different gauge groups $U_\phi(1)$ and $U_s(1)$ and the corresponding gauge fields A_μ and B_μ, the field definitions, c.f. Eq. (4.20), and the Lagrangian as well as the tree-level potential are unchanged compared to Eq. (4.21), but with the covariant derivatives now given by

$$D_\mu\phi = \partial_\mu\phi - iq_\phi g_\phi A_\mu\phi \,, \tag{4.28a}$$
$$D_\mu S = \partial_\mu S - iq_s g_s B_\mu S \,. \tag{4.28b}$$

In the Lagrangian we focus on the terms relevant for the analysis of effective potential minima, hence the ones that provide contributions to either tree-level or one-loop level terms, as a consequence we have to note that again we assume a $\mathbb{Z}_2$ symmetry between the fields ϕ and S such that operators of odd dimension in one of the fields are forbidden. Furthermore, for simplicity we set any gauge boson "mixing" terms, i.e. the product of the gauge fields' field strength tensors, to zero. This is clearly only possible with loss of generality but is the easiest model to test for RSSB features that are beyond the Gildener-Weinberg formalism. Again we fix the gauge such that only the real degree of freedom of ϕ and S contribute to the effective pontential like in Section 4.3 The charges of the fields with respect to the gauge groups are then generally set to

$$Q(\phi)_{U_\phi} = q_\phi, \qquad Q(\phi)_{U_s} = 0 \,, \tag{4.29a}$$
$$Q(S)_{U_\phi} = 0, \qquad Q(S)_{U_s} = q_s \,, \tag{4.29b}$$

resulting in the field dependent gauge masses

$$\hat{m}_A^2(\vartheta;\varphi_0) = q_\phi^2 g_\phi^2 \sin^2\vartheta \,, \tag{4.30a}$$
$$\hat{m}_B^2(\vartheta;\varphi_0) = q_s^2 g_s^2 \cos^2\vartheta \,, \tag{4.30b}$$

where we already used the same 2d spherical coordinates as in Eq. (4.22). Since the scalar content is unchanged to Section 4.3 the same scalar field dependent masses $\hat{m}_\pm^2(\vartheta;\varphi_0), \hat{m}_3^2(\vartheta;\varphi_0), \hat{m}_4^2(\vartheta;\varphi_0)$, c.f. Eqs. (4.6a), (4.16) and (4.24) contribute to the effective potential with the constants $c_i = \frac{3}{2}$, $c_l = \frac{5}{6}$ and multiplicities $n_i = 1$, $n_l = 3$ for $i = \pm, 3, 4$ and $l = A, B$. The β-functions and therefore the functions of the running couplings $\lambda_i(t)$ and $g_l(t)$ are given by

$$16\pi^2\beta_{g_\phi} = \frac{q_\phi^2}{3} g_\phi^3 \,, \tag{4.31a}$$
$$16\pi^2\beta_{g_s} = \frac{q_s^2}{3} g_s^3 \,, \tag{4.31b}$$
$$16\pi^2\beta_\lambda = 20\lambda^2 + \lambda_p^2 - 12q_\phi^2\lambda g_\phi^2 + 6q_\phi^4 g_\phi^4 \,, \tag{4.31c}$$
$$16\pi^2\beta_{\lambda_s} = 20\lambda_s^2 + \lambda_p^2 - 12q_s^2\lambda_s g_s^2 + 6q_s^4 g_s^4 \,, \tag{4.31d}$$
$$16\pi^2\beta_{\lambda_p} = 2\lambda_p\left(2\lambda_p + 4\lambda + 4\lambda_s - 3q_\phi^2 g_\phi^2 - 3q_s^2 g_s^2\right) \,. \tag{4.31e}$$

Comparing the above β-functions to the previous ones we already see that the quartic scalar and gauge couplings behave like before and by omitting gauge field strength contributions to the Lagrangian we ensured that the portal coupling is

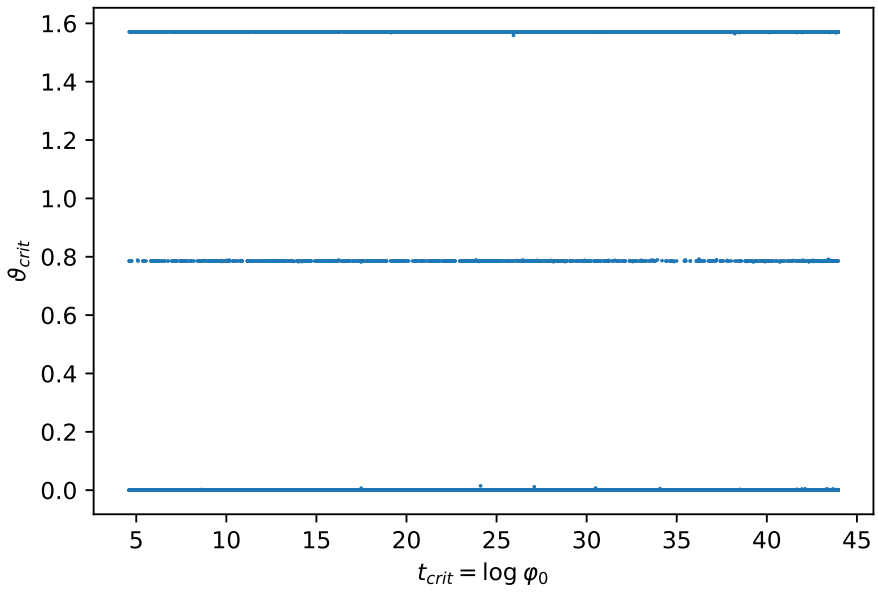

Figure 4.21: The critical angles ϑ_{crit} and scales t_{crit} that are allowed by randomly chosen individual initial couplings $\lambda_{i,0} \in [10^{-5}, 10^{-1}]$ and $g_{i,0} \in [10^{-1}, 1]$, for the symmetrical case of $q_\phi = q_s$, $\lambda_0 = \lambda_{s,0}$ and $g_{\phi,0} = g_{s,0} = 1$ and $\lambda_{p,0} > 0$.

renormalized in a multiplicative way again. Thus, the sign of $\lambda_p(t)$ does not change when evolving to lower or higher energies and there are no (fundamentally) new features of the couplings' RG-running. Starting off with the simple case of $q_\phi = q_s = 1$ we analyze symmetry breaking with respect to non-trivial angles for positive critical portal couplings $\lambda_p(t_{\text{crit}})$. Because of the portal coupling's multiplicative renormalization, c.f. Eq. (4.31), it is sufficient to search in the parameter region of initial $\lambda_{p,0} > 0$.

Because of the separate gauge contributions to the one-loop terms $A(\vartheta;\varphi_0)$ and $B(\vartheta;\varphi_0)$ via the masses in Eq. (4.30), we expect to find non-trivial angles for a simple symmetric case, where we chose $\lambda_0 = \lambda_{s,0} = 0$ and $g_{\phi,0} = g_{s,0}$. As a result the β-functions and therefore the functions of RG-running couplings for the gauge couplings and the quartic scalar couplings are identical, $\lambda(t) = \lambda_s(t)$, $g_\phi(t) = g_s(t)$ for all $t \in [t_{\text{EW}}, t_{\text{Pl}}]$. Investigating the criticality equations, starting with the radial one, c.f. Eq. (3.12a), we see that the combined gauge couplings contribution is maximal at $\vartheta = \frac{\pi}{4}$ but also non-zero for $\vartheta = 0, \frac{\pi}{2}$, while the angle at the which the angular tree-level term $\kappa(\vartheta_{\text{min}};\varphi_0)$ is minimal depends on the ratio between λ and λ_p. For $\lambda_p < 2\lambda$ this angle is given by $\vartheta_{\text{min}} = \frac{\pi}{4}$ and for $\lambda_p > 2\lambda$ by $\vartheta_{\text{min}} = 0, \frac{\pi}{2}$. In conclusion, under the assumption that the gauge couplings are large enough for *gauge-breaking*, for $\lambda_p(t_{\text{crit}}) < 2\lambda(t_{\text{crit}})$ we expect RSSB at the non-trivial angle $\vartheta_0 = \frac{\pi}{4}$ and still positive critical portal couplings and therefore a possibility of SSB that is not covered by the Gildener-Weinberg analysis, otherwise we are left with non-trivial vacua at trivial angles. In Fig. 4.21 we see the expected results for random initial couplings under the symmetric conditions of $\lambda_0 = \lambda_{s,0}$ and $g_{\phi,0} = g_{s,0}$. Since, $g_{\phi,0} = g_{s,0}$ are also varied there is also the case that the gauge sectors contribution is not large enough and the theory generates non-trivial minima via *scalar-breaking*,

resulting in trivial angles $\vartheta_0 = 0, \frac{\pi}{2}$. Having shown that in a "simple" scale-invariant two-scalar model with simple gauge groups ($U(1)$), there is already a case of RSSB that is not covered in an analysis via the Gildener-Weinberg formalism, we must note that this very symmetrical example is highly fine-tuned but possible. For example, the same analysis with our formalism, but without the symmetry conditions yields only very few points of RSSB at non-trivial angles, as seen in Fig. 4.22.

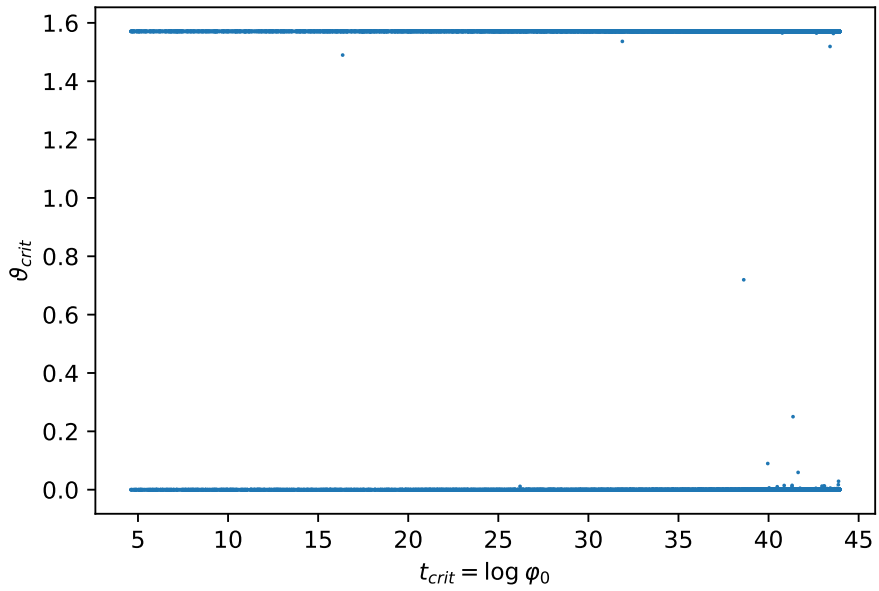

Figure 4.22: The critical angles ϑ_{crit} and scales t_{crit} that are allowed by randomly chosen individual initial couplings $\lambda_{i,0} \in [10^{-5}, 10^{-1}]$ and $g_{i,0} \in [10^{-1}, 1]$, with $q_\phi = q_s = 1$ and $\lambda_{p,0} > 0$.

Altogether, even though the case where we found SSB at positive critical portal couplings and non-trivial angles was very symmetrical and therefore needs fine tuning when setting the renormalized couplings at the Planck scale, it shows that even in fairly simple models like the classical scale-invariant two-scalar model coupled to two $U_i(1)$ gauge group provides possible cases for the generation of non-trivial minima by quantum corrections that are not considered in the widely used approach of the Gildener-Weinberg formalism. As a result, the initial assumption, that RSSB takes place if one of the Gildener-Weinberg conditions is fulfilled is not sufficient any more. Furthermore, one has to check whether the full criticality equations, c.f. Eq. (3.12) are not fulfilled at a higher scale, such that any assumptions or calculations for lower scales would have to include that one is already in the spontaneously broken phase of conformal symmetry when evolving the theory to lower scales than the critical one t_{crit}.

In the following section, Section 5, we recap our results for the systematics of RSSB from analyzing classical scale-invariant two-scalar models with different gauge sectors and discuss the connections for addressing the hierarchy problem via classical conformal multiscalar extensions of the standard model and their phenomenology.

5 Conclusion and outlook

Extensions of the SM are necessary to explain the unsolved problems of high-energy physics like dark matter, the hierarchy problem or the unification with gravity. But since there is no experimental evidence for the predictions of a supersymmetric standard model, alternatives like an extended conformal standard model (cSM) become more favorable. Following the observation that the SM itself is already (almost) scale-invariant at high energy-scales like the Planck scale, extensions to the cSM naturally address the electroweak hierarchy problem. They can be regarded as effective field theories for sub-Planck scale physics that generate the Higgs and all the other SM particles' masses dynamically via spontaneous symmetry breaking of the (tree-level) conformal symmetry by quantum (loop) corrections. It is necessary to extend the cSM via scalars and gauge bosons to counter the destabilization effects of the large top mass on the effective potential and generate the experimentally observed value for the vacuum expectation value of the Higgs boson.

Since the analytical minimization of the one-loop effective potential for classical conformal multiscalar theories is far from trivial, the Gildener-Weinberg approximation, assuming that a flat direction is formed at tree-level, is commonly used in the literature to analyze these. Yet S. Coleman and E. Weinberg already state in their original publication, Ref. [6], that this does not need to be the case to allow for the generation of non-trivial minima. There is another possibility of numerical brute-force minimization, which does not require additional assumptions but lacks the potential of gaining insight in the basic principles of RSSB in scale-invaraint multiscalar models. Therefore, we introduce a generalized formalism of exact criticality equations that are solved numerically to investigate the fundamental properties of RSSB in classically conformal multiscalar models. In Section 3, we derived generalized criticality equations and conditions for vacuum stability up to one-loop level that do not need any additional assumptions to the initial one of classical scale-invariance. With this formalism we gain another access to understanding the fundamentals of scale generation via RSSB and to the computation of non-trivial vacuum expectation values of the fields depending only on the values of the dimensionless couplings at the scale of renormalization. This leads us to a more intuitive concept of scale-setting in classically conformal theories as described in Section 3.2.

Analyzing the conformal symmetric two real scalar model in Section 4.1 we see that our general approach reproduces the results obtained with the Gildener-Weinberg approximations almost exactly. Investigating the dependency on the dimensionless couplings at renormalization scale of RSSB that generates non-trivial vacuum expectation values for the scalar fields in the right energy range, we see e.g. that asymmetric symmetry breaking along one of the fields $\vartheta_0 = 0$ or $\vartheta_0 = \frac{\pi}{2}$ already requires an initial asymmetry (hierarchy) in the dimensionless couplings. This can be understood via the intuitive nature of our criticality equations. Consequently, the assumption that at tree level a flat direction develops is not generally applicable to determine the properties of scale-setting, which is often neglected in the current literature, e.g. in Refs. [24, 38].

Given the intuitive nature of the criticality equations we can distinguish fundamentally different cases of RSSB when including gauge groups into the scale-

invariant two-scalar models. We observe *scalar-breaking* where an almost flat direction develops at tree-level, resulting in condensation similar to the one in the Gildener-Weinberg approximation. Furthermore, we can distinguish the case of *gauge-breaking*, where the one-loop terms, dominated by the contribution of the gauge field(s), are of the same order of magnitude as the tree-level (scalar) contributions and thus allow for RSSB. The latter form of symmetry breaking corresponds to the one displayed in the scalar QED case, c.f. Sections 2.2 and 3.4, which is not considered in the Gildener-Weinberg approximation. With this conceptional different form of RSSB our formalism offers the possibility to fundamentally distinguish forms of spontaneous symmetry breaking in conformal models by the respective particle sectors that are taking part. Furthermore, because of the analytically given criticality equations from Eq. (3.12) we can separate between interplay of contributions by particles with different spins directly at the critical scale and the effects of renormalization group running that connects the generation of non-trivial vacua with the conditions on the initial couplings. Conversely, in the Gildener-Weinberg approximation the conditions for symmetry breaking only depend on the scalar particle content of the theory, while the contributions from gauge bosons or fermions are implicitly included via the scalar couplings' RG-running. Hence, we expect our formalism to be more generally applicable and intuitive for understanding the fundamentals of scale-setting in conformal symmetric multiscalar models.

Our results from the analysis of the conformal two-scalar model is reproduced via the Gildener-Weinberg approach until we coupled the scalars to independent $U(1)$ gauge groups in Section 4.4. Thus, we conclude that depending on the gauge sector of the theory the foremost mechanism of RSSB is the RG-running of the couplings. Only when extending the gauge sector to a certain complexity, the analysis using our general approach yields possible regions of non-trivial vacua that are not included in the Gildener-Weinberg approach, c.f. Fig. 4.21. So far, trustworthy observations of these qualitatively new scenarios of RSSB were only made when coupling two massless complex scalars to independent $U(1)$ gauge groups with symmetric initial conditions and charges of the scalars under the corresponding $U(1)$. However, they serve as examples for the universality of our formalism and for the necessity of a general analysis in the context of full Coleman-Weinberg symmetry breaking instead of the Gildener-Weinberg approximation to show that a model extending the cSM solves the hierarchy problem.

In Ref. [22] it was shown that the minimal model of cSM extensions that is RG stable all the way up to the Planck scale and produces the correct radiative breaking of electroweak symmetry is the cSM with two additional scalar gauge singlets. T hus, the models discussed in Section 4 are phenomenologically not relevant. Yet the fundamental findings of distinguishable cases of RSSB and additional qualitatively new features not covered by the Gildener-Weinberg approximation are. Since our formalism can be generically used for arbitrary multiscalar fields without adding further assumptions than initial scale-invariance the next step would be the analysis of a three-scalar model with the right fermion and boson particle content to qualify as minimal extension of the cSM that adresses the electroweak hierarchy problem. Because of the generality of the theoretical formalism given in Section 3.1 and the numerical methods of Section 3.3 we do not expect this to raise insuperable problems

and hence is subject to future work.

In conclusion, given the generality of our approach, involving all particle contributions in the criticality equations as well as in the RG-running of the couplings we expect our results to be translatable to theories with extended particle content. Whereas we already saw that extended non-scalar particle content further limits the applicability of the Gildener-Weinberg approximation. Thus, the assumption that there exists a tree-level flat direction comes with some loss of generality as the generated non-trivial minimum along this flat direction is not necessary the global minimum and hence the true radiatively induced vacuum of the theory. Contrary to this, our approach of analyzing the radiatively induced spontaneous breakdown of conformal symmetry is appropriate to make a statement on whether a theory is viable to deal with the hierarchy problem via extension of the cSM and generate the correct non-trivial vacuum expectation values for the fields to match with experimental observations. Because of the exact criticality equations we can intuitively distinguish qualitatively different cases of RSSB, thus revealing the fundamental properties of scale-setting in classically conformal multiscalar theories.

A Appendix

A.1 Scaling of the Hessian determinant

From a computational point of view, it is a problem that the elements of the Hessian matrix in Eq. (3.13) scale differently with φ_0. However, as thankfully provided by Ref. [39], it turns out that all terms in calculating the determinant contain the same power of φ_0 so that it can be factored out in the end. To see why, we look only at the powers of φ_0 in each element of the full $n \times n$ Hessian matrix and calculate the determinant using the minor expansion formula with expansion with respect to the first row

$$\begin{vmatrix} \varphi_0^2 & \varphi_0^3 & \cdots & \varphi_0^3 \\ \varphi_0^3 & \varphi_0^4 & \cdots & \varphi_0^4 \\ \vdots & \vdots & \ddots & \vdots \\ \varphi_0^3 & \varphi_0^4 & \cdots & \varphi_0^4 \end{vmatrix} = \varphi_0^2 \cdot \begin{vmatrix} \varphi_0^4 & \cdots & \varphi_0^4 \\ \vdots & \ddots & \vdots \\ \varphi_0^4 & \cdots & \varphi_0^4 \end{vmatrix} + \varphi_0^3 \cdot \begin{vmatrix} \varphi_0^3 & \varphi_0^4 & \cdots & \varphi_0^4 \\ \vdots & \vdots & \ddots & \vdots \\ \varphi_0^3 & \varphi_0^4 & \cdots & \varphi_0^4 \end{vmatrix} , \tag{A.1}$$

where both matrices on the right-hand side are $(n-1)\times(n-1)$. Since the determinant is homogeneous of maximal degree, the first term on the right-hand side scales like $\varphi_0^2(\varphi_0^4)^{n-1} = \varphi_0^{4n-2}$. The determinant in the second term on the right-hand side can be further simplified by expanding it with respect to its first row giving

$$\varphi_0^3 \cdot \begin{vmatrix} \varphi_0^3 & \varphi_0^4 & \cdots & \varphi_0^4 \\ \vdots & \vdots & \ddots & \vdots \\ \varphi_0^3 & \varphi_0^4 & \cdots & \varphi_0^4 \end{vmatrix} = \varphi_0^3 \cdot \varphi_0^3 \cdot \begin{vmatrix} \varphi_0^4 & \cdots & \varphi_0^4 \\ \vdots & \ddots & \vdots \\ \varphi_0^4 & \cdots & \varphi_0^4 \end{vmatrix} , \tag{A.2}$$

where the determinant on the right-hand side is now $(n-2) \times (n-2)$. Using again homogeneity, this term can be seen to also scale like $(\varphi_0^3)^2(\varphi_0^4)^{n-2} = \varphi_0^{4n-2}$. In total, we have shown that

$$\det \mathrm{Hess}(\hat{V}_{\mathrm{eff}})(\varphi_0, \vec{\vartheta}_0; \varphi_0) = \varphi_0^{4n-2} \cdot \det \mathrm{H}(\vec{\vartheta}_0; \varphi_0) , \tag{A.3}$$

where the $n \times n$ matrix H is given by

$$\mathrm{H}(\vec{\vartheta}_0; \varphi_0) = \begin{pmatrix} 2B(\vec{\vartheta}_0; \varphi_0) & \frac{1}{2}\left[\vec{\nabla}_\vartheta B(\vec{\vartheta}_0; \varphi_0)\right]^{\mathsf{T}} \\ \frac{1}{2}\vec{\nabla}_\vartheta B(\vec{\vartheta}_0; \varphi_0) & \frac{1}{4}\,\mathrm{Hess}(\kappa + A)(\vec{\vartheta}_0; \varphi_0) \end{pmatrix} , \tag{A.4}$$

where $\mathrm{Hess}(\kappa + A)(\vec{\vartheta}_0; \varphi_0)$ denotes the angular Hessian

$$\mathrm{Hess}(\kappa + A)_{ij} = \frac{\partial^2(\kappa + A)}{\partial\vartheta_i \partial\vartheta_j} \qquad \text{with} \qquad i, j = 1, \ldots, n-1 , \tag{A.5}$$

evaluated at the vacuum $(\varphi_0, \vec{\vartheta}_0)$. Consequently, we can use the above matrix H to determine the stability properties of the one-loop vacuum in practice.

A.2 Scalar QED β_λ calculations

Given that $g(t) \simeq g_0 = \text{const}$ the derivative of λ's β-function is calculated to be

$$(4\pi)^2 \frac{\partial \beta_\lambda(\lambda)}{\partial \lambda} = 40\lambda - 12g^2 \,, \tag{A.6}$$

such that demanding Eq. (A.6) is identically zero, β_λ becomes stationary at $\lambda = \frac{3}{10}g^2$. Furthermore, the second derivative of β_λ with respect to λ shows that the before determined stationary point is a local minimum

$$(4\pi)^2 \frac{\partial^2 \beta_\lambda}{\partial \lambda^2} = 40 > 0 \,. \tag{A.7}$$

Investigating quartic couplings $\lambda(t) \geq 0$, we can now say that for all $\lambda(t) \geq 0$, $\beta_\lambda > 0$, since the value at the "domain wall" ($\lambda(t) = 0$) as well as the value at the minimum are positive

$$(4\pi)^2 \beta_\lambda(\lambda = \frac{3}{10}g^2) = \frac{21}{5}g^4 > 0 \,, \tag{A.8a}$$

$$(4\pi)^2 \beta_\lambda(\lambda = 0) = 6g^4 > 0 \,. \tag{A.8b}$$

A.3 Hessian determinant in the massless two-scalar model

The first partial derivatives of the effective potential with respect to the polar coordinates are given by

$$\frac{\partial \hat{V}_{\text{eff}}}{\partial \varphi} = \varphi^3 \left[\kappa(\vartheta;\varphi_0) + A(\vartheta;\varphi_0) + B(\vartheta;\varphi_0) \left(\ln \frac{\varphi^2}{\varphi_0^2} + \frac{1}{2} \right) \right] \,, \tag{A.9a}$$

$$\frac{\partial \hat{V}_{\text{eff}}}{\partial \vartheta} = \frac{\varphi^4}{4} \left[\kappa'(\vartheta;\varphi_0) + A'(\vartheta;\varphi_0) + B'(\vartheta;\varphi_0) \ln \frac{\varphi^2}{\varphi_0^2} \right] \,, \tag{A.9b}$$

where the prime denotes derivatives with respect to the angular variable ϑ. The second partial derivatives are computed to be

$$\frac{\partial^2 \hat{V}_{\text{eff}}}{\partial \varphi^2} = 3\varphi^2 \left[\kappa(\vartheta;\varphi_0) + A(\vartheta;\varphi_0) + B(\vartheta;\varphi_0) \left(\ln \frac{\varphi^2}{\varphi_0^2} + \frac{7}{6} \right) \right] \,, \tag{A.10a}$$

$$\frac{\partial^2 \hat{V}_{\text{eff}}}{\partial \vartheta^2} = \frac{\varphi^4}{4} \left[\kappa''(\vartheta;\varphi_0) + A''(\vartheta;\varphi_0) + B''(\vartheta;\varphi_0) \ln \frac{\varphi^2}{\varphi_0^2} \right] \,, \tag{A.10b}$$

$$\frac{\partial^2 \hat{V}_{\text{eff}}}{\partial \varphi \partial \vartheta} = \varphi^3 \left[\kappa'(\vartheta;\varphi_0) + A'(\vartheta;\varphi_0) + B'(\vartheta;\varphi_0) \left(\ln \frac{\varphi^2}{\varphi_0^2} + \frac{1}{2} \right) \right] \,. \tag{A.10c}$$

Evaluating Eq. (A.9) at the vacuum reproduces the left-hand sides of Eq. (3.12). Likewise, evaluating Eq. (A.10) at the stationary points and using the criticality

conditions in Eq. (3.12) gives

$$\left.\frac{\partial^2 \hat{V}_{\text{eff}}}{\partial \varphi^2}\right|_{\text{vac}} = 2\varphi_0^2 B(\vartheta_0;\varphi_0)\ , \tag{A.11a}$$

$$\left.\frac{\partial^2 \hat{V}_{\text{eff}}}{\partial \vartheta^2}\right|_{\text{vac}} = \frac{\varphi_0^4}{4}\left[\kappa''(\vartheta_0;\varphi_0) + A''(\vartheta_0;\varphi_0)\right]\ , \tag{A.11b}$$

$$\left.\frac{\partial^2 \hat{V}_{\text{eff}}}{\partial \varphi \partial \vartheta}\right|_{\text{vac}} = \frac{\varphi_0^3}{2} B'(\vartheta_0;\varphi_0)\ . \tag{A.11c}$$

The corresponding Hessian determinant $H(\varphi_0,\vartheta_0)$ can then be calculated as

$$H(\varphi_0,\vartheta_0) = \frac{\varphi_0^6}{4}\left[2B(\vartheta_0;\varphi_0)\Big(\kappa''(\vartheta_0;\varphi_0) + A''(\vartheta_0;\varphi_0)\Big) - B'(\vartheta_0;\varphi_0)^2\right] \tag{A.12a}$$

$$= \frac{\varphi_0^6}{4}\left(2B(\vartheta_0;\varphi_0)\left[\frac{\partial^2\left(\kappa(\vartheta;\varphi_0) + A(\vartheta;\varphi_0)\right)}{\partial\vartheta^2}\right]_{\vartheta=\vartheta_0} - \left[\frac{\partial B(\vartheta;\varphi_0)}{\partial\vartheta}\right]^2_{\vartheta=\vartheta_0}\right)\ . \tag{A.12b}$$

The stationary point (φ_0,ϑ_0) is a minimum of the one-loop effective potential and thus a proper stable vacuum if

$$H(\varphi_0,\vartheta_0) > 0 \qquad \text{and} \qquad B(\vartheta_0;\varphi_0) > 0\ , \tag{A.13}$$

where the second condition derives from the requirement that $\partial^2\hat{V}_{\text{eff}}/\partial\varphi^2$ (or equivalently $\partial^2\hat{V}_{\text{eff}}/\partial\vartheta^2$) must be positive for the stationary point to be a minimum.

A.4 Additional plots for two scalars one coupled to a gauge group

Here we show the results if one uses to the *top-down* approach to determine at which critical scale and angle one fulfills one of the Gildener-Weinberg conditions from Eq. (4.10) in the context of the model described in Section 4.2, i.e. the couplings' β-functions given by Eq. (4.18). The condensation scale depending on the initial couplings of the same order of magnitude are shown in Fig. A.1, whereas the critical angles are displayed in Fig. A.2. For further investigation of the structure in the critical angle distribution for non-trivial angles $\vartheta_0 \neq 0, \frac{\pi}{2}$ and therefore equivalently $\lambda_p < 0$ can be seen in Fig. A.3. For comparability with the plots from the two-scalar model $\lambda_{s,0} = \text{const.} = 0.3$ and following Section 4.2 the gauge coupling is also held constant for each plot and takes values of $g_0 = 0.652, 0.688, 0.738, 0.8308$. Furthermore, we give plots to investigate the effect of a variation in $\lambda_{s,0}$ in this model in Figs. A.4 and A.5, where we see, that there are no new features compared to Section 4.1.

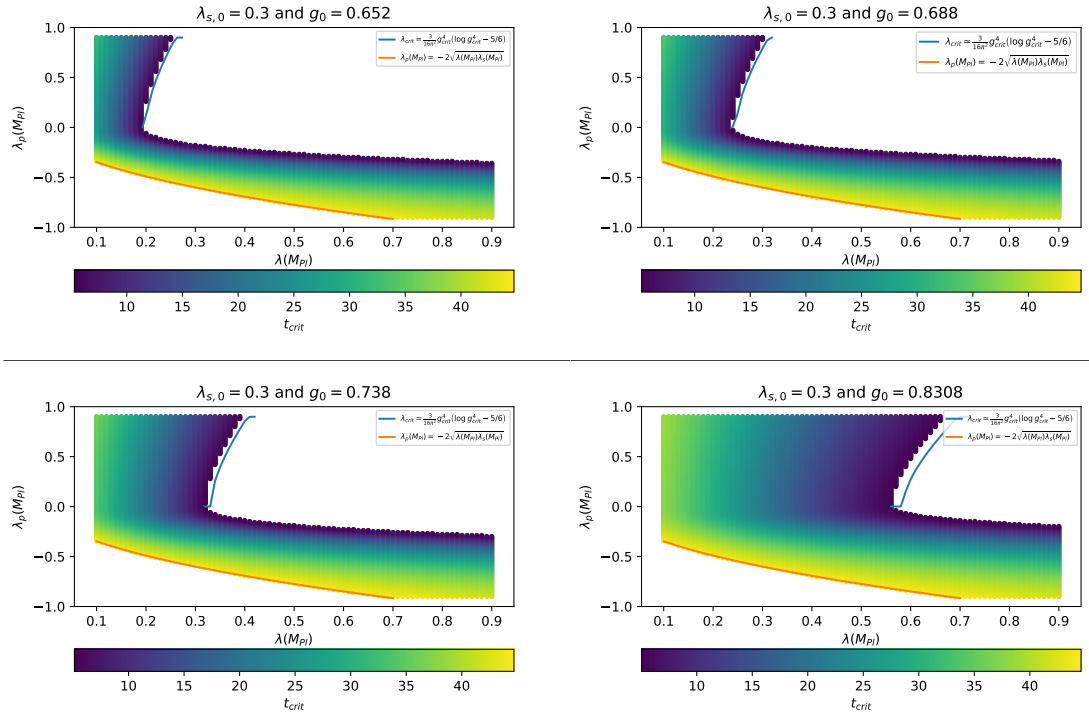

Figure A.1: Condensation scale t_{crit} depending on the initial portal $\lambda_{p,0}$ and quartic coupling λ_0, with different but constant $\lambda_{s,0}$ and g_0. Additionally, the tree-level stability condition and the gauge-breaking bounds (like in scalar QED) are plotted.

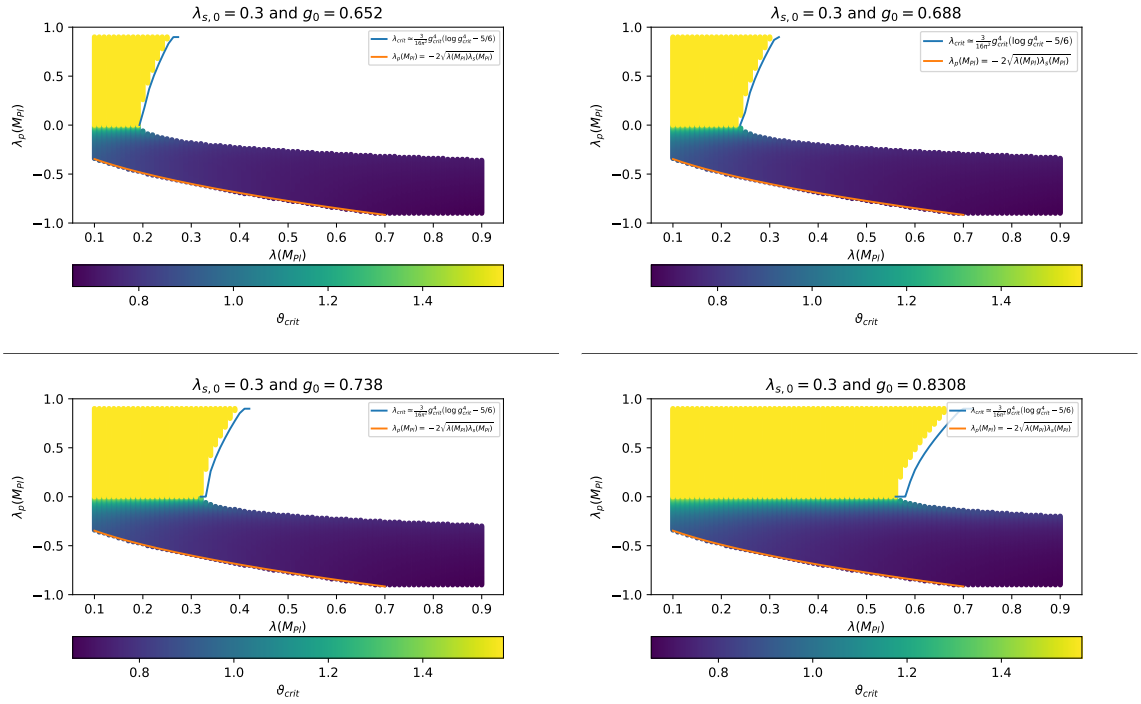

Figure A.2: Condensation angle ϑ_{crit} depending on the initial portal $\lambda_{p,0}$ and quartic coupling λ_0, with different but constant $\lambda_{s,0}$ and g_0. Additionally, the tree-level stability condition and the gauge-breaking bounds are plotted.

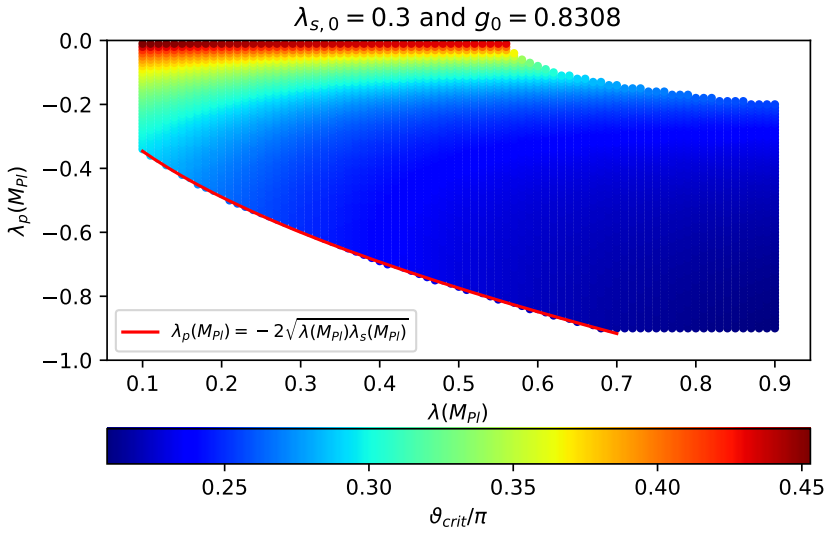

Figure A.3: The critical angles ϑ_{crit} depending on initial portal $\lambda_{p,0} < 0$ and quartic coupling λ_0, for constant $\lambda_{s,0} = 0.3$ and $g_0 = 0.8308$. Additionally the lower bound, given by tree-level stability of the potential, is plotted.

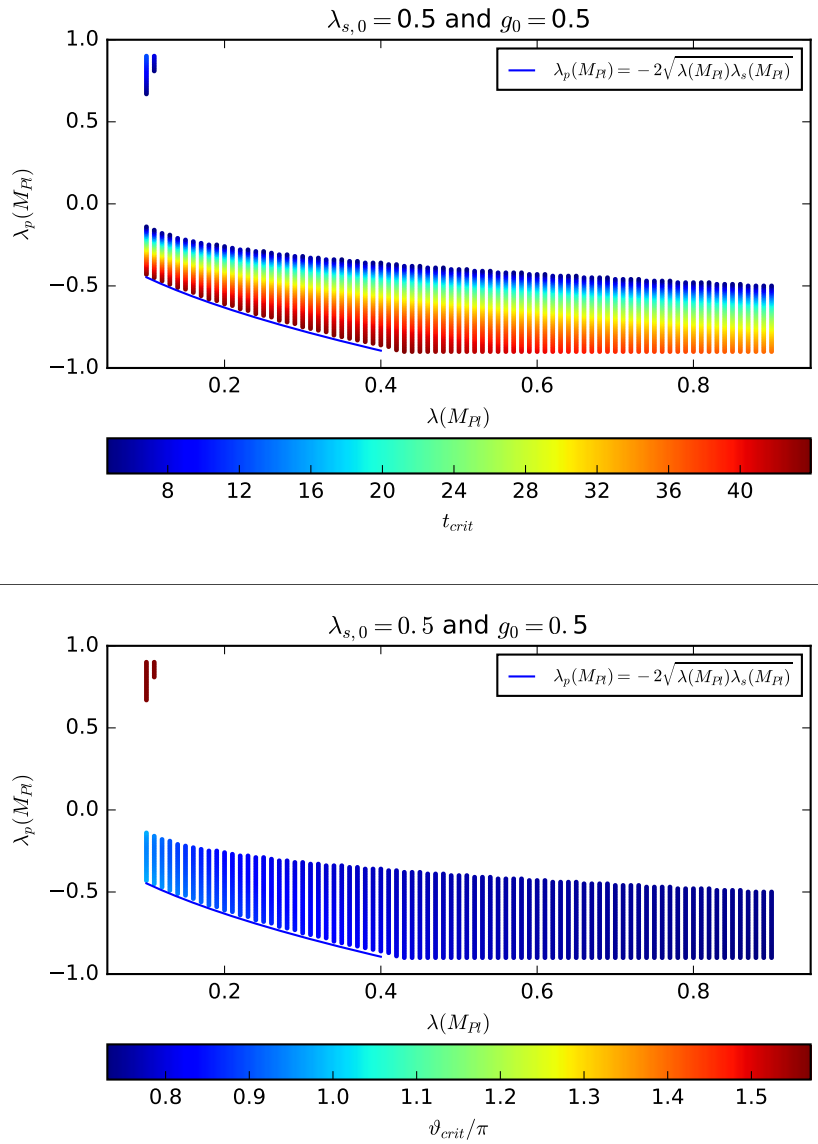

Figure A.4: The critical scales t_{crit} and angles ϑ_{crit} depending on initial portal $\lambda_{p,0}$ and quartic coupling λ_0, for constant $\lambda_{s,0} = 0.5$ and $g_0 = 0.5$. Additionally the lower bound, given by tree-level stability of the potential, is plotted.

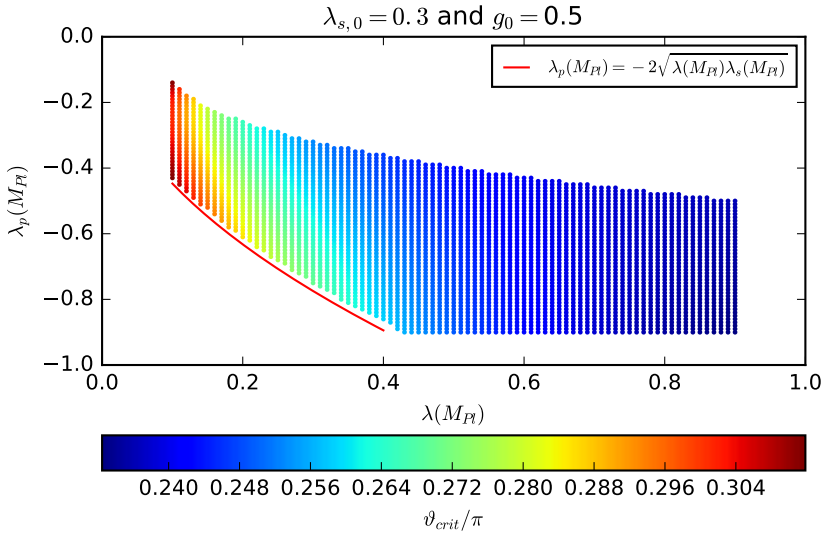

Figure A.5: The critical angles ϑ_{crit} depending on initial portal $\lambda_{p,0} < 0$ and quartic coupling λ_0, for constant $\lambda_{s,0} = 0.5$ and $g_0 = 0.5$. Additionally the lower bound, given by tree-level stability of the potential, is plotted.

A.5 Additional plots for two scalars both coupled to the same gauge group

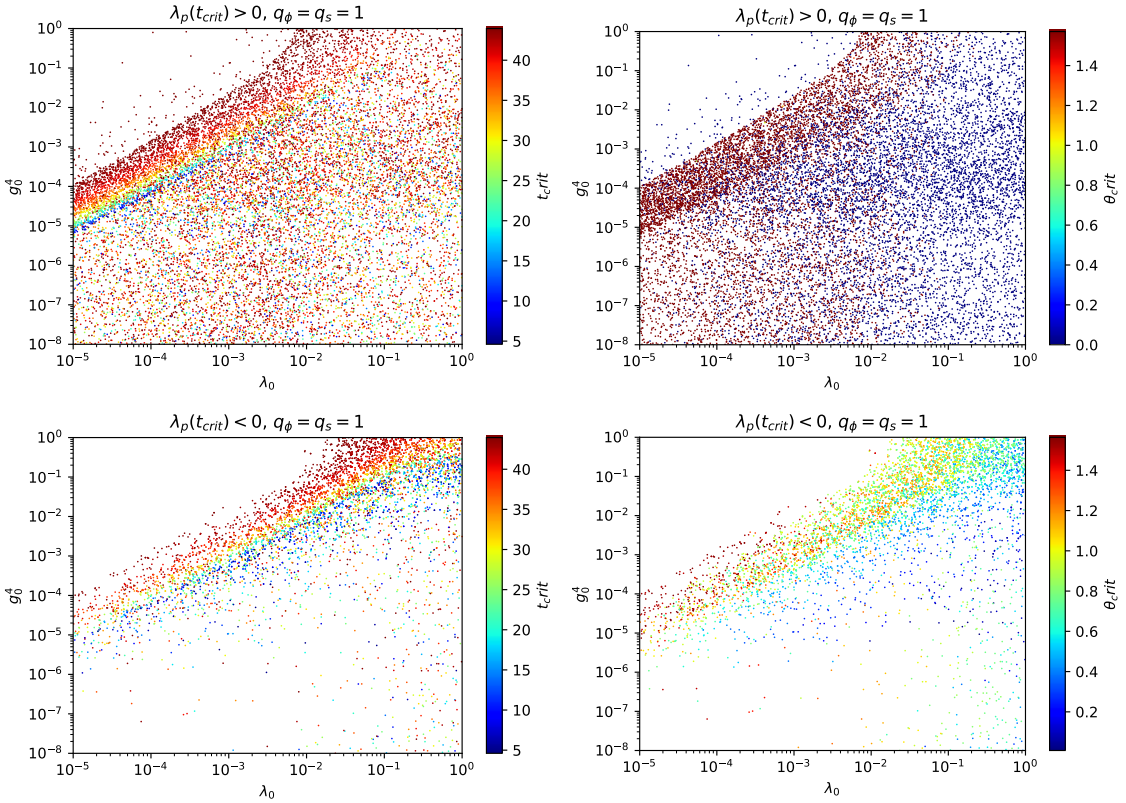

Figure A.6: The critical angles ϑ_{crit} and scales t_{crit} that are allowed by randomly chosen individual initial couplings $\lambda_{i,0} \in [10^{-5}, 1]$, and $g_0 \in [10^{-2}, 1]$ in dependence of the initial gauge g_0 and one quartic coupling λ_0. Divided by portal coupling at t_{crit}, the positive points are shown in the upper two plots, while negative ones are shown in the lower two.

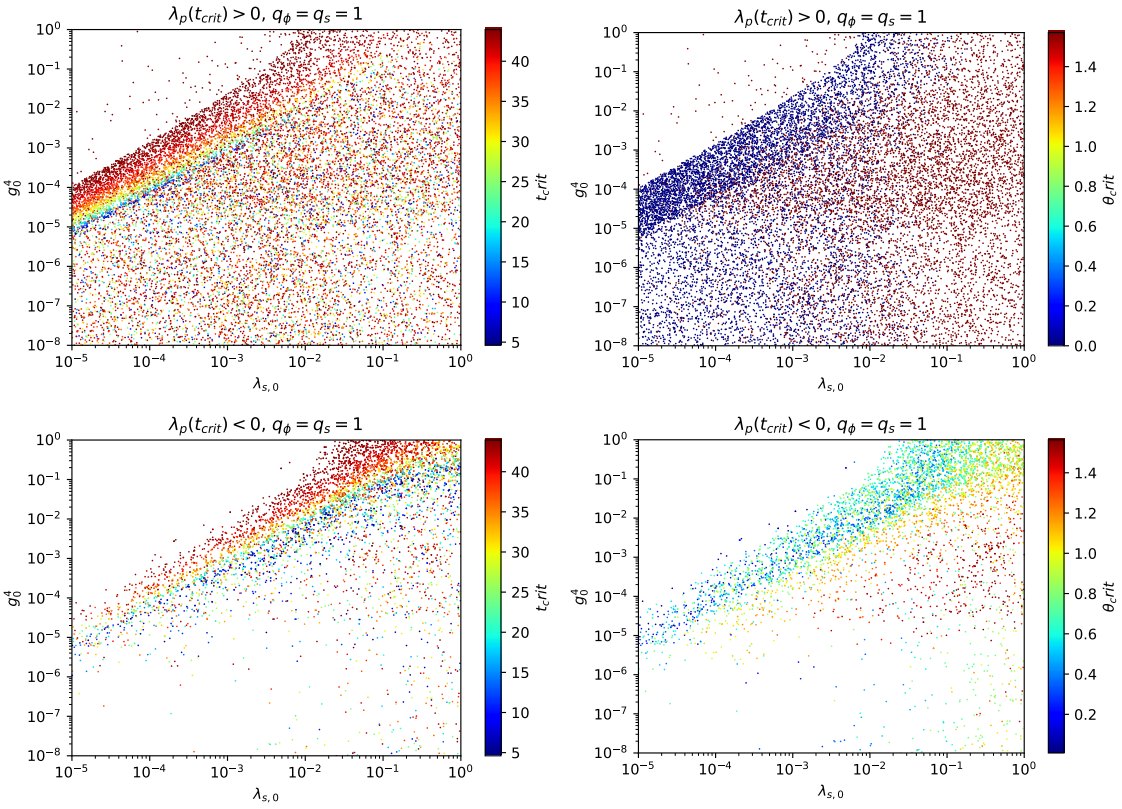

Figure A.7: The critical angles ϑ_{crit} and scales t_{crit} that are allowed by randomly chosen individual initial couplings $\lambda_{i,0} \in [10^{-5}, 1]$, and $g_0 \in [10^{-2}, 1]$ in dependence of the initial gauge g_0 and one quartic coupling $\lambda_{s,0}$. Divided by portal coupling at t_{crit}, the positive points are shown in the upper two plots, while negative ones are shown in the lower two.

A.6 Lists

List of Figures

References

[1]The NIST Reference on Constants, Units, and Uncertainty, *2018 CODATA Value: Planck mass energy equivalent*, Retrieved 17 December 2019.

[2]D. J. Gross and J. Wess, "Scale invariance, conformal invariance, and the high-energy behavior of scattering amplitudes", Phys. Rev. **D2**, 753–764 (1970).

[3]C. G. Callan Jr., S. R. Coleman, and R. Jackiw, "A New improved energy - momentum tensor", Annals Phys. **59**, 42–73 (1970).

[4]S. R. Coleman and R. Jackiw, "Why dilatation generators do not generate dilatations?", Annals Phys. **67**, 552–598 (1971).

[5]W. A. Bardeen, "On naturalness in the standard model", in Ontake Summer Institute on Particle Physics Ontake Mountain, Japan, August 27-September 2, 1995 (1995).

[6]S. R. Coleman and E. J. Weinberg, "Radiative Corrections as the Origin of Spontaneous Symmetry Breaking", Phys. Rev. **D7**, 1888–1910 (1973).

[7]R. Hempfling, "The next-to-minimal coleman-weinberg model", Physics Letters B **379**, 153–158 (1996).

[8]K. A. Meissner and H. Nicolai, "Conformal symmetry and the standard model", Physics Letters B **648**, 312–317 (2007).

[9]R. Foot, A. Kobakhidze, K. L. McDonald, and R. R. Volkas, "Solution to the hierarchy problem from an almost decoupled hidden sector within a classically scale invariant theory", Physical Review D **77** (2008) 10.1103/physrevd.77.035006.

[10]R. Foot, A. Kobakhidze, K. L. McDonald, and R. R. Volkas, "Neutrino mass in radiatively broken scale-invariant models", Physical Review D **76** (2007) 10.1103/physrevd.76.075014.

[11]M. Holthausen, M. Lindner, and M. A. Schmidt, "Radiative symmetry breaking of the minimal left-right symmetric model", Physical Review D **82** (2010) 10.1103/physrevd.82.055002.

[12]N. Haba, H. Ishida, N. Kitazawa, and Y. Yamaguchi, "A new dynamics of electroweak symmetry breaking with classically scale invariance", Phys. Lett. **B755**, 439–443 (2016).

[13]A. Ahriche, K. L. McDonald, and S. Nasri, "A Radiative Model for the Weak Scale and Neutrino Mass via Dark Matter", JHEP **02**, 038 (2016).

[14]P. Humbert, M. Lindner, and J. Smirnov, "The Inverse Seesaw in Conformal Electro-Weak Symmetry Breaking and Phenomenological Consequences", JHEP **06**, 035 (2015).

[15]M. Lindner, S. Schmidt, and J. Smirnov, "Neutrino Masses and Conformal Electro-Weak Symmetry Breaking", JHEP **10**, 177 (2014).

[16]K. Hashino, S. Kanemura, and Y. Orikasa, "Discriminative phenomenological features of scale invariant models for electroweak symmetry breaking", Phys. Lett. **B752**, 217–220 (2016).

[17]C. Englert, J. Jaeckel, V. V. Khoze, and M. Spannowsky, "Emergence of the Electroweak Scale through the Higgs Portal", JHEP **04**, 060 (2013).

[18]C. T. Hill, "Is the Higgs Boson Associated with Coleman-Weinberg Dynamical Symmetry Breaking?", Phys. Rev. **D89**, 073003 (2014).

[19]N. Haba, H. Ishida, R. Takahashi, and Y. Yamaguchi, "Gauge coupling unification in a classically scale invariant model", JHEP **02**, 058 (2016).

[20]N. Haba, H. Ishida, N. Okada, and Y. Yamaguchi, "Bosonic seesaw mechanism in a classically conformal extension of the Standard Model", Phys. Lett. **B754**, 349–352 (2016).

[21]A. Karam and K. Tamvakis, "Dark matter and neutrino masses from a scale-invariant multi-Higgs portal", Phys. Rev. **D92**, 075010 (2015).

[22]A. J. Helmboldt, P. Humbert, M. Lindner, and J. Smirnov, "Minimal conformal extensions of the higgs sector", Journal of High Energy Physics **2017** (2017) 10.1007/jhep07(2017)113.

[23]E. Gildener and S. Weinberg, "Symmetry Breaking and Scalar Bosons", Phys. Rev. **D13**, 3333 (1976).

[24]L. Alexander-Nunneley and A. Pilaftsis, "The minimal scale invariant extension of the standard model", Journal of High Energy Physics **2010** (2010) 10.1007/jhep09(2010)021.

[25]A. Farzinnia, H.-J. He, and J. Ren, "Natural electroweak symmetry breaking from scale invariant higgs mechanism", Physics Letters B **727**, 141–150 (2013).

[26]R. Foot, A. Kobakhidze, and R. R. Volkas, "Electroweak higgs as a pseudo-goldstone boson of broken scale invariance", Physics Letters B **655**, 156–161 (2007).

[27]A. Karam and K. Tamvakis, "Dark matter from a classically scale-invariantsu(3)x", Physical Review D **94** (2016) 10.1103/physrevd.94.055004.

[28]I. Buchbinder, S. Odintsov, and L. Shapiro, *Effective action in quantum gravity* (Taylor & Francis, 1992).

[29]M. Quiros, "Finite temperature field theory and phase transitions", in Proceedings, Summer School in High-energy physics and cosmology: Trieste, Italy, June 29-July 17, 1998 (1999), pp. 187–259.

[30]S. Weinberg, *The quantum theory of fields. Vol. 2: Modern applications* (Cambridge University Press, 1996).

[31]B. N. Swiezewska, "Higgs boson and vacuum stability in models with extended scalar sector", PhD thesis (Warsaw U., 2016).

[32]R. Jackiw, "Functional evaluation of the effective potential", Phys. Rev. D **9**, 1686–1701 (1974).

[33]T. Markkanen, S. Nurmi, A. Rajantie, and S. Stopyra, "The 1-loop effective potential for the standard model in curved spacetime", Journal of High Energy Physics **2018**, 40 (2018).

[34]A. Andreassen, W. Frost, and M. D. Schwartz, "Consistent use of effective potentials", Physical Review D **91** (2015) 10.1103/physrevd.91.016009.

[35]Z.-f. Cui, C. Shi, W.-m. Sun, Y.-l. Wang, and H.-s. Zong, "The wigner solution and qcd phase transitions in a modified pnjl model", The European Physical Journal C **74** (2014) 10.1140/epjc/s10052-014-2782-x.

[36]S. Hassani, *Mathematical physics, A modern introduction to its foundations*, eng, Second edition (Springer, Cham ; Heidelberg ; New York ; Dordrecht ; London, 2013), xxxi, 1205 Seiten.

[37]F. Lyonnet and I. Schienbein, "PyR@TE 2: A Python tool for computing RGEs at two-loop", Comput. Phys. Commun. **213**, 181–196 (2017).

[38]J. Haruna and H. Kawai, "Weak scale from Planck scale – Mass Scale Generation in Classically Conformal Two Scalar System –", (2019).

[39]A. J. Helmboldt, *Scaling of hessian determinant*, Internal communication.

[40]T. G. Steele and Z.-W. Wang, "Is radiative electroweak symmetry breaking consistent with a 125 gev higgs mass?", Physical Review Letters **110** (2013) 10.1103/physrevlett.110.151601.

[41]V. Elias, R. B. Mann, D. G. C. McKeon, and T. G. Steele, "Radiative electroweak symmetry breaking revisited", Physical Review Letters **91** (2003) 10.1103/physrevlett.91.251601.

Erklärung:

Ich versichere, dass ich diese Arbeit selbstständig verfasst habe und keine anderen als die angegebenen Quellen und Hilfsmittel benutzt habe.

Heidelberg, den 20.12.2019 .....